UNIVERSITY OF KWAZULU-NATAL

Index Modulation for Next-Generation Wireless Networks

Segun Emmanuel Oladoyinbo

2020

Index Modulation for Next-Generation Wireless Networks

By Segun Emmanuel Oladoyinbo

Student Number: 214574841

Submitted in fulfilment of the academic requirements of

Doctor of Philosophy in Engineering

School of Engineering, Electronic Engineering

College of Agriculture, Engineering and Science

University of KwaZulu-Natal

Howard College

South Africa

Supervised by: Dr. Narushan Pillay

Co-supervised by: Prof. HongJun Xu

August 2020

CERTIFICATION

As the candidate's Supervisor, I agree with the submission of this thesis.

Signed: Dr. Narushan Pillay

Date: 24th August 2020

DECLARATION 1 - PLAGIARISM

I, Segun Emmanuel Oladoyinbo declare that:

1. The research reported in this dissertation, except where otherwise indicated, is my original research.

2. This dissertation has not been submitted for any degree or examination at any other university.

3. This dissertation does not contain other persons’ data, pictures, graphs, or additional information unless specifically acknowledged as being sourced from other persons.

4. This dissertation does not contain other persons' writing unless specifically acknowledged as being sourced from other researchers. Where other written sources have been quoted, then:

a. Their words have been re-written but the general information attributed to them has been referenced

b. Where their exact words have been used, then their writing has been placed in italics and inside quotation marks and referenced.

5. This dissertation does not contain texts, graphics or tables copied and pasted from the internet, unless specifically acknowledged, and the source being detailed in the thesis and in the Reference section.

____

Signed: Oladoyinbo Segun

Date: 24th August 2020

DECLARATION 2 - PUBLICATIONS

The work in this dissertation has been published or submitted for publication. The details are as follows:

1. S. Oladoyinbo, N. Pillay, and H. Xu, "Media-based single-symbol generalized spatial modulation," International Journal of Communication Systems, vol. 32, no. 6, pp. 1-13, 2019. DOI: 10.1002/dac.3909.

2. S. Oladoyinbo, N. Pillay, and H. Xu, "Adaptive single-input multiple-output media-based modulation," [Under review with Digital Communications and Networks], 2020.

3. S. Oladoyinbo, N. Pillay, and H. Xu, "Single-symbol generalized quadrature spatial modulation," in Proceedings of the South African Telecommunication Networks and Applications Conference (SATNAC), pp. 370-375, Sep. 2018.

4. S. Oladoyinbo, N. Pillay, and H. Xu, "Generalised Quadrature Spatial Modulation in Two-way Decode-and-Forward Relaying Cooperative Networks," [Ready for submission to IEEE INFOCOM 2021: IEEE International Conference on Computer Communications 2021].

____

Signed: Oladoyinbo Segun

Date: 24th August 2020

ACKNOWLEDGMENTS

I thank God for making it a possibility "…but with God all things are possible", Matthew 19:26. I say a big thank you to my supervisors, Dr. Narushan Pillay and Prof H. Xu, for your time, encouragement and training as a researcher from the wealth of experience, guidance and unlimited access to your office. In addition, a big thank you to my parents: Elder. P.O Oladoyinbo and Mrs. W.A Oladoyinbo for your encouragement. Olayide, Desire, Olaoluwa, Seun, Ayobami, Ife, Joseph, I appreciate you all. Finally, to my loved ones, thank you all for your supports, motivations and prayers. Gracias.

DEDICATION

This thesis is dedicated to my wife (Dr. Olayide Oladoyinbo).

ABSTRACT

The desirability of high throughput and superior system performance for multimedia services requires schemes that can achieve high spectral efficiency. However, this imposes high system/hardware complexity due to the large number of antennas required at the transmitter. This led to the development of several innovative multiple-input multiple-output (MIMO) techniques in the research community, such as generalized spatial modulation (GSM).

GSM is a spatial modulation (SM) based scheme, which employs transmit antenna combinations coupled with identical symbols to convey additional information. This made the use of multiple transmit antennas possible in index modulation, improving the setback/limitation of hardware complexity experienced in the conventional MIMO and SM schemes.

Furthermore, in the literature, an improved spectral efficient quadrature spatial modulation (QSM) based scheme termed generalized quadrature spatial modulation (GQSM) is proposed. In GQSM, the antennas at the transmitter are divided into groups and a unique symbol is employed across multi-active transmit antenna groups. Hence, GQSM requires less transmit antennas to achieve a high data rate when compared to its counterparts. However, GQSM requires multiple radio frequency (RF) chains, considering unique symbols are employed in each transmit antenna group. This motivates us to investigate single-symbol GQSM (SS-GQSM), which employs identical symbols across each group requiring a single RF chain.

Recently, the application of RF mirrors termed media-based modulation (MBM) was introduced to the research community as a technique to enhance the spectral efficiency at a reduced hardware complexity. This motivates us to investigate MBM with single-symbol GSM to enhance its error performance and to mitigate the drawback of the requirement of multiple RF chains.

In addition, link adaptation has been stated in literature as a technique, which can enhance the performance of a single-input multiple-output (SIMO)/MIMO scheme. MBM achieves a high data rate coupled with enhanced system performance. However, to the author's best knowledge, link adaptation has not been investigated with MBM. This motivates us to propose an adaptive algorithm that employs different candidate transmission modes to enhance the reliability of the SIMO system. The proposed scheme is called adaptive SIMOMBM (ASIMOMBM).

Lately, two-way cooperative relaying has been proven as a spectral efficient relaying system. This technique employs two or more source nodes, which transmit information to the relay node simultaneously. Considering the advantages of GQSM stated earlier, this motivates us to investigate two-way decode-and-forward relaying for the GQSM scheme to improve the error performance of the conventional GQSM system.

Table of Contents

LIST OF FIGURES

LIST OF TABLES

LIST OF ACRONYMS

APM…………………………………………………………..Amplitude/Phase Modulation
ASIMOMBM………………...Adaptive Single-Input Multiple-Output Media-based Modulation
AWGN ………………………………………………………..Additive White Gaussian Noise
BER……………………………………………………………………………Bit Error Rate
CC……………………………………………………………….Computational Complexity
CSI……………………………………………………………….Channel State Information
DF-GQSM……………………Decode and Forward Generalized Quadrature Spatial Modulation
EDAS………………………………………………..Euclidean Distance Antenna Selection
GQSM……………………………………………Generalized Quadrature Spatial Modulation
GSM………………………………………………………..Generalized Spatial Modulation
GSM-MBM……………………………………..Generalized Spatial Media-based Modulation
i.i.d. …………………………………………………Independent and Identically Distributed
IAS………………………………………………………..Inter-Antenna Synchronization
IBEP……………………………………………………Instantaneous Bit Error Probability
ICI……………………………………………………………..Inter-Channel Interference
LCTAS-A-C……………………LCTAS based on Channel Amplitude and Antenna Correlation
MAP……………………………………………………………….Mirror Activation Pattern
MB-SSK……………………………………………………..Media-based Space Shift Keying
M-GSM…………………………Multiple Transmit Antenna for Generalized Spatial Modulation
MIMO………………………………………………………Multiple-Input Multiple-Output
ML……………………………………………………………………….Maximum Likelihood
PEP……………………………………………………………….Pairwise Error Probability
PSK……………………………………………………………………….Phase Shift Keying
QAM…………………………………………………….Quadrature Amplitude Modulation
QSM……………………………………………………….Quadrature Spatial Modulation
RF……………………………………………………………………………..Radio Frequency
SIMO…………………………………………………….….Single-Input Multiple-Output
SIMO-MBM……………………………Single-Input Multiple-Output Media-based Modulation
SM……………………………………………………………………………..Spatial Modulation
SS-GQSM……………………………………….Single-Symbol Generalized Spatial Modulation
SS-GSM-MBM………...………….Single-Symbol Generalized Spatial Media-based Modulation
SNR…………………………………………………………………...Signal-to-Noise Ratio
USTLD…………………………………………………Uncoded Space-Time Label Diversity
V-BLAST…………………………Vertical Bell Laboratories Layered Space-Time Architecture

CHAPTER 1

INTRODUCTION

The introduction and background study of this thesis are presented in this chapter.

INTRODUCTION

1 Multiple-Input Multiple-Output

The tremendous promise shown over the years concerning high transmission capacity and improved link reliability in multiple-input-multiple-output (MIMO) systems [1] motivates the development of several MIMO techniques in the research community. The spatial multiplexing MIMO system transmits data in parallel streams. Multiple antennas capture the data streams at the receiver, which is slightly different in amplitude and phase, such that each antenna is unique and treated independently, hence increasing throughput [2].

One of the main benefits of MIMO is the linear increment of its spectral efficiency, which results in a high-capacity gain and the multi-transmission of data streams improves the link reliability (diversity gain) coupled with the enhancement of the signal-to-noise ratio (SNR). However, MIMO systems experience some drawbacks to its practical realization, such as inter-antenna synchronization (IAS), inter-channel interference (ICI) and high power consumption due to multi-active transmit antennas [3, 4].

1.1 System model for the Multiple-Input Multiple-Output scheme

Figure 1.1 presents a detailed system model of a MIMO system with multiple transmit antennas and multiple receive antennas.

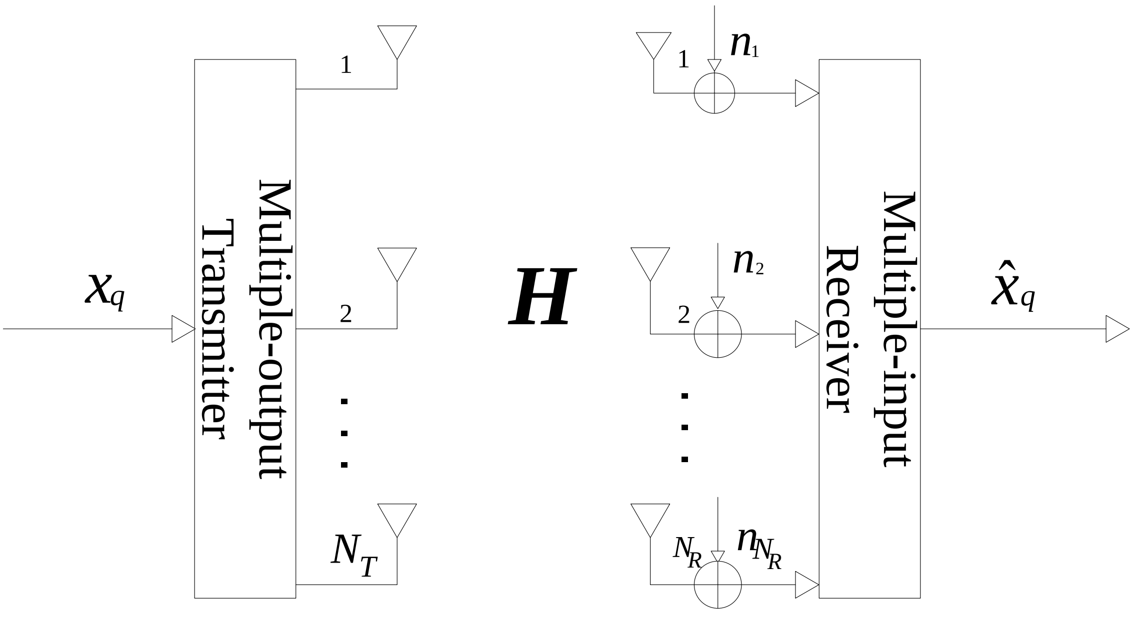

Figure 1.1 MIMO system with multiple transceivers [5]

The channel employed is a frequency-flat Rayleigh fading channel, this is mostly seen where there is a high environmental multipath propagation effect on the radio wave or where line-of-sight (LOS) is absent. The channel matrix $\boldsymbol{H}$ of dimension $N_R \times N_T$ between the multi-active transmitter N_T and multi-active receiver N_R is:

$$\boldsymbol{H} = \begin{bmatrix} h_{1,1} & \cdots & h_{1,N_T} \\ \vdots & \ddots & \vdots \\ h_{N_R,1} & \cdots & h_{N_R,N_T} \end{bmatrix} \tag{1-1}$$

where $h_{i,j}$ represents the j^{th} column corresponding to the channel matrix $\boldsymbol{H}$, $i \in [1: N_R]$ and $j \in [1: N_T]$.

Considering an example of a vector $\boldsymbol{x}_q$ of dimension $N_T \times 1$ transmitted over a multipath channel $\boldsymbol{H}$, which is with independent and identically distributed (i.i.d) entries. The vector $\boldsymbol{x}_q$ is transmitted with the existence of additive white Gaussian noise (AWGN) $\boldsymbol{n}$ with i.i.d entries and $CN(0,1)$ distribution. Hence, the vector $\boldsymbol{y}$ of dimension $N_R \times 1$ received at the receiver is described as:

$$\boldsymbol{y} = \sqrt{\frac{\rho}{N_T}}\, \boldsymbol{H}\boldsymbol{x}_q + \boldsymbol{n} \tag{1-2}$$

where ρ is the average SNR.

In the next sub-section, several techniques employed to improve the limitations of MIMO systems with relevant examples are discussed. This includes spatial multiplexing, spatial diversity and pre-coding techniques. In addition to these techniques, cooperative networks, link adaptation and smart antennas are employed to enhance the performance of the MIMO systems.

1.2 Spatial multiplexing and spatial diversity

The spatial multiplexing technique is employed in MIMO to enhance the data rate. This made the technique (spatial multiplexing) a suitable scheme for future wireless communication [5, 6]. Especially in multimedia services, considering the high demand for an increase in transmission capacity.

The input signals/bits in spatial multiplexing are divided into streams. These streams are transmitted with a unique transmit antennas in the same frequency channel. This enables the simultaneous transmission of user information/messages to multiple receivers [6].

Similarly, link reliability is achieved in MIMO via spatial diversity, which is the variation of the channel in time, frequency and space. However, this technique (spatial diversity) has a limitation of inter-symbol interference (ISI) due to the dispersion of the channel, which can be avoided if there is enough space between the transmitted symbols. However, this will result in decreased throughput [7, 8].

Various examples of improved MIMO schemes will be discussed in the next sub-section, starting with vertical-Bell Laboratories layered space-time architecture (V-BLAST) [9].

1.2.1 Vertical-Bell Laboratories layered space-time architecture

In V-BLAST [9], the block of N_T (number of transmit antennas) symbols are compressed into a single message block, which is mapped to a single transmit antenna [4], eliminating the ICI experienced in the conventional MIMO scheme. The V-BLAST architecture takes advantage of spatial multiplexing to enhance its spectral efficiency by sending out N_T signals at each time slot.

Considering an example of a V-BLAST technology in an indoor environment, this can achieve a spectral efficiency higher than 15 bpcu or b/s/Hz, assuming a practical SNR range [9]. However, the multi-active transmit antennas in this architecture requires N_T radio frequency (RF) chains coupled with IAS.

1.3 Index modulation

Index modulation-based scheme employs transmit antennas innovatively to convey additional information, such that spatial multiplexing gain is achieved coupled with an increase in data rate. Details of index modulation-based schemes are presented in the next sub-section.

1.3.1 Spatial Modulation

Spatial modulation (SM) [10] employs transmit antennas innovatively to mitigates the major setbacks of IAS and ICI experienced in the conventional MIMO schemes [5, 10-12]. In SM, just one antenna is required at the transmitter at every instant, hence, enabling the use of a single RF chain possible [11]. SM exhibits an improved system performance compared to V-BLAST [10]. This is achieved via the maximization of the space modulation technique.

Furthermore, SM exploits spatial multiplexing techniques to achieve a high data rate coupled with enhanced system performance. This is achieved by separating the input bitstream into two sections; the initial segment chooses one antenna from the variety of the available antennas at the transmitter, while the second part is modulated into amplitude/phase modulation (APM) constellation symbol. The modulated signal is sent out via the active transmit antenna. Figure 1.2 presents a detailed transmission model of SM.

The spectral efficiency associated with the SM scheme is $\log_2 MN_T$ b/s/Hz, where M represents the modulation order. Taking an example of 2×4 4-QAM, employing the notation (N_T, N_R, M).

This achieves a data rate of 3 b/s/Hz. The initial part of the bit selects the antenna to be used for transmission and the last two bits modulate the APM symbol. The mapped bits are sent out via a single transmit antenna. A clarified mapping process of SM is tabulated in Table 1.1.

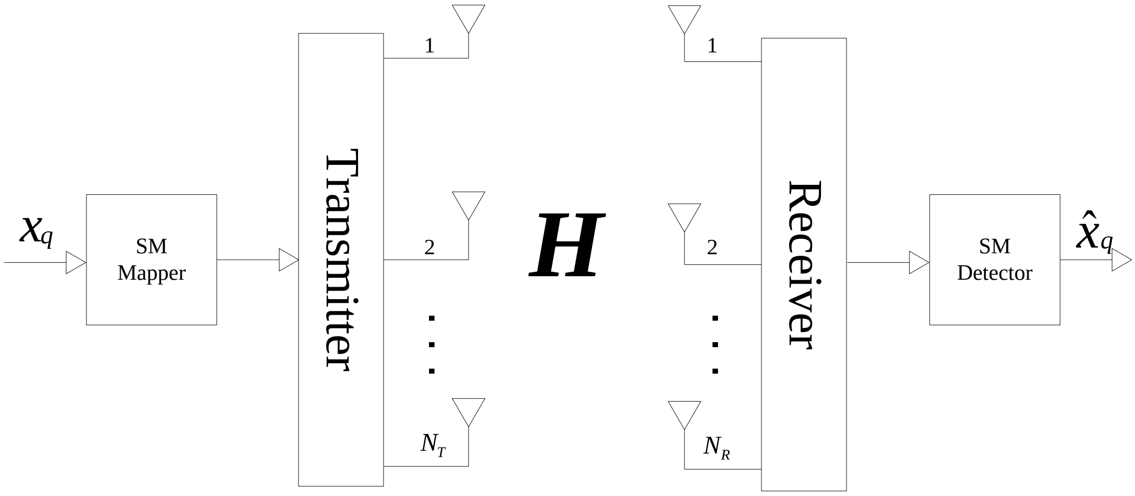

Figure 1.2 Transmission model for the SM system [7].

Table 1.1 Mapping process for the SM system.

Input bits	Antenna index	Symbol x_q	Transmitted signal
0 1 1	[0] ⇒ 1	[1 1] ⇒1-1i	[1-1i, 0]
1 0 0	[1] ⇒ 2	[0 0] ⇒ 1+1i	[0, 1+1i]
0 1 0	[0] ⇒ 1	[1 0] ⇒ -1-1i	[-1-1i, 0]
1 1 1	[1] ⇒ 2	[1 1] ⇒ 1-1i	[0, 1-1i]
1 0 0	[1] ⇒ 2	[0 0] ⇒ 1+1i	[0, 1+1i]
1 1 1	[1] ⇒ 2	[1 1] ⇒ 1-1i	[0, 1-1i]
1 0 0	[1] ⇒ 2	[0 0] ⇒ 1+1i	[0, 1+1i]
0 1 0	[0] ⇒ 1	[1 0] ⇒ -1-1i	[-1-1i, 0]

The vector $\boldsymbol{y}$ received at the receiver becomes:

$$\boldsymbol{y} = \sqrt{\rho}\boldsymbol{H}x_q + \boldsymbol{n} \tag{1-3}$$

where $\boldsymbol{H}$ is the channel matrix, $\boldsymbol{n}$ is the AWGN and ρ represents the SNR associated with each receive antennas.

1.3.2 Differential Spatial Modulation

In [13], a special case of SM termed differential SM (DSM) was proposed. This improves the requirement of the CSI/complex channel estimation and symbol detection algorithm needed in SM. DSM maintains the benefits of the conventional SM system while eliminating the necessity of CSI needed in SM. The SNR gain achieved in DSM is approximately 3 dB over SM in terms of error performance.

Despite the benefits of SM and DSM, the system is still not practically realizable due to the system complexity, considering the logarithmic relationship of the spectral efficiency and the transmit antennas [9]. This motivates the investigation of space shift keying (SSK).

1.3.3 Space Shift Keying

A particular case of SM termed SSK was investigated in [14]. This employs only the spatial domain to relay information, such that the APM symbol present in SM is wholly eliminated. This results in reduced system complexity. However, SSK still imposes high hardware complexity to achieve high spectral efficiency. This led to bi-space shift keying (Bi-SSK) [15].

1.3.4 Bi-Space Shift Keying

In [15], an SSK-based scheme was proposed termed Bi-SSK. This scheme maintains the benefits of SSK, such as low-complexity detection, whilst doubling the spectral efficiency of SSK. Bi-SSK simultaneously transmits information via two transmit antennas at every transmission interval, enabling the scheme to achieve high throughput. This improves the limitation of SSK in terms of hardware complexity. However, Bi-SSK only rectified the setback of SSK but did little in terms of the error performance enhancement. A similar technique termed generalized spatial modulation (GSM) [16] is discussed in the next sub-section.

1.3.5 Generalized Spatial Modulation

GSM [16] employs transmit antenna combinations to activate more than two transmit antennas at every transmission instant. The activated transmit antennas are employed to transmit the modulated APM symbols. This improves the setback/limitation of hardware complexity experienced in index modulation schemes mentioned earlier. Furthermore, the spectral efficiency associated with GSM is $\log_2(M) + \left\lfloor \log_2 \binom{N_T}{N_a} \right\rfloor$ b/s/Hz, where N_a, N_T, M are the required number of transmit antennas at each transmission instant, the total number of transmit antennas and the modulation order, respectively. Despite the improvement of hardware complexity achieved in GSM, the reliability of the scheme is not well improved as SM exhibits a superior error performance.

Furthermore, in [17], a multi-active transmit antenna GSM (MA-GSM) was proposed. The data rate associated with MA-GSM is $N_a\log_2(M) + \left\lfloor \log_2 \binom{N_T}{N_a} \right\rfloor$ b/s/Hz. MA-GSM achieves better performance in terms of hardware complexity, error performance and throughput. As a 10 b/s/Hz QPSK system, requires only 4 transmit antennas in the proposed scheme, which requires 8 transmits antennas in the conventional GSM system and 64 transmit antennas in SM. Thus, improving the system complexity with respect to the high data rate.

The input bits $\log_2(M) + \left\lfloor \log_2 \binom{N_T}{N_a} \right\rfloor$ for GSM and $N_a\log_2(M) + \left\lfloor \log_2 \binom{N_T}{N_a} \right\rfloor$ for MA-GSM are grouped/sections into two segments, such that the first segment maps/modulate the APM symbol and the second segment maps the antenna index based on $\left\lfloor \log_2 \binom{N_T}{N_a} \right\rfloor$.

1.3.6 Quadrature spatial modulation

Another example to consider is quadrature spatial modulation (QSM) [18], this is an SM-based scheme, which extends its spatial constellation to quadrature dimension in an innovative manner. In QSM, the APM constellation symbol is split into real and imaginary components. The first dimension relays the real component to the receiver while the quadrature dimension sends out the imaginary component.

Both ICI and IAS are avoided in QSM by modulating the decomposed symbol into the cosine and sine carriers, respectively [18], hence, enabling the use of a single RF chain possible similar to SM. This improves the setback of SM by employing additional $\log_2 N_T$. The error performance of QSM is superior to SM and MA-GSM [18-20].

1.3.6.1 System model for QSM

In Figure 1.3, an example of a QSM system equipped with multiple transceivers is presented.

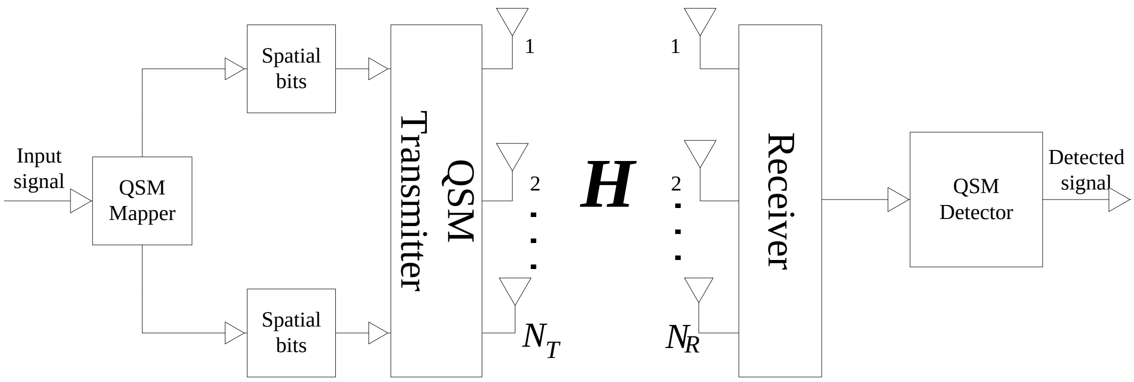

Figure 1.3 An example of a QSM system.

QSM achieved a data rate m of $\log_2 MN_T^2$ b/s/Hz. In QSM, the APM symbol x_q is sectioned into real and imaginary components and mapped into the $\log_2 M$ bits. The required transmit antenna to transmit the real part of the modulated symbol is activated by $\log_2 N_T$, while an additional $\log_2 N_T$ bits activate the second transmit antenna, which is employed to transmit the imaginary component. Table 1.2 tabulates an example of the mapping process for QSM.

Table 1.2 Mapping process for the QSM system.

Configuration	Input Bits $\log_2 MN_T^2$	First $\log_2 M$ bits	Second $\log_2 N_T$ bits	Third $\log_2 N_T$ bits
$M = 4$ $N_T = 2$ $N_R = 4$	0 0 0 1	$\log_2 4$ $= 2$ bits [0 0] $x_q = -1 + i$ $x_{Re}^q = -1$ $x_{Im}^q = +1$	$\log_2 2$ $= 1$ bit [0] $\ell_R = 1$	$\log_2 2$ $= 1$ bit [1] $\ell_I = 2$
$M = 16$ $N_T = 4$ $N_R = 4$	1 0 0 1 1 1 0 1	$\log_2 16$ $= 4$ bits [1 0 0 1] $x_q = +3 + i$ $x_{Re}^q = +3$ $x_{Im}^q = +1$	$\log_2 4$ $= 2$ bits [1 1] $\ell_R = 4$	$\log_2 4$ $= 2$ bits [0 1] $\ell_I = 2$

Considering a QSM scheme with 2 antennas at the transmitter and 4-QAM modulation order yields 4 bpcu or b/s/Hz. In SM, the same configuration settings yield 3 bpcu or b/s/Hz. The first two bits modulate the 4-QAM symbol x_q, while the third bit activates the antenna index ℓ_R and the fourth bit activates the antenna index ℓ_I, which are used to transmit the real and imaginary components, respectively.

The decomposed symbol x_q is transmitted via a channel $\boldsymbol{H}$ with the existence of AWGN $\boldsymbol{n}$ with $CN(0,1)$ distribution. Thus, the received vector $\boldsymbol{y}$ becomes:

$$\boldsymbol{y} = \boldsymbol{h}_{\ell_R} x_{Re}^q + i\boldsymbol{h}_{\ell_I} x_{Im}^q + \boldsymbol{n} \tag{1-4}$$

where ρ is the average SNR, $x_q = x_{Re}^q + i x_{Im}^q$, ℓ_R and ℓ_I is the corresponding transmit antenna employed to transmit the decomposed symbol.

Reducing the hardware complexity imposed in QSM led to the investigation of generalized quadrature spatial modulation (GQSM). This scheme achieves a high data rate at a reduced system complexity, similar to MA-GSM. This is elaborated in the next sub-section.

1.3.7 Generalized Quadrature Spatial Modulation

GQSM [21] divide the transmit antennas into groups and employs a unique symbol across the multi-active transmit antenna groups. The spectral efficiency associated with the GQSM system [21] is $n_b\left(\log_2 M + N_{T_\ell}\right)$ b/s/Hz, where n_b, N_{T_ℓ} and M represents the antenna groups, the available antennas in each group and the modulation order, respectively. Hence, a configuration setting with 4 transmit antennas, i.e. $n_b = \frac{N_T}{2}$ and 4-QAM in GQSM coupled with $N_{T_\ell} = 2$, yields a data rate of 8 b/s/Hz. The same configuration settings in the conventional QSM system and MA-GSM scheme will yield only 6 b/s/Hz. The system model of GQSM is presented in the next sub-section.

1.3.7.1 System model of Generalized Quadrature Spatial Modulation

Figure 1.4 presents an example of a GQSM system with N_T transmits antennas, n_b groups, i.e. $n_b = \frac{N_T}{2}$ and N_R receive antennas.

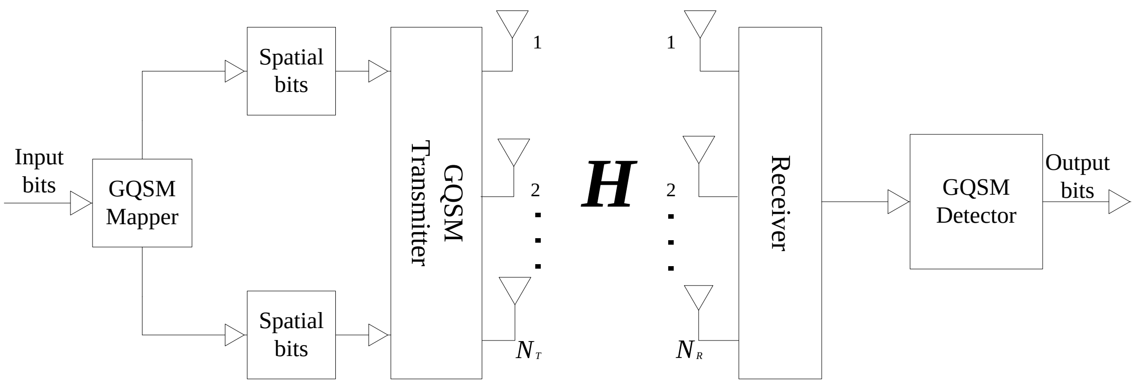

Figure 1.4 System model for the GQSM system.

The main benefit of GQSM is the high data rate achieved at a reduced hardware complexity. GQSM is a suitable scheme for multimedia services and massive MIMO with respect to transmission capacity. Taking another example of GQSM with the configuration settings of 6×4, 16-QAM, this achieves a data rate of 18 b/s/Hz. To achieve this spectral efficiency in QSM, 32 transmit antennas with 256-QAM is required. However, GQSM requires multiple RF chains. The $n_b \log_2 M$ bits modulates the vector $\boldsymbol{x}_q^j$, while $N_{T_\ell} n_b$ bits select the transmit antennas required for transmission. Thereafter, a complex channel matrix $\boldsymbol{H}_j$ of dimension $N_R \times N_{T_\ell}$ is employed to relay the modulated vector $\boldsymbol{x}_q^j$ with the existence of AWGN $\boldsymbol{n}$, of dimension $N_R \times 1$. The vector $\boldsymbol{y}$ received at the receiver is expressed as:

$$\boldsymbol{y} = \sqrt{\rho / n_b} \sum_{j=1}^{n_b} \boldsymbol{H}_j \, \boldsymbol{x}_q^j + \boldsymbol{n} \tag{1-5}$$

where $\boldsymbol{x}_q^j$ is the transmission block of the decomposed symbol of all groups and ρ is the average SNR. The mapping process for GQSM is revealed in Table 1.3.

Several limitations are associated with GQSM [21], including high hardware complexity and high computational complexity (CC) due to the simultaneous transmission of unique symbols, which limits its practical implementation.

Table 1.3 Mapping process for GQSM

Configuration	Input Bits	First n_b bits	Second n_b bits	Third $\log_2 M$ bits	Fourth $\log_2 M$ bits	Group 1	Group 2
$M = 16$ $N_T = 4$ $n_b = 2$	110101 101101	[11] $N_{T_1} = 1$ $N_{T_2} = 1$	[01] $N_{T_1} = 1$ $N_{T_2} = 2$	[1101] $1 + 1i$	[0110] $-1 - 3i$	$[1 + 1i, 0]$	$[-1, -3i]$

Furthermore, the desirability of high throughput in wireless communication to accomplish the demand of high transmission capacity and superior system performance in multimedia services [21-22] motivates the investigation of a channel-based modulation technique termed media-based modulation (MBM). This achieves a high data rate at a reduced system complexity suitable for multimedia services compared to other index modulation techniques. This is discussed in the next sub-section.

1.3.8 Media-based modulation

Recently, MBM [23-25] was introduced as a technique to enhance the data rate of the MIMO schemes by maximizing the linear relationship between the RF mirrors (m_{rf}) and the spectral efficiency. MBM achieves high throughput at a reduced hardware complexity. This is accomplished by utilizing RF mirrors to make distinctive channel fade realizations, known as mirror activation patterns (MAPs). An example to consider is [23, 25], where an equivalent SM system would require $2^{m_{rf}}$ antennas at the transmitter to meet the spectral efficiency as a single-input multiple-output (SIMO) aided MBM (SIMO-MBM) system. Thus, SIMO-MBM is more desirable than SM, in terms of data rate.

Some other advantages of MBM are as follows [24]:

a) In MBM, the constellation size is independent of the transmit energy; therefore, an improvement in spectral efficiency can be easily achieved. In addition, the increment in the constellation size efficiently enables constellation diversity to transforms a static multi-path fading channel into an AWGN with an efficient signal energy equivalent to the average energy received.

b) There is no basic constraint on the separation of mirrors in MBM. Hence, RF mirrors can be positioned side by side. Similarly, a subset of a distinguished/distinct channel can be chosen from the N_m channel permutation resulting in superior system performance.

c) The RF mirrors around each transmit unit in MBM are treated independently enabling a superior error performance to be achieved [26], i.e. the spatial portion of the scheme is employed to linearly increases the throughput. Based on the above advantages, numerous research works have been presented.

In [23, 24], MBM was investigated in GSM (GSM-MBM) and QSM (QSM-MBM), respectively. Employing RF mirrors coupled with unique MAP indices to activate or de-activate the RF mirrors at every transmission instant.

1.3.8.1 Generalized Spatial Modulation-Media-based Modulation

The GSM-MBM scheme [23], follows the MA-GSM scheme [17], which employs multiple APM symbols coupled with the transmit antenna combination to activate N_a transmit antennas at every transmission instant. GSM-MBM achieves high spectral efficiency, considering the simultaneous transmission of the APM symbols, coupled with the additional information conveyed via the MAP indices. The next sub-section illustrates a typical transmission model for the SM-MBM system.

1.3.8.1.1 System model for Generalized Spatial Modulation-Media-based Modulation

A typical example of GSM-MBM is presented in Figure 1.5. The transmit antennas are considered independently as a transmit unit with the dimension $N_R \times N_m$, each surrounded with m_{rf} RF mirrors, where N_m represents $2^{m_{rf}}$.

The spectral efficiency associated with GSM-MBM is $N_a \log_2(M) + \left\lfloor \log_2 \binom{N_T}{N_a} \right\rfloor + N_a m_{rf}$ b/s/Hz, where M, N_T, N_a and m_{rf} represents the modulation order, the transmit antennas consider as transmit units in GSM-MBM, the active transmit units and RF mirrors, respectively. Given the set of the transmit antenna combination $N_c = \binom{N_T}{N_a}$ and the usable transmit antenna combinations N_s, where $N_s = 2^{\log_2(N_c)}$.

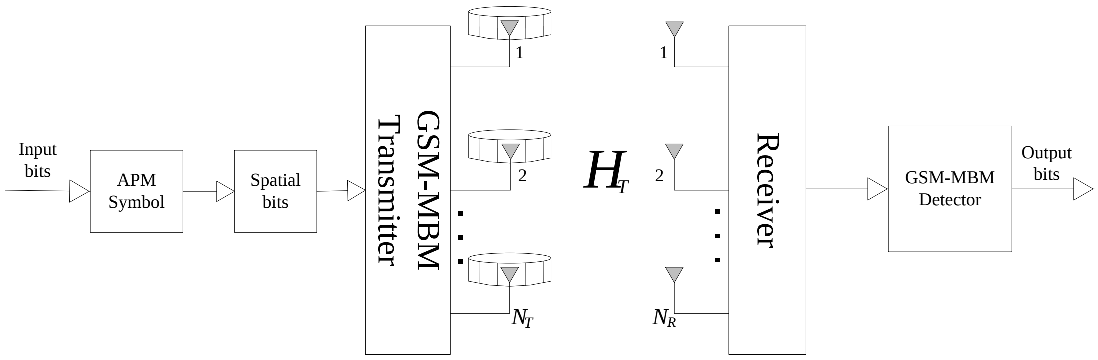

Figure 1.5 A typical example of GSM-MBM.

Considering an example of GSM-MBM with 4-QAM modulation order, 4 transmit units and 2 RF mirrors, i.e. 4×4 4-QAM with $m_{rf} = 2$ and $N_a = 2$. This configuration achieves a data rate of 10 b/s/Hz. In GSM, this configuration achieves only 4 b/s/Hz. Assuming [1 0 1 1 0 0 0 1 1 0] bits are generated based on $N_a \log_2(M) + \left\lfloor \log_2 \binom{N_T}{N_a} \right\rfloor + N_a m_{rf}$ b/s/Hz. [1 0 1 1] modulates the APM symbols based on $N_a \log_2(M)$. In this case, $1 + 1i$ and $1 - 1i$ APM symbols are selected. Similarly, the [0 0] bit activates the transmit unit combination needed for transmission. In this case, the first antenna combination is selected based on the input bits [0 0]. The third segment [0 1] bit activates the first required RF mirror and the fourth segment [1 0] bit activates the second required RF mirror.

The channel $\boldsymbol{H}_{k_j}$ of dimension $N_R \times N_m$ across N_T is used for transmission. Therefore, the received vector $\boldsymbol{y}$ is expressed as:

$$\boldsymbol{y} = \sqrt{\rho / N_a} \sum_{j=1}^{N_a} \boldsymbol{H}_{k_j} \boldsymbol{e}_{\ell_{k_j}} x_q + n \tag{1-6}$$

where ρ is the SNR, x_q is the symbol $q \in [1{:}M]$, $\boldsymbol{e}_{\ell_{k_j}}$ represents the MAP index of $N_m \times 1$ dimension with the ℓ^{th} column set to unity, $j \in [1{:}N_a]$, $\ell \in [1{:}N_m]$.

1.3.8.2 Quadrature Spatial Modulation-Media-based Modulation

In [24], MBM was investigated in QSM, employing RF mirrors to achieve a high data rate coupled with improved system performance. In QSM-MBM, the decomposed symbol is modulated into the sine and cosine carriers, respectively, maintaining the benefits of conventional QSM, including the use of one RF chain. A substantial improvement is achieved in QSM-MBM compared to the conventional QSM scheme.

1.3.8.3 Uncoded space-time label diversity media-based modulation

Likewise, in [27], MBM is investigated in uncoded space-time label diversity (USTLD-MBM), employing a pre-coding technique coupled with label diversity to achieve coding gain and transmit diversity. Significant improvement is achieved over the conventional USTLD and space-time channel modulation of [28] in terms of system reliability and complexity. Hence, MBM-based schemes exhibited improved system performance and reduced hardware complexity.

1.4 Pre-coding

In this technique, the user information is pre-coded before transmission, enhancing the performance of the system. This technique has the benefit of summing up the transmitted signals from different antennas. Thus, improving the signal gain at the receiver and reducing fading effects [28]. Examples of MIMO systems, which employ a precoding technique, are discussed in the next sub-section.

1.4.1 The Alamouti space-time block code

The Alamouti space-time block code (STBC) [29] employs a spatial diversity to improve the system performance by sending two symbols x_1 and x_2 in code word and in two time slots. The transmitted code word is $\boldsymbol{X} = \begin{bmatrix} x_1 & x_2 \\ -x_2^* & x_1^* \end{bmatrix}$.

In the Alamouti STBC, the CC increases exponentially with the size of the constellation, making the practical implementation not only tricky but expensive [29].

1.4.2 Space Time Block Code-Spatial Modulation

In [30], STBC was investigated in SM. The proposed scheme combines the pre-coding technique of STBC with SM, maximizing the benefits of the pre-coding technique of STBC to achieve coding gain. The code word of STBC is extended in STBC-SM such that $\boldsymbol{X}$ becomes:

$$\begin{aligned} x_1 &= [x_{11}\ x_{12}] = \left\{ \begin{bmatrix} x_1 & x_2 & 0 & 0 \\ -x_2^* & x_1^* & 0 & 0 \end{bmatrix} \begin{bmatrix} 0 & 0 & x_1 & x_2 \\ 0 & 0 & -x_2^* & x_1^* \end{bmatrix} \right\} \\ x_2 &= [x_{21}\ x_{22}] = \left\{ \begin{bmatrix} 0 & x_1 & x_2 & 0 \\ 0 & -x_2^* & x_1^* & 0 \end{bmatrix} \begin{bmatrix} x_2 & 0 & 0 & x_1 \\ x_1^* & 0 & 0 & -x_2^* \end{bmatrix} \right\} \end{aligned} \tag{1-7}$$

In the above example, 4 transmit antennas are considered and the transmitted information is expanded to the spatial domain, corresponding to the active or inactive status of the transmit antennas, including the time and space domains.

1.4.3 Space Time-Quadrature Spatial Modulation

Similarly, in [31], ST-QSM scheme was investigated. This technique enhanced the system performance of the conventional QSM, outperforming STBC and STBC-SM mentioned earlier. ST-QSM section the antennas at the transmitter into groups and maps user information to the indices of the antennas enabled for transmission.

Furthermore, a unique APM symbol is employed in ST-QSM, which is further decomposed into real and imaginary components prior to transmission. Thereafter, the Alamouti's STBC principle is employed in each transmission interval. Hence, the code word $\boldsymbol{X}$ for ST-QSM is defined as:

$$\boldsymbol{X} = \begin{bmatrix} x_{11} & x_{12} & x_{13} & x_{14} \\ -x_{12}^{*} & x_{11}^{*} & -x_{14}^{*} & x_{13} \end{bmatrix} \tag{1-8}$$

In the above example, 4 transmit antennas are considered.

1.5 Cooperative networks

Cooperative communication systems have shown tremendous promise with regards to link reliability and extension in-network coverage. This is achieved by employing multiple nodes available in the network as a virtual node (antenna) to transmit users' information [32]. Thereby extending the coverage of the wireless network via cooperative relaying [33]. The relaying techniques employed in the cooperative network includes:

1.5.1 Decode-and-forward (DF)

In DF, the received signal at the relay node is decoded and filtered prior to the re-transmission of the information to the destination, such that the reliability of the system is enhanced.

1.5.2 Amplify-and-forward (AF)

Firstly, data/message is transmitted to the relay. After that, the received message at the relay is amplified and then forwarded to the destination. AF needs two orthogonal time slots to complete a transmission between the source and the destination [33]. This is further discussed in Chapter 5 of this dissertation.

1.5.3 One-way relaying

In one-way relaying [33], the source node transmits the user information to a relay node, which is decoded/amplified; thereafter, the decoded/amplified message is re-transmitted to the destination. In one-way relaying, higher modulation order/a huge number of antennas is required at the transmitter to achieve high throughput and this results in high hardware complexity.

1.5.4 Two-way relaying

In the literature [33-35], two-way relaying has been proven as a spectral efficient relaying system. This technique employs two or more nodes, which simultaneously transmit data. The transmitted data is decoded at the relay node or amplified, thereafter a network coding principle is applied to the decoded/amplified message, such that the message from source nodes is extracted as a single message block and re-transmitted to the source nodes.

There are two major types of cooperative network, which are categorized based on the relaying technique employed, this includes:

1.5.5 Half-duplex cooperative networks

The major limitation/setback of cooperative networks is the inability to relay data at the same time employing the same frequency. This causes the non-maximization of the system resources, such as the allocation of dedicated bandwidth at the relay for transmissions.

In [36], several techniques to mitigate these setbacks were proposed, which includes enabling the source node to be operative with the relay node during transmissions, employing non-orthogonal protocols. Another approach is overlapping several relay nodes for transmission, enabling the system to behave like an ideal full-duplex operation. A similar technique termed two-way relaying was proposed, which employs two or more nodes to transfer information via a relay node. Lastly, the concept of cognitive radio was investigated, this enables the relay node to transmit information when the primary nodes are idle.

Similarly, in [37], an efficient half-duplex cooperative network, which employs the Alamouti STBC in an innovative manner for a three-node relaying was proposed. However, the proposed system is limited to $\frac{1}{2}$ symbols per channel use, considering Alamouti STBC requires four symbol periods.

1.5.6 Full-duplex cooperative networks

In [38], a full-duplex cooperative network was proposed, this improves the setback of half-duplex constraint experienced in cooperative networks by transmitting/receiving data simultaneously. However, a full-duplex cooperative network experiences a loopback interference at the relay node output. In [39], the full-duplex technique is exploited at the relay to form the Alamouti codewords for three unique nodes. This mitigates the loopback interference experienced in [38]. The proposed full-duplex Alamouti scheme exhibits significant improvement compared to the conventional half-duplex cooperative networks.

Achieving schemes with full-rate, full-diversity with spatial multiplexing such as V-BLAST [9], which can give high multiplexing gain for multiple transmit antennas with linear CC is impossible [17]. This is due to the coupling of symbols in time and space, resulting in high ICI and simultaneous transmission of data requires IAS at the transmitter [40].

In the literature [41, 42], it has been stated that link adaptation can augment the performance of SIMO/MIMO systems. The application of transmit/receive diversity or a combination of both allows tremendous enhancement in terms of link reliability. This is further discussed in the next sub-section.

1.6 Link adaptation

Link adaption is the process of optimizing the wireless communication link according to the condition of the link at a particular instant, so as to enhance the system efficiency [43]. Figure 1.6 presents an example of an adaptive system with a perfect feedback link, which connects the adaptive unit to the transmitter.

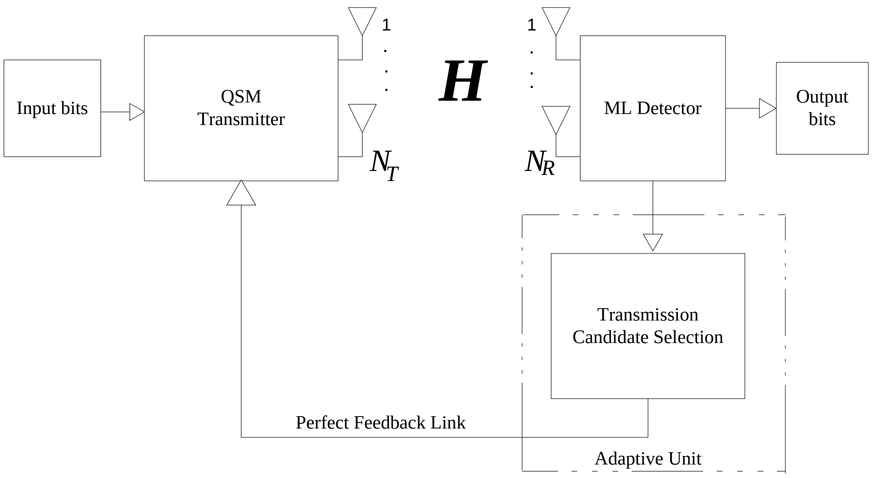

Figure 1.6 System model of a typical adaptive system.

In [42, 44, 45], link adaptation was employed in several ways, viz. adaptive selection of candidates modes, transmit antenna selection or the combination to enhance the reliability of the system.

In [42], link adaptation was investigated in SM termed adaptive SM (ASM). The estimated channel state information (CSI) is employed as the decision metric to select the optimum candidate for transmission. Another link adaptation technique was investigated in SM in [46], employing a power allocation algorithm to improve the effect of power imbalance stated in [47].

Similarly, in [44], two unique transmit pre-coding algorithms were proposed. The first one employs an algorithm, which determines the minimum Euclidean distance among the constellation points. The second algorithm in [44] was based on minimizing the bit error rate (BER) of the SM system. The second algorithm proposed in [44] (employing the minimum BER) achieved significant improvement compared to the first algorithm.

Likewise, transmit antenna selection, a transmit diversity technique has been richly explored in the SM system to achieve a considerable SNR gain compared to the conventional SM.

1.6.1 Transmit antenna selection

In [48, 49], Euclidean distance-based antenna selection (EDAS) was investigated in SM, taking advantage of the ICI and IAS free property of SM to separate the QAM signal sets, achieving an improved scheme. A reduced CC version of this approach was investigated in [50], employing the approach of only one search across the symmetrical constellation sets, making SM practically implementable.

In [34, 35], the availability of additional antennas as a cheap way of accomplishing a diversity gain was investigated. In addition, a transmit antenna selection algorithm was employed to activates the required transmit antennas at each transmission instant. A similar approach was employed in [38], where the system performance of SSK was enhanced via the increment of the available of transmit antennas and using an antenna selection algorithm to activate the required number of antennas.

Similarly, in [51] EDAS algorithm was investigated in QSM termed EDAS-QSM. The EDAS-QSM scheme achieves a tremendous diversity gain compared to conventional QSM. However, this imposes a high CC due to the exhaustive search. To further reduce the CC imposed on the scheme, an algorithm in the form of reduced-complexity EDAS for QSM was proposed, this achieved a reduced CC, whilst preserving the error performance.

In [52], a reduced CC sub-optimal based transmit antenna selection algorithm was proposed by Pillay *et al.*, where the amplitude and correlation of the antenna were employed to select the best channel prior to transmission. This technique exhibits a very low CC when compared to EDAS-SM (an optimal technique). Hence, making SM more realizable.

1.7 Research motivation and problem statement

SM [10] employs transmit antennas innovatively to mitigate the major setbacks of IAS and ICI experienced in MIMO schemes. The requirement of a single RF chain in SM enables the scheme to maximize the space modulation technique.

The desirability of high throughput and superior system performance for multimedia services requires schemes that can achieve high spectral efficiency. However, this imposes high system/hardware complexity due to the huge number of antennas required at the transmitter [16]. This prompted the investigation of GSM [16].

GSM [16] employs the transmit antenna combinations coupled with identical symbols to convey additional information. This made the use of multiple transmit antennas possible in index modulation, improving the setback/limitation of hardware complexity experienced in index modulation schemes. In [17], a similar scheme was proposed termed MA-GSM, which employs unique symbols across the transmit antenna combination. The proposed MA-GSM outperforms the GSM system of [16]. However, MA-GSM requires multiple RF chains.

Recently, the application of RF mirrors was introduced to the research community as a technique to enhance the spectral efficiency at a reduced hardware complexity [23, 24, 26, 27]. In MBM, the modulation alphabet can be created by a single transmit antenna [53]. This motivates us to investigate MBM with GSM of [16] to mitigate the drawback of MA-GSM mentioned earlier.

Furthermore, in [23], GSM-MBM was proposed. This scheme achieves a high data rate coupled with improved link reliability at the cost of a high system complexity, including the requirement of multiple RF chains similar to MA-GSM.

In addition, link adaptation has been stated in literature as a technique, which can enhance the performance of a SIMO/MIMO scheme. This is evident in [41, 42, 54], where link adaptation is employed in SIMO/MIMO system to enhance the reliability of the system.

In [23, 25], MBM is investigated in a SIMO system termed SIMO-MBM. The proposed scheme achieves a high data rate coupled with enhanced system performance. However, to the author's best knowledge, link adaptation has not been investigated with MBM. This motivates us to propose an adaptive algorithm that employs different candidate transmission modes to enhance the reliability of the system. The proposed scheme is called adaptive SIMOMBM (ASIMOMBM).

Furthermore, the data rate enhancement of SM only increases in $\log_2 N_T$ compared to other index modulation schemes, this brought about an enhanced spectral efficient SM called QSM.

In [21], an improved spectral efficient QSM scheme termed GQSM is proposed. In GQSM, the antennas at the transmitter are divided into groups and a unique symbol is employed across multi-active transmit antenna groups. Hence, GQSM requires less transmit antennas to achieve a high data rate when compared to SM, GSM, and QSM [21]. However, GQSM requires multiple RF chains considering unique symbols are employed in each transmit antenna group. This motivates us to investigate single-symbol GQSM (SS-GQSM), which employs identical symbols across each group requiring a single RF chain.

Lately, cooperative networks have been employed to enhance link reliability via the use of multiple nodes in the communication network to transmit users' information [32]. In the literature [33-35], two-way cooperative relaying has been proven as a spectral efficient relaying system. This technique employs two or more source nodes, which transmit information to the relay node simultaneously. An example to consider is [33], where two-way DF relaying was investigated in QSM. This scheme outperforms QSM and one-way DF-QSM relaying.

Considering the advantages of GQSM stated earlier over QSM, such as achieving a high data rate at a reduced hardware complexity. Considering an example of a 6×4 4-QAM two-way DF-GQSM relaying scheme, this yields a data rate of 12 bpcu or b/s/Hz. The two-way DF-QSM system will require 8 transmit antennas coupled with a 64-QAM modulation order to match this spectral efficiency. This motivates us to investigate two-way DF relaying in the GQSM scheme to enhance the reliability of the two-way DF-QSM relaying technique.

1.8 Research objectives

The following are the objectives of this research:

1. Investigation of link adaptation in SIMO-MBM schemes.
2. Formulation of instantaneous bit error probability (IBEP) for ASIMOMBM using a lower bound approach and union bound.
3. Application of MBM based on RF mirrors in single-symbol GSM-MBM.
4. Formulation of the performance analysis for single-symbol GSM-MBM.
5. Investigation of single-symbol GQSM scheme and formulation of the performance analysis, employing a lower bound approach.
6. Application of two-way DF relaying cooperative network in GQSM.

1.9 Organization of the thesis

The paper format is used in this thesis, in which each paper form the Chapters of this thesis. The rest of the thesis is structured as follows:

Chapter 2 presents a detailed system model of an adaptive media-based SIMO system, together with the numerical results. The formulation of the IBEP for ASIMOMBM is presented in this chapter.

Chapter 3 provides a detailed transmission/system model for a single-symbol GSM-MBM coupled with the formulation of the performance analysis.

Chapter 4 presents the single-symbol GQSM system with the claimed advantages of the system in terms of CC, thereafter, comparisons with the conventional GQSM system are drawn.

Chapter 5 presents the two-way DF-GQSM system, coupled with the performance analysis and its benefits over one-way DF-GQSM.

Chapter 6 concludes the thesis.

1.10 Major contributions of the research

The study in this thesis is either published as a journal paper or in conference proceedings, or submitted for review. The details are as follows:

a) Paper A

S. Oladoyinbo, N. Pillay, and H. Xu, “Adaptive single-input multiple-output media-based modulation,” [*Under review with Digital communications and networks*].

Contributions of the paper:

1. Investigation of link adaptation in SIMO-MBM based schemes, employing a decision metric of the minimum IBEP.
2. Formulation of the IBEP for all candidate mode employed, which includes: SIMO, media-based SSK and SIMO-MBM.

b) Paper B

S. Oladoyinbo, N. Pillay, and H. Xu, “Media-based single-symbol generalized spatial modulation,” International Journal of Communication Systems, vol. 32, no. 6, pp. 1-13, 2019. DOI: 10.1002/dac.3909

Contributions of the paper:

1. Investigation of MBM with a single-symbol GSM system.
2. Formulation of the performance analysis for single-symbol GSM.
3. Introduction of the MAP selection algorithm in the proposed scheme, employing an exhaustive search among the transmission vectors to selects the optimal MAP.
4. Investigation of the effect of channel amplitude and antenna correlation has a MAP selection technique in the proposed scheme.

c) Paper C

S. Oladoyinbo, N. Pillay, and H. Xu, “Single-symbol generalized quadrature spatial modulation,” in *Proceedings of the South African Telecommunication Networks and Applications Conference (SATNAC),* pp. 370-375, Sep. 2018.

Contributions of the paper:

1. Investigation of an identical symbol set across a unique transmit antenna group in the proposed SS-GQSM system.

2. Formulation of the theoretical analysis for the proposed SS-GQSM.

3. Investigation of Euclidean distance antenna selection algorithm in the proposed SS-GQSM and multi-symbol GQSM schemes.

4. Investigation of the effect of channel amplitude and antenna correlation has the selection criteria for the transmit antenna selection algorithm.

d) Paper D

S. Oladoyinbo, N. Pillay, and H. Xu, "Generalised quadrature spatial modulation in two-way decode and forward relaying cooperative networks," [*Ready for submission to IEEE INFOCOM 2021: IEEE International Conference on Computer Communications 2021].*

Contributions of the paper:

1. Investigation of two-way DF relaying with GQSM scheme, employing two source nodes, which simultaneously transmit user information to the relay.

2. Investigation of a benchmark scheme (one-way DF relaying) with GQSM, which transmits user information to the relay node as against simultaneous transmission of information from both nodes in two-way DF relaying.

1.11 Notation used in the thesis

Bold italics variables represent vectors/matrices, while regular variables represent scalar quantities. $[\cdot]^T$, $(\cdot)^H$, $|\cdot|$, $||\cdot||_F$ and $(\cdot)^*$ represents transpose, Hermitian, Euclidean norm, Frobenius norm and the complex conjugate of a number, respectively. $Q(\cdot)$ denotes the Gaussian Q-function, $Re\{\cdot\}$ is the real component of a complex value, while $Im\{\cdot\}$ is the imaginary component of a complex value. $\underset{w}{\arg\min}(\cdot)$ is the least value of an argument with corresponding to w, while $\underset{w}{\arg\max}(\cdot)$ is the maximum value of an argument with corresponding to w, $\binom{\cdot}{\cdot}$ is the binomial coefficient and $\lfloor\cdot\rfloor$ is the nearest integer less than the input argument.

References

[1] A. Goldsmith, Wireless Communications, 1st ed., New York: Cambridge University Press, 2005.

[2] S. E. Krouk, Modulation and Coding Techniques in Wireless Communications: John Wiley & Sons Ltd, 2011.

[3] A. Goldsmith, N. Jindal, and S. Vishwanath, "Capacity limits of MIMO channels," *IEEE Journal on Selected Areas in Communications,* vol. 21, no. 5, pp. 684-702, Jun 2003.

[4] R. Y. Mesleh, H. Hass, L. Yeonwoo, and Y. Sangboh, "Interchannel Interference Avoidance in MIMO Transmission by Exploiting Spatial Information," in *Proceedings of the IEEE 16th International Symposium on Personal, Indoor and Mobile Radio Communications, (PIMRC 2005),* pp. 141-145, Sep. 2005.

[5] N. R. Naidoo, H. Xu, and T. Quazi, "Spatial modulation: optimal detector asymptotic performance and multiple-stage detection," *IET Communications,* vol. 5, no. 10, pp. 1368 - 1376, Jul. 2010.

[6] X. Wang, J. Geng, X. Zhang, and D. Yang, "Spatial Multiplexing with Opportunistic Multiuser Scheduling in Ad Hoc Networks," in *Proceedings of the IEEE Vehicular Technology Conference (VTC Fall),* pp. 1-5, Sep. 2012.

[7] Cisco, "Multipath and Diversity," *Technical Report on Wireless Communications*, available at http://www.cisco.com/c/ en/us/support /docs/wireless-mobility/wireless-lan-wlan/27147-multipath.html, Jul. 2019.

[8] T. Ngoc-Anh, V. V. Mai, T. C. Thang, and A. T. Pham, "Impact of reflections and ISI on the throughput of TCP over VLC networks with ARQ-SR protocol," in *Proceedings of the IEEE 4th International Conference on Photonics (ICP)*, pp. 172-174, Oct. 2013.

[9] P. Wolniansky, G. J. Foschini, D. Golden, and R. Valenzuela, "V-BLAST: an architecture for realizing very high data rates over the rich-scattering wireless channel," in *Proceedings of the International Symposium on Signals, System and Electronic. (ISSSE 98)*, pp. 295-300, Sep. 1998.

[10] R. Y. Mesleh, H. Haas, S. Sinanovic, A. Chang Wook, and Y. Sangboh, "Spatial Modulation," *IEEE Transactions on Vehicular Technology,* vol. 57, no. 4, pp. 2228-2241, Jul. 2008.

[11] J. Jeganathan, A. Ghrayeb, and L. Szczecinski, "Spatial modulation: optimal detection and performance analysis," *IEEE Wireless Communications Letters*, vol. 12, no. 8, pp. 545-547, Aug. 2008.

[12] Z. Jianping, "Signal Vector-Based List Detection for Spatial Modulation," *IEEE Wireless Communications Letters,* vol. 1, no. 4, pp. 265-267, May. 2012.

[13] Y. Bian, X. Cheng, M. Wen, L. Yang, H. V. Poor, and B. Jiao, "Differential Spatial Modulation," *IEEE Transactions on Vehicular Technology*, vol. 64, no. 7, pp. 3262-3268, Jul. 2015.

[14] J. Jeganathan, L. Szczecinski, and A. Ceron, "Space Shift Keying Modulation for MIMO Channels," *IEEE Wireless Communications Letters,* vol. 8, no. 7, pp. 3692-3703, Jul. 2009.

[15] H. Liang, R. Y. Chang, W. Chung, H. Zhang, and S. Kuo, "Bi-Space Shift Keying Modulation for MIMO Systems," *IEEE Communications Letters,* vol. 16, no. 8, pp. 1161-1164, Aug. 2012.

[16] A. Younis, N. Serafimovski, R. Mesleh, and H. Haas, "Generalised spatial modulation," in *Proceedings of the 2010 Conference Record of the Forty-Fourth Asilomar Conference on Signals, Systems and Computers*, pp. 1498-1502, 2010.

[17] F. Jinlin, H. Chunping, X. Wei, Y. Lei, and H. Yonghong, "Generalised spatial modulation with multiple active transmit antennas," in *Proceedings of the IEEE GLOBECOM Workshops (GC Wkshps),* pp. 839-844, Dec. 2010.

[18] R. Mesleh, S. S. Ikki, and H. M. Aggoune, "Quadrature Spatial Modulation," *IEEE Transactions on Vehicular Technology,* vol. 64, no. 6, pp. 2738-2742, Jul. 2014.

[19] R. Mesleh, S. S. Ikki, "A High Spectral Efficiency Spatial Modulation Technique," in *Proceedings of the 80th IEEE Vehicular Technology Conference (VTC Fall 2014),* pp. 14-17, Sep. 2014.

[20] S. Naidu, N. Pillay, and H. Xu, "A Study of Quadrature Spatial Modulation," in *Proceedings of the Southern Africa Telecommunication Networks and Applications Conference (SATNAC),* Sep. 2015.

[21] J. R Castillo-Soria, R. Ramirez-Gutierrez, "Generalized Quadrature Spatial Modulation Scheme using Antenna Grouping," *Electronics and Telecommunications Research Institute Journal,* vol. 39, no. 5, pp. 707-717, Oct. 2017.

[22] W. Jintao, J. Shuyun, and S. Jian, "Generalised Spatial Modulation System with Multiple Active Transmit Antennas and Low Complexity Detection Scheme," *IEEE Transactions on Wireless Communications,* vol. 11, no. 4, pp. 1605-1615, Apr. 2012.

[23] Y. Naresh, A. Chockalingam, "On Media-based Modulation using RF Mirrors," *IEEE Transactions on Vehicular Technology,* vol. 66, no. 6, pp. 4967 - 4983, Oct. 2016.

[24] N. Pillay, H. Xu, "Quadrature Spatial Media-based Modulation with RF Mirrors," *IET Communications*, vol. 11, no. 16, pp. 2440-2448, Nov. 2017.

[25] R. Pillay, H. Xu, and N. Pillay, "A Study of Single-Input Multiple-Output Media-based Modulation with RF Mirrors," in *Proceedings of the Southern Africa Telecommunication Networks and Applications Conference (SATNAC),* Spain, 2017.

[26] A. Khandani, "Media-based modulation: Converting static Rayleigh fading to AWGN," in *Proceedings of the IEEE International Symposium on Information Theory*, 2014.

[27] N. Pillay, H. Xu, "Uncoded Space-Time Labeling Diversity-Application of Media-based Modulation with RF Mirrors," *IEEE Communications Letters*, vol. 22, no. 2, Feb. 2017.

[28] E. Basar, I. Altunbas, "Space-Time Channel Modulation," *IEEE Transactions on Vehicular Technology,* vol. 66, no. 8, pp. 7609-7614, Aug. 2017.

[29] L. Tsung-Hsien, "Analysis of the Alamouti STBC MIMO System With Spatial Division Multiplexing Over the Rayleigh Fading Channel," *IEEE Transactions on Wireless Communications*, vol. 14, no. 9, pp. 5156-5170, May 2015.

[30] E. Basar, U. Aygolu, E. Panayirci, and H. V. Poor, "Space-Time Block Coded Spatial Modulation," *IEEE Transactions on Wireless Communications,* vol. 59, no. 3, pp. 823-832, Mar. 2011.

[31] Z. Yigit, E. Basar, "Space-time quadrature spatial modulation," in *Proceedings of the IEEE International Black Sea Conference on Communications and Networking (BlackSeaCom)*, Istanbul, pp. 1-5, 2017.

[32] Y. Li, M. Daneshmand, and W. Duan, "A Cooperative Relay Method and Performance for Wireless Networks," in *Proceedings of the 2nd International Symposium on Intelligence Information Processing and Trusted Computing,* Hubei, 2011.

[33] S. Althunibat, R. Mesleh, "Performance analysis of quadrature spatial modulation in two-way relaying cooperative networks," *IET Communications*, vol. 12, no. 4, pp. 462-72, Mar. 2018.

[34] A. W. Rankov, "Achievable rate regions for the two-way relay channel," in *Proceedings of the IEEE International Symposium on Information Theory*, Jul. 2006.

[35] H. Ju, E. Oh, and D. Hong, "Catching resource-devouring worms in next-generation wireless relay systems: Two-way relay and full-duplex relay," *IEEE Communications Magazine*, vol. 47, no. 9, pp. 58-65, Sep. 2009.

[36] Z. Ding, B. Rong, J. S. Thompson, C. Wang, and S. Yang, "On combating the half-duplex constraint in modern cooperative networks: protocols and techniques," *IEEE Wireless Communications*, vol. 19, no. 6, pp. 20-27, Dec. 2012.

[37] K. Azarian, P. Schniter, "On the Achievable Diversity-Multiplexing Tradeoff in Half-duplex Cooperative Channels," *IEEE Transactions on Information Theory*, vol. 51, no 12, pp. 4152–72, Dec. 2005.

[38] I. Krikidis, A. Himal, and A. Suraweera, "Full-Duplex Cooperative Diversity with Alamouti Space-Time Code," *IEEE Wireless Communications Letters*, vol. 2, no. 5, pp. 519-522, Oct. 2013.

[39] J. I. Choi, K. Srinivasan, P. Levis, and S. Katti, "Achieving single channel, full duplex wireless communication," in *Proceedings of the 2010 International Conference on Computer and Networks*, pp. 1-12, 2010.

[40] N. R. Naidoo, "Performance analysis and enhancement schemes for spatial modulation," MSc Thesis, School of Electrical, Electronics and Computer Engineering, University of KwaZulu-Natal, Dec. 2010.

[41] P. Yang, Y. Xiao, Y. Yu, and S. Li, "Adaptive Spatial Modulation for Wireless MIMO Transmission Systems," *IEEE Communications Letters*, vol. 15, no. 6, pp. 602-604, Jun. 2011.

[42] P. Yang, Y. Xiao, L. Li, Q. Tang, Y. Yu, and S. Li, "Link Adaptation for Spatial Modulation With Limited Feedback," *IEEE Transactions on Vehicular Technology*, vol. 61, no. 8, pp. 3808-3813, Oct. 2012.

[43] T. ABC, "Link Adaptation," available at http://www.telecomabc.com/l/link-adaptation .html, accessed on Jul. 2019.

[44] P. Yang, Y. L. Guan, Y. Xiao, M. Di Renzo, S. Li, and L. Hanzo, "Transmit Pre-coded Spatial Modulation: Maximizing the Minimum Euclidean Distance Versus Minimizing

the Bit Error Ratio," *IEEE Transactions on Wireless Communications*, vol. 15, no. 3, pp. 2054-2068, Nov. 2015.

[45] P. Yang, Y. Xiao, Y. L. Guan, S. Li, and L. Hanzo, "Transmit Antenna Selection for Multiple-Input Multiple-Output Spatial Modulation Systems," *IEEE Transactions on Wireless Communications,* vol. 64, no. 5, pp. 2035-2048, Mar. 2016.

[46] P. Yang, Y. Xiao, S. Li, and L. Hanzo, "A Low-Complexity Power Allocation Algorithm for Multiple-Input Multiple-Output Spatial Modulation Systems," *IEEE Transactions on Vehicular Technology,* vol. 65, no. 3, pp. 1819-1825, Mar. 2015.

[47] M. Di Renzo, H. Haas, "Improving the performance of space shift keying (SSK) modulation via opportunistic power allocation," *IEEE Communications Letters,* vol. 14, no. 6, pp. 500-502, Jun. 2010.

[48] R. Rajashekar, K. V. S. Hari, and L. Hanzo, "Antenna Selection in Spatial Modulation Systems," *IEEE Wireless Communications Letters,* vol. 17, no. 3, pp. 521-524, Jan. 2013.

[49] N. Pillay, H. Xu, "Comments on "Antenna Selection in Spatial Modulation Systems", *IEEE Wireless Communications Letters,* vol. 17, no. 9, pp. 1681-1683, Aug. 2013.

[50] W. Nan, L. Wenlong, M. Hongzhi, J. Minglu, and H. Xu, "Further Complexity Reduction Using Rotational Symmetry for EDAS in Spatial Modulation," *IEEE Communications Letters,* vol. 18, no. 10, pp. 1835-1838, Oct. 2014.

[51] S. Naidu, N. Pillay, and H. Xu, "Transmit Antenna Selection Schemes for Quadrature Spatial Modulation," *Springer Wireless Personal Communications,* vol. 99, no. 1, pp. 299–317, Mar. 2018.

[52] N. Pillay, H. Xu, "Low-complexity transmit antenna selection schemes for spatial modulation," *IET Communications,* vol. 9, no. 2, pp. 239-248, Jan. 2015.

[53] Y. Naresh, A. Chockalingam, "On media-based modulation using RF mirrors," in *Proceedings of the 2016 Information Theory and Applications Workshop (ITA),* pp. 1-10, 2016.

[54] R. Rajashekar, K. V. S. Hari, and L. Hanzo, "Quantifying the Transmit Diversity Order of Euclidean Distance Based Antenna Selection in Spatial Modulation," *IEEE Signal Processing Letters,* vol. 22, no. 9, pp. 1434-1437, Mar. 2015.

CHAPTER 2

Journal Article 1

This is submitted to Digital Communications and Networks for publication. The detail is as follows:

S. Oladoyinbo, N. Pillay, H. Xu, “Adaptive Single-Input Multiple-Output Media-Based Modulation,” [*Under review with Digital Communication and Networks*], 2020.

Adaptive Single-Input Multiple-Output Media-Based Modulation

2 Introduction

A tremendous promise has been shown over the years with regards to the high capacity transmission and improved link reliability in multiple-input multiple-output (MIMO) systems [1]. This has led to a vast amount of interest in the research community. However, MIMO systems have some drawbacks to its practical realization, such as inter-antenna synchronization (IAS) and inter-channel interference (ICI) due to multi-active transmit antennas [2, 3].

Furthermore, achieving a high data rate in MIMO requires a large number of antennas, which limits its practical implementation due to the hardware complexity/cost.

Spatial modulation (SM) [4], an innovative MIMO scheme, requires only a single radio frequency (RF) chain to improve upon the major setbacks of conventional MIMO. The basic idea behind the SM system is the use of both the amplitude/phase modulation (APM) and transmit antenna index to convey information. Improvements achieved in SM have spawned a wealth of research in MIMO systems.

However, the system complexity imposed for high data rates by the SM system is high, considering the logarithmic relationship between the total number of transmit antennas and the spectral efficiency compared to vertical Bell laboratories layered space-time architecture (V-BLAST) [5]. This has led to the investigation of various techniques for reducing the system complexity of the SM system.

In [6], space shift keying (SSK) modulation, a special case of SM was investigated. In SSK, only the spatial domain is exploited to relay information. Resulting in reduced system complexity. However, SSK still requires a large number of transmit antennas required for high data rate, which increases the complexity of the system.

Media-based modulation (MBM) [7] has been recently introduced in the research community. MBM reduces the imposed hardware complexity when compared to SM and SSK. This is due to the linear relationship between the number of radio frequency (RF) mirrors and the spectral efficiency, which is achieved by employing RF mirrors to create different channel fade realizations, known as mirror activation patterns (MAPs) [7].

Some other advantages of MBM are [8]: a) the received constellation size is independent of the transmit power; hence, a substantial increase in spectral efficiency is easily realizable. Furthermore, as the constellation size increase, constellation diversity effectively converts a static multipath fading channel into an additive white Gaussian noise (AWGN) channel with effective signal energy equal to the average received energy, b) a subset of channel realizations may be selected from the N_m distinct channel perturbations that result in superior error performance. Similarly, transmit antennas are sufficiently separated so as to achieve an independent fading, while RF mirrors can be placed side-by-side. As there is no fundamental constraint on mirror separation, based on the above advantages, numerous research works have been presented.

In [9], a single-input multiple-output (SIMO) aided MBM (SIMO-MBM) system was proposed. Due to the linear relationship between the number of RF mirrors (m_{rf}) and the spectral efficiency in SIMO-MBM, an equivalent SM system would require $2^{m_{rf}}$ transmit antennas to achieve the same spectral efficiency. Therefore, SIMO-MBM is more desirable than SM, in terms of data rate.

In [7, 8], MBM was investigated for generalized SM (MBM-GSM) and quadrature SM (MBM-QSM), respectively. The MBM-GSM scheme [7], follows the conventional GSM scheme, employing the transmit antenna combination to activate two transmit antennas at every transmission instant coupled with the spatial dimension to convey information similar to [4].

MBM-QSM [8] decomposes the modulated symbol into in-phase and quadrature components, which are transmitted via the sine and cosine carriers, respectively. Hence, requiring only a single RF chain. A substantial improvement in terms of error performance is achieved in MBM-GSM and MBM-QSM. However, MBM-GSM requires multiple RF chains.

Likewise, in [10], MBM is investigated in uncoded space-time label diversity (USTLD-MBM). The Monte Carlo simulation results obtained demonstrate a significant improvement over the conventional USTLD and the recently proposed space-time channel modulation [11] for fast frequency-flat Rayleigh fading channels in terms of error performance and system complexity.

In [12-14], link adaptation has been employed in several ways, viz. adaptive modulation, transmit precoding (TPC), antenna selection and combinations thereof to enhance the error performance of a SIMO/MIMO system substantially. However, it is not investigated for MBM.

Considering the availability of a single transmit antenna and a mirror unit, transmission candidates may be adopted as follows: SIMO (Mode 1) may use the single transmit antenna while keeping all mirrors OFF. Media-based SSK (MB-SSK) (Mode 2) may employ only the RF mirrors to transmit, while SIMO-MBM (Mode 3) employs both the transmit antennas and RF mirrors to transmit. Note, the transmission candidate configurations are chosen, such as to meet a particular target spectral efficiency.

Given channel knowledge, at the receiver, the transmission candidate mode that minimizes the instantaneous bit error probability (IBEP) is selected and transmitted to the transmitter via a perfect feedback link.

The advantage of using the IBEP is that a look-up table (LUT) approach can be invoked or employed to decrease the imposed computational complexity (CC).

Hence, the contributions of this paper are as follows: we investigate link adaptation in SIMO based schemes, called adaptive single-input multiple-output media-based modulation (ASIMOMBM).

The structure of the remainder of the paper is as follows: In Section 2, the proposed ASIMOMBM system model is presented. Analysis of the IBEP is presented in Section 3. In Section 4, the CC of the proposed ASIMOMBM is formulated. Numerical analysis of the proposed ASIMOMBM is presented in Section 5, while conclusions are drawn in Section 6.

Notation: Bold italic lowercase/uppercase symbols denote vectors/matrices, while regular letters represent scalar quantities. $\|\cdot\|_F$ represents Frobenius norm, $Q(\cdot)$ represents the Gaussian Q-function, $E\{\cdot\}$ is the expectation operator, $\underset{w}{\operatorname{argmin}}(\cdot)/\underset{w}{\operatorname{argmax}}(\cdot)$ represents the minimum or maximum value of an argument with respect to w, $R\{\cdot\}$ represents the real part of a complex number and i represents a complex number.

2.1 System model of ASIMOMBM

The system model of the proposed ASIMOMBM scheme is illustrated in Figure 2.1. A single transmit antenna with m_{rf} RF mirrors located around the transmit antenna and N_R receive antennas are assumed.

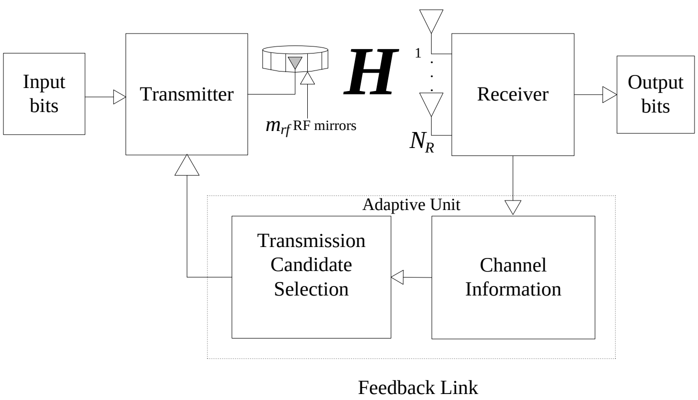

Figure 2.1 System model of the proposed ASIMOMBM scheme.

In the ASIMOMBM system, three transmission candidate modes are employed, which are chosen to satisfy a target spectral efficiency. These are based on: SIMO (Mode 1), MB-SSK (Mode 2) and SIMO-MBM (Mode 3). The total spectral efficiency associated with each mode is $m_{SIMO} = \log_2 M$ b/s/Hz, $m_{MB-SSK} = m_{rf}$ b/s/Hz and $m_{SIMO-MBM} = \log_2 M + m_{rf}$ b/s/Hz, respectively, where M is the order of the APM constellation, and m_{rf} is the number of RF mirrors located around the transmit antenna. The $\log_2 M$ bits modulate the constellation symbol x_q, $q \in [1: M]$ for the SIMO-MBM and SIMO systems. In addition, the m_{rf} bits activate the RF mirrors to transmit the modulated symbol for the SIMO-MBM and MB-SSK schemes.

As an example, the following configuration settings maybe employed for a target spectral efficiency of 4 b/s/Hz: Mode 1: 1×2 16-QAM, Mode 2: 1×2 with $m_{rf} = 4$ and Mode 3: 1×2 4-QAM with $m_{rf} = 2$ are employed as the transmission candidate modes.

Assuming a slowly varying frequency-flat Rayleigh fading channel and full channel knowledge thereof at the receiver, the IBEP for each transmission candidate mode is first computed at the transmission candidate selection module (refer to Figure 2.1), the module then selects the mode that minimizes the IBEP. The IBEP for selection of the mode is discussed in Section 3. Finally, the index of the candidate is transmitted along a perfect low bandwidth feedback link to the transmitter for the next transmission instant.

The $N_R \times 1$ received signal vector $\boldsymbol{y}_{SIMO}$, $\boldsymbol{y}_{MB-SSK}$ and $\boldsymbol{y}_{SIMO-MBM}$ for each of the candidate modes may be defined as [6, 9]:

$$\boldsymbol{y}_{SIMO} = \sqrt{\rho}\, \boldsymbol{h} x_q + \boldsymbol{\eta} \tag{2-1a}$$

$$\boldsymbol{y}_{\substack{MB-SSK \\ SIMO-MBM}} = \sqrt{\rho}\, \boldsymbol{H} \boldsymbol{z}_{\substack{MB-SSK \\ SIMO-MBM}} + \boldsymbol{\eta} \tag{2-1b}$$

where ρ is the average signal-to-noise ratio (SNR), $\boldsymbol{z}_{MB-SSK} = \boldsymbol{e}_\ell x$, where x is a tone and $\boldsymbol{e}_\ell$ is an $N_m \times 1$ vector with one unit entry at the ℓ^{th} position corresponding to the chosen MAP. Likewise, $\boldsymbol{z}_{SIMO-MBM} = \boldsymbol{e}_\ell x_q$ for SIMO-MBM, where the symbol x_q is drawn from an M-ary quadrature amplitude modulation (M-QAM) or an M-ary phase shift keying (M-PSK) constellation, $q \in [1: M]$ and it is assumed that $E\left\{|x_q|^2\right\} = 1$. $\boldsymbol{H}$ and $\boldsymbol{h}$ are the frequency-flat Rayleigh fading channel gain matrix and vector with dimension $N_R \times N_m$ and $N_R \times 1$, respectively. In each of the modes, the message signal is received in the presence of additive white Gaussian noise (AWGN), which is represented as $\boldsymbol{\eta}$ with dimension $N_R \times 1$. The entries of $\boldsymbol{H}$, $\boldsymbol{h}$ and $\boldsymbol{\eta}$ are independent and identically distributed (i.i.d.) according to CN (0,1).

The optimal maximum likelihood (ML) detector for each of the candidate modes SIMO, MB-SSK and SIMO-MBM, respectively may be defined as follows:

Mode 1:

$$[x_{\hat{q}}] = \underset{q\in[1:M]}{\operatorname{argmin}}\left(\left\|\boldsymbol{y}_{SIMO} - \sqrt{\rho}\,\boldsymbol{h}x_q\right\|_F^2\right) \tag{2-2a}$$

$$= \underset{q\in[1:M]}{\operatorname{argmin}}(\|\boldsymbol{g}_{SIMO}\|_F^2 - 2R\{\boldsymbol{y}_{SIMO}^H\,\boldsymbol{g}_{SIMO}\})$$

Mode 2:

$$[\hat{\ell}] = \underset{\ell\in[1:N_m]}{\operatorname{argmin}}\left(\left\|\boldsymbol{y}_{MB-SSK} - \sqrt{\rho}\,\boldsymbol{H}\boldsymbol{z}_{MB-SSK}\right\|_F^2\right) \tag{2-2b}$$

$$= \underset{\ell\in[1:N_m]}{\operatorname{argmin}}(\|\boldsymbol{g}_{MB-SSK}\|_F^2 - 2R\{\boldsymbol{y}_{MB-SSK}^H\boldsymbol{g}_{MB-SSK}\})$$

Mode 3:

$$[\hat{\ell}, x_{\hat{q}}] = \underset{\substack{q\in[1:M]\\ \ell\in[1:N_m]}}{\operatorname{argmin}}\left(\left\|\boldsymbol{y}_{SIMO-MBM} - \sqrt{\rho}\,\boldsymbol{H}\boldsymbol{z}_{SIMO-MBM}\right\|_F^2\right) \tag{2-2c}$$

$$= \underset{\substack{q\in[1:M]\\ \ell\in[1:N_m]}}{\operatorname{argmin}}(\|\boldsymbol{g}_{SIMO-MBM}\|_F^2 - 2R\{\boldsymbol{y}_{SIMO-MBM}^H\boldsymbol{g}_{SIMO-MBM}\})$$

where $\boldsymbol{g}_{SIMO} = \sqrt{\rho}\,\boldsymbol{h}x_q$ and $\boldsymbol{g}_{\substack{MB-SSK\\ SIMO-MBM}} = \sqrt{\rho}\,\boldsymbol{H}\boldsymbol{z}_{\substack{MB-SSK\\ SIMO-MBM}}$

In the next section, the IBEP expression for each candidate mode is formulated. The selection of the active transmission mode is based on the IBEP.

2.2 Analysis of the Instantaneous Bit Error Probability for ASIMOMBM

In this section, the IBEP for each candidate mode employed is formulated.

Mode 1 (SIMO):

The IBEP for the SIMO-based M-QAM system is formulated as [9]:

$$P_{e_{M-QAM}} = \frac{1}{\log_2 M}\left[4\left(1-\frac{1}{\sqrt{M}}\right)Q\left(\sqrt{\frac{3\rho\|\boldsymbol{h}\|_F^2}{(M-1)}}\right) - 4\left(1-\frac{1}{\sqrt{M}}\right)^2 Q^2\left(\sqrt{\frac{3\rho\|\boldsymbol{h}\|_F^2}{(M-1)}}\right)\right] \quad \text{(2-3a)}$$

where $\boldsymbol{h}$ is the frequency-flat Rayleigh fading channel gain with dimension $N_R \times 1$ and M is the APM symbol employed.

In addition, the IBEP for the SIMO-based M-PSK system is computed as [1] (pg. 174):

$$P_{e_{M-PSK}} = \frac{2}{\log_2 M} Q\left(\sqrt{\|\boldsymbol{h}\|_F^2 \rho} \sin\left(\frac{\pi}{M}\right)\right) \quad \text{(2-3b)}$$

Note, in (2-3a, 2-3b), the $Q(\cdot)$ is completed via the bound given in [15] as:

$Q(x) = \frac{(1-\exp(-1.40x))\exp(-\frac{1}{2}x^2)}{1.135\sqrt{2\pi}x}$.

Mode 2 (MB-SSK):

The IBEP for the MB-SSK scheme can be evaluated similar to [6]. The IBEP for M-QAM and M-PSK are the same in the case of MB-SSK scheme, considering the APM symbol is eliminated. The general expression can be expressed as [6]:

$$P_{e_{MB-SSK}} \leq \sum_{\ell=1}^{N_m} \sum_{\hat{\ell}=1}^{N_m} \frac{2 \cdot N(\ell, \hat{\ell})}{N_m} P(\boldsymbol{e}_\ell \to \boldsymbol{e}_{\hat{\ell}} | \boldsymbol{H}) \quad \text{(2-4)}$$

where $P(\boldsymbol{e}_\ell \to \boldsymbol{e}_{\hat{\ell}} | \boldsymbol{H})$ is the conditional pairwise error probability (PEP) of incorrectly choosing the estimated MAP index $\boldsymbol{e}_{\hat{\ell}}$ given that the MAP index $\boldsymbol{e}_\ell$ was transmitted and $N(\ell, \hat{\ell})$ is the associated number of bit errors between the activation patterns of the RF mirrors ℓ and $\hat{\ell}$.

Employing the triangle inequality [16], the PEP can be derived as:

$$P(\boldsymbol{e}_\ell \to \boldsymbol{e}_{\hat{\ell}} | \boldsymbol{H}) = P\left(\left\|\boldsymbol{y}_{MB-SSK} - \sqrt{\rho}\,\overline{\boldsymbol{g}}\right\|_F > \left\|\boldsymbol{y}_{MB-SSK} - \sqrt{\rho}\,\widehat{\overline{\boldsymbol{g}}}\right\|_F\right) \quad \text{(2-5)}$$

where $\overline{\boldsymbol{g}} = \boldsymbol{H}\boldsymbol{e}_\ell$, $\widehat{\overline{\boldsymbol{g}}} = \boldsymbol{H}\boldsymbol{e}_{\hat{\ell}}$. $\boldsymbol{H}$, $\boldsymbol{e}_\ell$ are with dimension $N_R \times N_m$ and $N_m \times 1$, respectively. By simplification, (2-5) becomes:

$$P(\boldsymbol{e}_\ell \to \boldsymbol{e}_{\hat{\ell}} | \boldsymbol{H}) = P\left(\|\boldsymbol{\eta}\|_F > \frac{\left\|\sqrt{\rho}\overline{\boldsymbol{g}} - \sqrt{\rho}\widehat{\overline{\boldsymbol{g}}}\right\|_F}{2\sqrt{N_R}}\right) \quad \text{(2-6)}$$

$$P\left(\boldsymbol{e}_\ell \to \boldsymbol{e}_{\hat{\ell}} | \boldsymbol{H}\right) = P\left(n > \frac{d}{2}\right)$$

where $d = \left\|\overline{\boldsymbol{g}} - \widehat{\overline{\boldsymbol{g}}}\right\|_F$. Therefore,

$$P\left(\boldsymbol{e}_\ell \to \boldsymbol{e}_{\hat{\ell}} | \boldsymbol{H}\right) = \frac{(1 - \exp{(-1.40\beta)})\exp{(-\frac{1}{2}\beta^2)}}{1.135\sqrt{2\pi}\beta} \tag{2-7}$$

where $\beta = \sqrt{\frac{\rho}{2}} \cdot \left\|\overline{\boldsymbol{g}} - \widehat{\overline{\boldsymbol{g}}}\right\|_F$.

Mode 3 (SIMO-MBM):

The IBEP for the SIMO-MBM scheme can be computed employing a lower-bound approach similar to [16] as:

$$P_{e_{SIMO-MBM}} \geq P_a + P_{e_{\substack{M-QAM \\ M-PSK}}} - P_a P_{e_{\substack{M-QAM \\ M-PSK}}} \tag{2-8}$$

where P_a is the bit error probability of the antenna index given that the symbol x_q is perfectly detected and P_e is the bit error probability of the estimated symbol given that the antenna index is perfectly detected. The bit error probability of the transmit antenna index estimation P_a is evaluated similar to [16] as:

$$P_a \leq \sum_{q=1}^{M} \sum_{\ell=1}^{N_m} \sum_{\hat{\ell}=1}^{N_m} \frac{N\left(\ell, \hat{\ell}\right) P\left(x_{\ell q} \to x_{\hat{\ell} q} | \boldsymbol{H}\right)}{M N_m} \tag{2-9}$$

To get the PEP, we compute the joint probability distribution of the channel gain employing moment generating function and alternative form of Q-function over a Rayleigh frequency-flat fading channel with $CN(0,1)$. The derived bit error probability of the transmit antenna index P_a considering the symbol is perfectly detected can be computed as:

$$P\left(x_{\ell q} \to x_{\hat{\ell} q} | \boldsymbol{H}\right) = P\left(\left\|\boldsymbol{y}_{SIMO-MBM} - \sqrt{\rho}\overline{\boldsymbol{g}} x_{\ell q}\right\|_F > \left\|\boldsymbol{y}_{SIMO-MBM} - \sqrt{\rho}\widehat{\overline{\boldsymbol{g}}} x_{\hat{\ell} q}\right\|_F\right)$$

where $\overline{\boldsymbol{g}} = \boldsymbol{H}\boldsymbol{e}_\ell$ and $\widehat{\overline{\boldsymbol{g}}} = \boldsymbol{H}\boldsymbol{e}_{\hat{\ell}}$. Employing the triangle inequality [16], (11) becomes:

$$P\left(x_{\ell q} \to x_{\hat{\ell} q} | \boldsymbol{H}\right) = P\left(2\|\boldsymbol{\eta}\|_F > \left\|\sqrt{\rho}\overline{\boldsymbol{g}} x_{\ell q} - \sqrt{\rho}\widehat{\overline{\boldsymbol{g}}} x_{\hat{\ell} q}\right\|_F\right) \tag{2-10}$$

where $\|\boldsymbol{\eta}\|_F = \sqrt{\sum_{k=1}^{N_R}(\eta_k^I)^2 + \sum_{k=1}^{N_R}(\eta_k^Q)^2}$ and the k^{th} element of $\boldsymbol{\eta}$ is given as [17]: $\eta_k = \eta_k^I + (\sqrt{-1})\eta_k^Q$. I and Q represents the in-phase and quadrature components of the complex number. Let $\eta^2 = \min\begin{Bmatrix}(\eta_1^I)^2, (\eta_2^I)^2, \cdots, (\eta_{N_R}^I)^2, \\ (\eta_1^Q)^2, (\eta_2^Q)^2, \cdots, (\eta_{N_R}^Q)^2\end{Bmatrix}$, we get:

$$P(x_{\ell q} \to x_{\hat{\ell} q}|\boldsymbol{H}) = P\left(2\sqrt{\sum_{k=1}^{N_R}(\eta_k^I)^2 + \sum_{k=1}^{N_R}(\eta_k^Q)^2} > \left\|\sqrt{\rho}\bar{\boldsymbol{g}}x_{\ell q} - \sqrt{\rho}\hat{\bar{\boldsymbol{g}}}x_{\hat{\ell} q}\right\|_F\right)$$

Finally, with some manipulation and the use of Q-function we arrived at:

$$= P\left(2\sqrt{2N_R\eta^2} > \left\|\sqrt{\rho}\bar{\boldsymbol{g}}x_{\ell q} - \sqrt{\rho}\hat{\bar{\boldsymbol{g}}}x_{\hat{\ell} q}\right\|_F\right)$$

$$P(x_{\ell q} \to x_{\hat{\ell} q}|\boldsymbol{H}) = P\left(\eta > \frac{\left\|\sqrt{\rho}\bar{\boldsymbol{g}}x_{\ell q} - \sqrt{\rho}\hat{\bar{\boldsymbol{g}}}x_{\hat{\ell} q}\right\|_F}{2\sqrt{2N_R}}\right) \quad \text{(2-11a)}$$

Employing an alternative form of Q-function and taking $P(x_{\ell q} \to x_{\hat{\ell} q}|\boldsymbol{H})$ over joint probability distribution of the channel gain. Therefore,

$$P(x_{\ell q} \to x_{\hat{\ell} q}|\boldsymbol{H}) = \frac{(1 - \exp(-1.40\alpha))\exp(-\frac{1}{2}\alpha^2)}{1.135\sqrt{2\pi}\alpha} \quad \text{(2-11b)}$$

where $\alpha = \frac{\left\|\sqrt{\rho}\bar{\boldsymbol{g}}x_{\ell q} - \sqrt{\rho}\hat{\bar{\boldsymbol{g}}}x_{\hat{\ell} q}\right\|_F}{2\sqrt{N_R}}$.

2.3 Computational complexity

The receiver complexity δ for each candidate mode is formulated based on floating-point operations (flops) similar to [18].

2.4 Computational complexity of Single-Input Multiple-Output

Considering a single-mode transmission, $\|\boldsymbol{h}\|_F^2$ can be re-written as $\boldsymbol{h}^H\boldsymbol{h}$, of dimension $1 \times N_R$ by $N_R \times 1$ imposing a $2N_R - 1$ flops, which is evaluated N_T times and a look-up table (LUT) approach can be employed for the bond $\frac{(1-\exp(-1.40x))\exp(-\frac{1}{2}x^2)}{1.135\sqrt{2\pi}x}$ [19, 20]. It can be validated that

$4\left(1-\frac{1}{\sqrt{M}}\right)$ and $\frac{3}{(M-1)}$ can be precomputed in the IBEP expression formulated for M-QAM in (3a). Likewise, in (3b), the IBEP expression $\sqrt{\|\boldsymbol{h}\|_F^2\rho}\,\sin\left(\frac{\pi}{M}\right)$ for M-PSK can be precomputed. Therefore, M-QAM and M-PSK imposes the same CC. This yield $N_T(2N_R-1)$ flops for M-QAM and M-PSK, respectively.

2.5 Computational complexity of Media-based-Space Shift Keying

The LUT approach is employed for $Q(\cdot)$ bound in MB-SSK (Mode 2). Likewise, considering $\overline{\boldsymbol{g}}=\boldsymbol{H}\boldsymbol{e}_\ell$, where $\boldsymbol{H}$ is of dimension $N_R\times N_m$ and $\boldsymbol{e}_\ell$ of dimension $N_m\times 1$. Therefore, the inner subtraction and product of the Frobenius norm of $\|\overline{\boldsymbol{g}}-\hat{\overline{\boldsymbol{g}}}\|_F$ in (7), imposes N_R and $2N_R-1$ flops, respectively. In addition, $\frac{2\cdot N(\ell,\hat{\ell})}{N_m}$ imposes 2 flops, which is evaluated across N_m^2 times. This yield $N_m^2(3N_R+1)$ flops.

2.6 Computational complexity of Single-Input Multiple-Output-MBM

The IBEP for the symbol error for M-QAM and M-PSK has been evaluated initially in Mode 1. Therefore, $\frac{N(\ell,\hat{\ell})P(x_q\rightarrow x_{\hat{q}}|\boldsymbol{H})}{MN_m}$ in (9) imposes 3 flops. Considering $\overline{\boldsymbol{g}}=\boldsymbol{H}\boldsymbol{e}_\ell$, where $\boldsymbol{H}$ is of dimension $N_R\times N_m$ and $\boldsymbol{e}_\ell$ of dimension $N_m\times 1$. The inner subtraction and product of the Frobenius norm of $\|\sqrt{\rho}\overline{\boldsymbol{g}}x_q-\sqrt{\rho}\hat{\overline{\boldsymbol{g}}}x_{\hat{q}}\|_F$ imposes N_R and $2N_R-1$ flops, respectively, which is required across M and evaluated N_m^2 times. Likewise, the division and $2\sqrt{N_R}$ in (11) imposes 2 flops. This yields a total of $MN_m^2(3N_R+4)$ flops.

Hence, the overall CC imposed by ASIMOMBM is:

$$\delta_{M-QAM}=N_T(2N_R-1)+3N_m^2N_R(1+M)+N_m^2(1+4M) \tag{2-12a}$$

$$\delta_{M-PSK}=N_T(2N_R-1)+3N_m^2N_R(1+M)+N_m^2(1+4M) \tag{2-12b}$$

2.7 Numerical analysis and discussion

In this section, the Monte Carlo simulation results obtained for the proposed ASIMOMBM system is presented. We consider the bit error rate (BER) versus SNR in dB. Full knowledge of the channel is assumed at the receiver and a perfect low-bandwidth feedback link to the transmitter is employed. In all cases, ML detection is assumed and two receive antennas are considered in all cases, i.e. $N_R=2$. The notation $(N_T,\ N_{R,}\ M)$, $(N_T,\ N_{R,}\ m_{rf})$ and $(N_T,\ N_{R,}\ M, m_{rf})$ is employed to denote the configuration of SIMO, MB-SSK and SIMO-MBM, respectively.

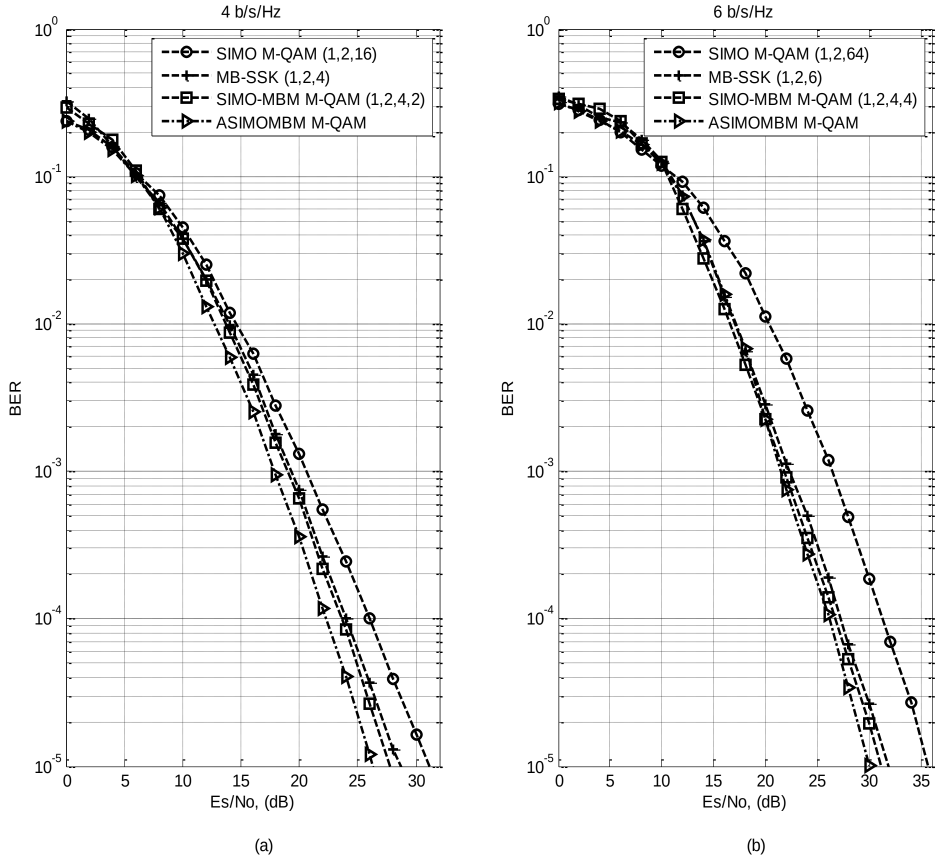

Figure 2.2 Comparison of BER performance for (a) 4 b/s/Hz and (b) 6 b/s/Hz for M-QAM.

Figure 2.2(a) and Figure 2.2(b) demonstrates the performance comparison between the conventional SIMO system, MB-SSK, SIMO-MBM and ASIMOMBM system, with a spectral efficiency of 4 b/s/Hz and 6 b/s/Hz, respectively. In the Monte Carlo simulation results obtained, the proposed scheme (ASIMOMBM) outperforms its counterparts.

In Figure 2.2, it is clearly evident that employing the ASIMOMBM system achieves a better performance when compared to SIMO, MB-SSK and SIMO-MBM systems.

Table 2.1 summarizes the SNR gains achieved with respect to the proposed scheme when compared to the conventional SIMO system, MB-SSK and SIMO-MBM systems.

Table 2.1: SNR gain (dB) of the ASIMOMBM system, based on M-QAM employing $N_R = 2$

Scheme	SNR gain of ASIMOMBM at a BER of 10^{-5}	
	4 b/s/Hz	6 b/s/Hz
SIMO	4.4 dB	5.1 dB
MB-SSK	2.1 dB	1.3 dB
SIMO-MBM	1.1 dB	1.0 dB

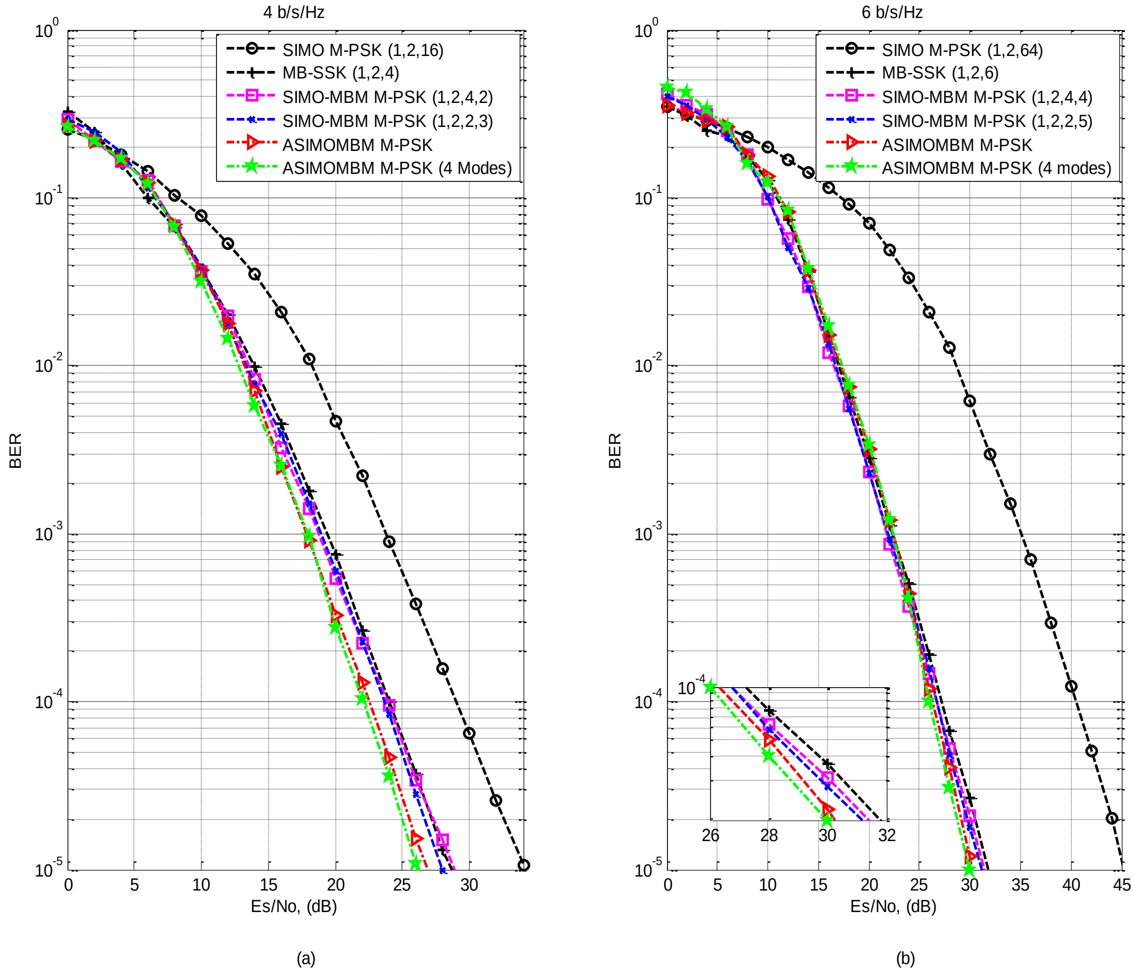

Figure 2.3 Comparison of BER performance for 4 b/s/Hz and 6 b/s/Hz for M-PSK.

Table 2.2: SNR gain (dB) of the ASIMOMBM based on M-PSK with $N_R = 2$

Scheme	SNR gain of ASIMOMBM at a BER of 10^{-5}	
	4 b/s/Hz	6 b/s/Hz
SIMO-PSK	6 dB	15 dB
MB-SSK-PSK	2 dB	2 dB
SIMO-MBM-PSK	1 dB	0.5 dB

Figure 2.3(a) and Figure 2.3(b) presents the performance comparison between the conventional SIMO system, MB-SSK, SIMO-MBM and ASIMOMBM system with M-PSK APM, with a target spectral efficiency of 4 b/s/Hz and 6 b/s/Hz, respectively. In the Monte Carlo simulation results obtained, the ASIMOMBM system outperforms its counterparts. The SNR gains achieved with respect to the proposed scheme is tabulated in Table 2.2.

Table 2.3 presents the imposed CC on ASIMOMBM, with the following settings for M-QAM and M-PSK: the 4 b/s/Hz system is equipped with a modulation order of 16-QAM and 16-PSK, respectively, i.e. $M = 16$. Likewise, the 6 b/s/Hz system is equipped with a modulation order of 64-QAM and 64-PSK, respectively, i.e. $M = 64$. Each system is equipped with 4 RF mirrors, such that $N_m = 16$ and two receive antennas.

Table 2.3: Imposed CC for ASIMOMBM for M-QAM and M-PSK with $N_R = 2$.

Scheme	4 b/s/Hz	6 b/s/Hz
M-QAM	42,767	165,647
M-PSK	42,759	165,639

2.8 Conclusion

In this Chapter, an adaptive scheme for SIMO employing RF mirrors was investigated to improve error performance. A decision metric to choose the transmission candidate mode was based on minimizing the IBEP per transmission instant. The Monte Carlo simulation results obtained reveal an improvement over its counterparts, viz. the conventional SIMO, MB-SSK and SIMO-MBM.

References

[1] A. Goldsmith, Wireless Communications, 1st ed., New York: Cambridge University Press, 2005.

[2] A. Goldsmith, N. Jindal and S. Vishwanath, "Capacity limits of MIMO channels," *IEEE Journal on Selected Areas in Communications*, vol. 21, pp. 684-702, Jun. 2003.

[3] R. Y. Mesleh, H. Hass, L. Yeonwoo, and Y. Sangboh, "Interchannel Interferenece Avoidance in MIMO Transmission by Exploiting Spatial Information," in *Proceedings of the IEEE 16th International Symposium on Personal, Indoor and Mobile Radio Communications, (PIMRC)*, pp. 141-145, 2005.

[4] R. Y. Mesleh, H. Haas, S. Sinanovic, A. Chang Wook, and Y. Sangboh, "Spatial Modulation," *IEEE Transactions on Vehicular Technology*, vol. 57, no. 4, pp. 2228-2241, Jul. 2008.

[5] P. Wolniansky, G. J. Foschini, D. Golden, and R. Valenzuela, "V-BLAST: an architecture for realizing very high data rates over the rich-scattering wireless channel," in *Proceedings of the International Symposium on Signals, System and Electronics. (ISSSE)*, pp. 295-300, Sep. 1998.

[6] J. Jeganathan, L. Szczecinski, and A. Ceron, "Space Shift Keying Modulation for MIMO Channels," *IEEE Wireless Communications*, vol. 8, no. 7, pp. 3692-3703, Jul. 2009.

[7] Y. Naresh and A. Chockalingam.: "On Media-based Modulation using RF Mirrors," *IEEE Transactions on Vehicular Technology*, vol. 66, no. 6, pp. 4967 - 4983, Oct. 2016.

[8] N. Pillay, H. Xu, "Quadrature spatial media-based modulation with RF mirrors," *IET Communications*, vol. 11, no. 16, pp. 2440 - 2448, Nov. 2017.

[9] R. Pillay, N. Pillay, H. Xu, "A Study of Single-Input Multiple-Output Media-based Modulation with RF Mirrors," in *Proceedings of the Southern Africa Telecommunication Networks and Applications Conference (SATNAC)*, Sep. 2017.

[10] N. Pillay, H. Xu, "Uncoded Space-Time Labeling Diversity-Application of Media-based Modulat-ion with RF Mirrors," *IEEE Communications Letters*, vol. 22, no. 2, pp. 272-275, Feb. 2018.

[11] E. Basar and I. Altunbas, "Space-Time Channel Modulation," *IEEE Transactions on Vehicular Technology*, vol. 66, no. 8, pp. 7609-7614, Aug. 2017.

[12] Y. Ping, X. Yue, L. Lei, T. Qian, Y. Yi, and L. Shaoqian, "Link Adaptation for Spatial Modulation With Limited Feedback," *IEEE Transactions on Vehicular Technology*, vol. 61, no. 8, pp. 3808-3813, Oct. 2012.

[13] P. Yang, Y. L. Guan, Y. Xiao, M. Di Renzo, S. Li, and L. Hanzo, "Transmit Pre-coded Spatial Modulation: Maximizing the Minimum Euclidean Distance Versus Minimizing the Bit Error Ratio," *IEEE Transactions on Wireless Communications*, vol. 15, no. 3, pp. 2054-2068, Mar. 2016.

[14] P. Yang, Y. Xiao, Y. L. Guan, S. Li, and L. Hanzo, "Transmit Antenna Selection for Multiple-Input Multiple-Output Spatial Modulation Systems," *IEEE Transactions on Wireless Communications*, vol. 64, no. 5, pp. 2035-2048, May 2016.

[15] G. Karagiannidis and A. S. Lioumpas, "An Improved Approximation for the Gaussian Q-Function," *IEEE Communications Letters*, vol. 11, no. 8, pp. 644-646, Aug. 2007.

[16] N. R. Naidoo, H. Xu, T. Quazi, "Spatial modulation: optimal detector asymptotic performance and multiple-stage detection," *IET Communications*, vol. 5, no. 10, pp. 1368 - 1376, Jul. 2010.

[17] N. Pillay, H. Xu, "A study of single transmit antenna selection with modulation," *SAIEE Africa Research Journal*, vol. 109, no. 4, pp. 250-259, Nov. 2018.

[18] N. Pillay, H. Xu, "Low Complexity Detection and Transmit Antenna Selection for Spatial Modulation," *SAIEE Africa Research Journal*, vol. 105, no. 1, pp. 4-12, Mar. 2014.

[19] N. N. Schraudolph, "A Fast, Compact Approximation of the Exponential Function," *Neural Computation*, vol. 11, no. 4, pp. 853-862, 15 May 1999.

[20] L. Denga, N. Pitsianisbc, X. Sunb, "Automated Optimization of Look-Up-Table Implementation for Function Evaluation on FPGAs," *in Proceedings of the SPIE Conference*, Jan. 2010.

CHAPTER 3

Journal Article 2

This article has been published in the International Journal of Communication Systems (IJCS). The detail is as follows:

S. Oladoyinbo, N. Pillay, H. Xu, "Media-based Single-Symbol Generalized Spatial Modulation," International Journal of Communication Systems, vol. 32, no. 6, pp. 1-13, 2019.
DOI: 10.1002/dac.3909

Media-Based Single-Symbol Generalized Spatial Modulation

3 Introduction

Spatial modulation (SM) [1], is an innovative form of multiple-input multiple-output (MIMO) scheme, which employs the spatial dimension to convey additional information. The requirement for a single radio frequency (RF) chain in SM eliminates inter-antenna synchronization (IAS) and inter-channel interference (ICI) experienced in conventional MIMO systems. However, the major criticism of SM is its data rate enhancement, which is proportional to the logarithm base-two of the total number of transmit antennas. This is unlike other spatial multiplexing techniques, such as vertical Bell laboratories layered space-time architecture (V-BLAST) [2], where the data rate increases linearly with the number of transmit antennas.

In addition, the demand for high data rates in multimedia services requires schemes with superior error performance and throughput. However, an increase in spectral efficiency leads to a high complexity due to a large number of transmit antennas required for transmission [3]. This is another setback in SM, due to the transmit antenna constraint, which led to the introduction of single-symbol generalized spatial modulation (GSM) [3], employing the same symbol across multi-active transmit antennas.

GSM [3] maps information bits to the index of a transmit antenna combination, allowing a relatively large number of points to be chosen in the spatial constellation. This alleviates the requirement for a large number of transmit antennas, as in the case of SM. However, the error performance of GSM is slightly degraded when compared to SM due to the average power effect.

In [4], a multi-symbol GSM system (M-GSM) was proposed, where multiple amplitude/phase modulation (APM) symbols are transmitted via the selected transmit antenna combination. It is evident from the Monte Carlo simulation results obtained [4], that M-GSM achieves a significant improvement in terms of error performance over the GSM system of [3]. However, M-GSM experiences several setbacks, such as the requirement of multiple RF chains and high system/computational complexity (CC), hence limiting practical implementation and increasing cost.

Recently, media-based modulation (MBM) [5-8] employing RF mirrors [6-8] was proposed. This creates unique channel fade realizations based on the status of the mirrors being either active or in-active. MBM has the benefit of linearly increasing the throughput [5] and improving the error performance of a MIMO system. In MBM, high throughput is achieved by considering the RF mirrors around each transmit antenna independently, such that the number of bits related to the spatial portion of the system linearly increases with the total number of the RF mirrors employed.

Furthermore, improved error performance is achieved with MBM via the selective use of the RF mirrors, which create different channel fade realizations that form the modulation alphabet. In MBM, only a single transmit antenna is needed to create the modulation alphabet [8]. Additionally, in classical systems, transmit antennas are sufficiently separated, in order to yield independent fading, while RF mirrors can be placed side-by-side in the MBM-based scheme, as there is no fundamental constraint on mirror separation. Several other advantages were discussed in [5].

In [8, 9], an MBM-based scheme was investigated for the M-GSM system of [4] termed generalized spatial media-based modulation (GSM-MBM), where multiple APM constellation symbols are employed. The scheme yields a high spectral efficiency since it employs simultaneous transmission of symbols and mirror activation pattern (MAP) indexing coupled with multiple RF chain imposing high CC.

However, the same disadvantages of M-GSM, as outlined earlier, apply to the scheme of [8, 9]. Hence, we are motivated to investigate MBM for the single-symbol GSM scheme of [3] to mitigate the drawbacks of [9].

The contributions of this paper are as follows: a) We formulate a single-symbol GSM system with RF mirror-based MBM, hereinafter referred to as S-GSM-MBM. We investigate the use of unique MAP indices at each transmit unit for the proposed scheme. b) The theoretical average bit error probability (ABEP) is formulated to validate the simulation results obtained for the proposed scheme. c) In order to further improve error performance, MAP selection algorithm for S-GSM-MBM is introduced. Based on complete channel knowledge, we investigate the effect of an optimal MAP selection approach in the S-GSM-MBM system, which is based on maximizing the minimum Euclidean distance among transmission vectors.

Likewise, the effect of sub-optimal MAP selection, based on computing the channel amplitude and antenna correlation to eliminate the poor channel(s) at every transmission instant is investigated. The Monte Carlo simulation results obtained demonstrate a trade-off between the CC and error performance.

The structure of the remainder of the paper is as follows: In Section 2, the system model of the proposed S-GSM-MBM system is presented. Section 3 formulates the theoretical ABEP and MAP selection for S-GSM-MBM is presented in Section 4. Numerical analysis of the proposed S-GSM-MBM is presented in Section 5, while conclusions are drawn in Section 6.
Notation: Bold italic lowercase/uppercase symbols denote vectors/matrices, while regular letters represent scalar quantities. $\|\cdot\|_F$ represents Frobenius norm, $Q(\cdot)$ represents the Gaussian Q-

function, $\underset{w}{\operatorname{argmin}}(\cdot)/\underset{w}{\operatorname{argmax}}(\cdot)$ represents the minimum/maximum value of an argument with respect to w, $\binom{\cdot}{\cdot}$ represents the binomial coefficient, i represents a complex number, $R\{\cdot\}$ represent the real part of a complex number and $\lfloor\cdot\rfloor$ represents the nearest integer less than the input argument.

3.1 Single-Generalized Spatial Modulation-Media-based Modulation

In this section, we first investigate an S-GSM-MBM system, where N_a MAP indices are employed to activate the RF mirrors at every transmission instant.

3.1.1 System model

Figure 3.1 presents the system model of the proposed S-GSM-MBM system equipped with N_T transmit units, each surrounded with m_{rf} RF mirrors and N_R antennas at the receiver, to transmit an APM symbol via the channel $\boldsymbol{H}_T$ of dimension $N_R \times N_m N_T$, where $\boldsymbol{H}_T = [\boldsymbol{H}_1\ \boldsymbol{H}_2 \cdots \boldsymbol{H}_{N_T}]$ and $N_m = 2^{m_{rf}}$.

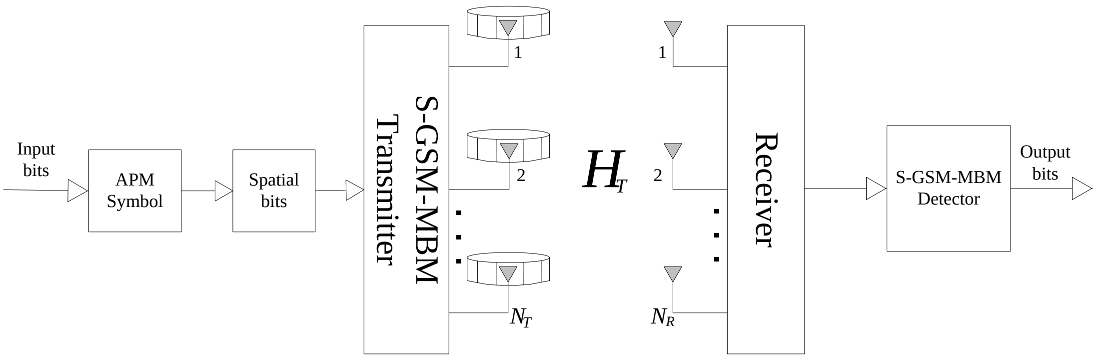

Figure 3.1 System model of the proposed S-GSM-MBM system

The spectral efficiency of the proposed S-GSM-MBM is given as $m = \log_2(M) + \left\lfloor \log_2 \binom{N_T}{N_a} \right\rfloor + N_a m_{rf}$ b/s/Hz, where M, N_T, N_a and m_{rf} represents the APM constellation size, total number of transmit antennas, number of active transmit units and number of RF mirrors at each transmit unit, respectively.

Hence, a system with the following settings: $M = 4$, $N_T = 4$, $N_a = 2$ and $m_{rf} = 2$, i.e. $N_m = 4$ will yield a spectral efficiency of 8 b/s/Hz. The spectral efficiency of the same configuration in a conventional GSM system will yield only 4 b/s/Hz. In this case, unique MAP indices at each transmit unit are employed to activate the RF mirrors, which will be employed to transmit the modulated symbol.

Given the set of $N_c = \binom{N_T}{N_a}$ transmit antenna combinations, N_s antenna combinations are selected, where $N_s = 2^{\lfloor \log_2(N_c) \rfloor}$. The channel $\boldsymbol{H}_{k_j}$, $j \in [1{:}\, N_a]$, employed for transmission is independent and identically distributed (i.i.d) as $CN(0, 1)$ with $N_R \times N_m$ dimension corresponding to the k^{th} combination of the form $k = (k_1 \cdots k_{N_a})$ in the presence of additive white Gaussian noise (AWGN) $\boldsymbol{n}$ of dimension $N_R \times 1$. The modulated symbol is transmitted through a channel $\boldsymbol{H}_{k_j}$ of $N_R \times N_m$ dimension. Therefore, the $N_R \times 1$ received signal vector $\boldsymbol{y}$ can be written as:

$$\boldsymbol{y} = \sqrt{\rho / N_a} \sum_{j=1}^{N_a} \boldsymbol{H}_{k_j} \boldsymbol{e}_{\ell_{k_j}} x_q + \boldsymbol{n} \tag{3-1}$$

where ρ is the signal-to-noise ratio (SNR), x_q, $q \in [1{:}\, M]$ represents the APM symbol, $\ell \in [1{:}\, N_m]$, $j \in [1{:}\, N_a]$, $\boldsymbol{e}_{\ell_{k_j}}$ is an $N_m \times 1$ vector with ℓ^{th} non-zero position corresponding to the chosen MAP, set to unity. Table 1 presents an illustration of the mapping procedure for the S-GSM-MBM system.

Table 3.1: Example of mapping process for the S-GSM-MBM system using 4-QAM.

Configuration	Input bits $\mathrm{m} = \log_2(M) + \left\lfloor \log_2 \binom{N_T}{N_a} \right\rfloor + N_a m_{rf}$	Symbol bits $\log_2 M$ bits	Antenna bits $\left\lfloor \log_2 \binom{N_T}{N_a} \right\rfloor$ bits	MAP index m_{rf} bits	MAP index m_{rf} bits
	$N_a = 2$	$\log_2 M$ bits	$\left\lfloor \log_2 \binom{N_T}{N_a} \right\rfloor$ bits	m_{rf} bits $m_{rf} = 2$	m_{rf} bits $m_{rf} = 2$
$M = 4$ $N_T = 4$ $N_R = 4$	1 0 1 0 0 0 0 1	[1 0] $x_q = 1 + 1i$	[1 0] $j = 3$	[0 0] $\boldsymbol{e}_{\ell_1} = [1\ 0\ 0\ 0]^T$	[0 1] $\boldsymbol{e}_{\ell_2} = [0\ 1\ 0\ 0]^T$
$M = 4$ $N_T = 4$ $N_R = 4$	1 1 0 1 0 0 0 1	[1 1] $x_q = 1 - 1i$	[0 1] $j = 2$	[0 0] $\boldsymbol{e}_{\ell_1} = [1\ 0\ 0\ 0]^T$	[0 1] $\boldsymbol{e}_{\ell_2} = [0\ 1\ 0\ 0]^T$

Table 1 presents an example of the mapping process for the proposed S-GSM-MBM system. The input bits [1 0 1 0 0 0 0 1] are divided into four sections, such that one section modulates the APM symbol [1 0] based on $\log_2 M$, the second section [1 0] choose the transmit unit based on $\left\lfloor \log_2 \binom{N_T}{N_a} \right\rfloor$, the third section [0 0] selects the RF mirror to transmit the first APM symbol and the fourth section [0 1] selects the second RF mirror to be employed to transmit the redundant copy of the APM symbol each based on m_{rf}.

3.1.2 Maximum Likelihood detector

The received signal vector $\boldsymbol{y}$ is detected optimally employing the maximum likelihood (ML) detector, which searches the entire signal space of M constellation points, all possible transmit antenna index combinations and MAP indices. The S-GSM-MBM ML detector can be defined as [9]:

$$\left[\hat{\ell}_{k_1}, \cdots, \hat{\ell}_{k_{N_a}}, \hat{k}, x_{\hat{q}}\right] = \underset{\substack{q \in [1:M] \\ \ell \in [1:N_m] \\ k \in \boldsymbol{\chi}}}{\operatorname{argmin}} \left(\left\| \boldsymbol{y} - \sqrt{\rho/N_a} \sum_{j=1}^{N_a} \boldsymbol{H}_{k_j} \boldsymbol{e}_{\ell_{k_j}} x_q \right\|_F^2 \right) \tag{3-2a}$$

where $\boldsymbol{\chi}$ is the set of all transmit antenna combinations, the k^{th} combination is of the form $(k_1 \cdots k_{N_a})$. The detection rule of (2a) can be simplified as:

$$\left[\hat{\ell}_{k_1}, \cdots, \hat{\ell}_{k_{N_a}}, \hat{k}, x_{\hat{q}}\right] = \underset{\substack{q \in [1:M] \\ \ell \in [1:N_m] \\ k \in \boldsymbol{\chi}}}{\operatorname{argmin}} (\|\boldsymbol{g}\|_F^2 - 2R\{\boldsymbol{y}^H \boldsymbol{g}\}) \tag{3-2b}$$

where $\boldsymbol{g} = \sqrt{\rho/N_a} \sum_{j=1}^{N_a} \boldsymbol{H}_{k_j} \boldsymbol{e}_{\ell_{k_j}} x_q$.

3.2 Computational complexity at the receiver

The receiver complexity for the proposed S-GSM-MBM system is formulated based on complex multiplications and complex additions of the ML algorithm, similar to [10]. The ML detector searches over $q \in [1:M]$, $\ell \in [1:N_m]$ and $k \in \boldsymbol{\chi}$ resulting in 2^m points. Considering the received signal vector $\boldsymbol{y}$ of dimension $N_R \times 1$ with channel matrix $\boldsymbol{H}_{k_j}$ of dimension $N_R \times N_m$, where k_j corresponds to the chosen transmit units, the MAP vector of dimension $N_m \times 1$ and the symbol x_q across M modulation order and N_a transmit units. The complexity of resolving $\boldsymbol{g}$ yields $N_R N_a$ complex multiplications, which searches across M and the complexity of computing $\|\boldsymbol{g}\|_F^2$ yields N_R complex multiplications. Similarly, resolving $\boldsymbol{y}^H \boldsymbol{g}$ yields N_R complex multiplications and $N_R - 1$ complex additions.

Hence, the complexity of (3-2b) for the proposed S-GSM-MBM across N_R receive antennas and 2^m points is:

$$\delta_{MB-GSM} = 2^m(N_R(N_a + 3) + M - 1) \tag{3-3a}$$

GSM-MBM of [9], employs unique MAP indices, coupled with unique symbols across N_a transmit units. Therefore, the ML detector searches over M^{N_a}. Hence, resolving $\boldsymbol{g}$ and computing $||\boldsymbol{g}||_F^2$ in [9], yields $N_R N_a$ complex multiplications across M^{N_a} and N_R complex multiplications, respectively. Resolving $\boldsymbol{y}^H \boldsymbol{g}$ yields N_R complex multiplications and $N_R - 1$ complex additions. Hence, the complexity of GSM-MBM of [9] across N_R receive antennas and 2^m points is:

$$\delta_{MB-GSM[9]} = 2^m(N_R(N_a + 3) + M^{N_a} - 1) \tag{3-3b}$$

Table 3.2 illustrates the complexity comparison for the proposed scheme and GSM-MBM of [9], employing the ML detector of (3-2b).

Table 3.2: Receiver complexity comparison for the ML detector, employing $N_R = 4$ and $M = 4$.

Scheme	8 b/s/Hz $N_a = 2$	10 b/s/Hz $N_a = 2$	12 b/s/Hz $N_a = 3$	14 b/s/Hz $N_a = 3$
S-GSM-MBM	5,888	23,552	110,592	442,368
GSM-MBM [9]	8,960	35,840	159,744	638,976

3.3 Average BER analysis for the proposed scheme

In the single-symbol GSM system, one symbol is transmitted across multiple active antennas, based on the analysis of average BER for conventional SM [11], minor modifications may be made to the analytical result for single-symbol GSM. In [11], the average BER is given as:

$$\begin{aligned} P_e &\geq 1 - ((1 - P_a)(1 - P_b)) \\ &= P_a + P_b - P_a P_b \end{aligned} \tag{3-4}$$

where P_e is decomposed into two parts, P_a the bit error probability of the antenna index estimation given that the APM symbol is perfectly detected and P_b the bit error probability of the estimated symbol given that the antenna index is perfectly detected.

For single-symbol GSM, we treat the system as if a single antenna was employed, similar to SM. Still, the antenna error needs to be adjusted since multiple transmit antennas convey the APM symbol. Based on N_a active antennas, the antenna error is modified as $N_a P_a$ using an average SNR $\frac{\rho}{N_a}$.

For the symbol error, we simply modify the average SNR as $\frac{\rho}{N_a}$. These modifications result in a bound for the single-symbol GSM system. We apply these modifications, taking into account RF mirrors around transmit antennas, to arrive at the average BER of the S-GSM-MBM system. Hence, employing a union bound on PEP, P_a can be computed as [11]:

$$P_a \leq \sum_{q=1}^{M}\sum_{\hat{j}=1}^{W}\sum_{j=1}^{W}\frac{N(j,\hat{j})\mu^{N_R}\sum_{k=0}^{N_R-1}\binom{N_R-1+k}{k}[1-\mu]^k}{G} \tag{3-5}$$

where $G = WM\log_2(W)$ with $W = N_T N_m$, $\mu = \frac{1}{2}\left(1-\sqrt{\frac{\gamma}{\gamma+1}}\right)$, $N(j,\hat{j})$ represents the number of bit errors between the transmit antenna j and the estimated transmit antenna $\hat{j}$. $\gamma = \frac{\rho}{N_a}|x_q|^2$, due to N_a active transmit antennas.

Employing square M-QAM, P_b is computed similar to [11] and [12] as:

$$\begin{aligned} P_b = \frac{1}{\log_2 M}\Bigg(\frac{a}{c}\Bigg[\frac{1}{2}\left(\frac{2}{b\rho+2}\right)^{N_R} - \frac{a}{2}\left(\frac{1}{b\rho+1}\right)^{N_R} + (1 \\ - a)\sum_{i=1}^{c-1}\left(\frac{2\sin^2\theta}{b\rho+2\sin^2\theta}\right)^{N_R} + \sum_{i=c}^{2c-1}\left(\frac{2\sin^2\theta}{b\rho+2\sin^2\theta}\right)^{N_R}\Bigg]\Bigg) \end{aligned} \tag{3-6}$$

where $a = 1-\frac{1}{\sqrt{M}}$, $b = \frac{3}{M-1}$, $\theta = \frac{i\pi}{4c}$ and c is the number of summations $c > 10$, for convergence of the trapezoidal approximation of the Q-function [12]. ρ is considered as $\frac{\rho}{N_a}$. Hence, the overall error $P_e \geq N_a P_a + P_b - N_a P_a P_b$.

3.4 MAP selection for S-GSM-MBM system

Similar to Fig. 1, a system model with N_T transmit antennas, each surrounded with M_{rf} RF mirrors, $M_{rf} > m_{rf}$, which creates $N_{m_T} = 2^{M_{rf}}$ distinct MAPs. The system requires only $2^{m_{rf}}$ MAPs out of the total $2^{M_{rf}}$ possibilities per transmission interval, so as to achieve the required spectral efficiency. Therefore, based on complete channel knowledge at the receiver, a MAP selection algorithm is required to select $2^{m_{rf}}$ MAPs out of $2^{M_{rf}}$ MAPs for each transmit unit. The index of the chosen MAPs is relayed to the transmitter via a perfect feedback link for the next transmission interval. RF mirrors that are not used are simply switched OFF, such that only m_{rf} RF mirrors are controlled.

In the literature, different optimization criteria have been investigated. For example, in [13-15], an optimal Euclidean distance-based transmit antenna selection (EDAS) technique was employed to further improve the system reliability, based on the maximization of the minimum Euclidean distance between transmission vectors. However, the method has a high CC.

On this note, in [16-17], a low-complexity sub-optimal antenna selection algorithm based on the maximization of the channel amplitude and minimization of the antenna correlation was proposed in order to reduce the CC of [14-15]. Similarly, in [18], the same algorithm based on [14-15] was employed with a corresponding low-complexity algorithm approach. A trade-off in terms of CC and error performance was demonstrated in the results obtained.
In this section, we investigate the effect of optimal and sub-optimal MAP selection algorithms for the proposed S-GSM-MBM system, employing the following techniques:

a) MAP selection based on EDAS
b) MAP selection based on channel amplitude (norm-based).
c) MAP selection based on channel amplitude and antenna correlation.

Since the CC and memory requirements of $N_a > 2$ are extremely high when applied to S-GSM-MBM, which renders the method impractical. Two actives transmit antennas, i.e. $N_a = 2$ are considered for all MAP selection algorithm considered in this paper.

3.4.1 Euclidean distance-based MAP selection

In this section, an optimal approach to select the MAPs that maximize the minimum Euclidean distance between the transmit vectors is presented. The performance achieved in the system is greatly improved at the cost of high CC and memory requirements. Let $N_s = \binom{N_{m_T}}{N_m}$ denote the number of enumerations of selecting N_m MAPs out of N_{m_T} MAPs for the k^{th} transmit unit. Employing the nearest neighbour approximation similar to [19], the PEP of the GSM system for a given channel is:

$$P(x_q \to x_{\hat{q}}) = \lambda Q\left(\sqrt{\frac{\rho}{N_a} d_{min}^2\left(\boldsymbol{H}_{k_j}\right)}\right) \tag{3-7}$$

where λ is the number of neighbor points, $Q(\cdot)$ is the Gaussian Q-function, $d_{min}^2\left(\boldsymbol{H}_{k_j}\right)$ is the minimum squared Euclidean distance between a pair of symbols given as $\min_{k\in\chi}\left\|\boldsymbol{h}_{k_1}x_q + \boldsymbol{h}_{k_2}x_q - \boldsymbol{h}_{\hat{k}_1}x_{\hat{q}} - \boldsymbol{h}_{\hat{k}_2}x_{\hat{q}}\right\|_F^2$. The minimum Euclidean distance must be maximized in order to improve the error performance of the system by adjusting the transmit parameters of $d_{min}^{2}\left(\boldsymbol{H}_{k_j}\right)$. Hence, the Euclidean distance metric for the S-GSM-MBM system can be formulated as [19]:

$$I_{ED}^{i} = \min_{\substack{k \in \chi \\ q \in 1:M \\ x_q \neq x_{\hat{q}}}} \left\| \boldsymbol{h}_{k_1} x_q + \boldsymbol{h}_{k_2} x_q - \boldsymbol{h}_{\hat{k}_1} x_{\hat{q}} - \boldsymbol{h}_{\hat{k}_2} x_{\hat{q}} \right\|_F^2 \tag{3-8}$$

where $\boldsymbol{h}_{k_j}$ and $\boldsymbol{h}_{\hat{k}_j}$ are the $N_R \times 1$ channel vector gain representing the selected and estimated transmit antennas of the k^{th} combination. The optimal enumeration of MAPs is then chosen based on:

$$I_{selected} = \underset{i \in [1:N_S]}{\operatorname{argmax}} \left(I_{ED}^{i} \right) \tag{3-9}$$

3.4.2 Norm-based MAP selection

In this section, the effect of maximizing the channel amplitude based on the channel that exhibits the highest energy is investigated. The channel vectors are arranged in ascending order such that the channel corresponding to each transmit antenna set with the highest energy is employed for the next transmission interval, such that:

$$\|\boldsymbol{h}_1\|_F^2 \geq \|\boldsymbol{h}_2\|_F^2 \geq \cdots \geq \left\|\boldsymbol{h}_{N_m}\right\|_F^2 \geq \cdots \geq \left\|\boldsymbol{h}_{N_{m_T}}\right\|_F^2 \tag{3-10}$$

The selected N_m MAPs are then employed in the subsequent transmission interval.

3.4.3 Channel amplitude and antenna correlation mirror activation pattern selection

In [16], a low-complexity antenna sub-optimal selection technique is investigated for the SM system, which demonstrates a low CC when compared to the EDAS approach of [18]. This is due to the exhaustive search of the EDAS system between the transmit vectors. Therefore, comparing the optimal MAP selection algorithm presented earlier with a low-complexity MAP selection in S-GSM-MBM system in terms of error performance will be worthwhile. This motivates us to investigate a low-complexity MAP selection based on channel amplitude and antenna correlation in the S-GSM-MBM system.

In the proposed topology, the combination of channel amplitude and antenna correlation is employed, discarding transmit antennas based on low amplitude and high correlation similar to [16], [20]. An algorithm based on the channel amplitude and antenna correlation as applied to S-GSM-MBM proceeds as follows:

Algorithm one

Step 1: Construct an $N_R \times N_{m_T} \times N_T$ channel matrix:

$$\boldsymbol{H} = [\boldsymbol{h}_1 \quad \boldsymbol{h}_2 \quad \cdots \quad \boldsymbol{h}_{N_{m_T}}] \tag{3-11}$$

Step 2: Sort the vectors in (11) by computing the vector norm and arrange them in ascending order.

Step 3: Select the first $N_m + 1$ vectors of the sorted vector, to form the matrix $\boldsymbol{H}$:

$$\boldsymbol{H} = [\boldsymbol{h}_1\ \boldsymbol{h}_2 \ldots \boldsymbol{h}_{N_m+1}] \tag{3-12}$$

Step 4: Compute the angle of correlation [15, 16] for all possible pairs of the MAP combinations $(\boldsymbol{h}_{k_1}, \boldsymbol{h}_{k_2})$:

$$\theta = \arccos\left(\frac{\left|\boldsymbol{h}_{k_1}{}^{H}\boldsymbol{h}_{k_2}\right|}{\left\|\boldsymbol{h}_{k_1}\right\|_F \left\|\boldsymbol{h}_{k_2}\right\|_F}\right) \tag{3-13}$$

where the number of combinations is given by $\binom{N_m+1}{N_a}$.

Step 5: Select the channel gain vector corresponding to the largest correlation (smallest angle), and eliminate the channel gain vector with the smallest vector norm.

The selected channel vector is then relayed to the transmitter via the perfect feedback link and employed in the next transmission interval.

3.5 Numerical analysis and discussion

In this section, the Monte Carlo simulation results obtained for the S-GSM-MBM system is presented. We consider the average BER versus the average SNR in dB. Full knowledge of the channel is assumed at the receiver. In all cases, ML detection is employed.

3.5.1 Average BER performance of S-GSM-MBM system

In Fig. 3-2, the system performance of the S-GSM-MBM scheme is demonstrated. Likewise, the evaluated theoretical ABEP results formulated in Section 3 is presented. We employ the notation $\left(N_T,\ N_{R,}\ M,\ N_a,\ m_{rf}\right)$. A system configuration setting of 4×4, 4-QAM with $N_a = 2$, which yields a spectral efficiency of 8 b/s/Hz is considered in Fig. 3-2. Similarly, a spectral efficiency of 10 b/s/Hz is considered, with a configuration setting of 8×4, 4-QAM. In each setting, unique MAP indices are employed to activate the required RF mirrors. The Monte Carlo simulation results obtained reveal a tight fit with the average theoretical result obtained validating the scheme for both the 8 b/s/Hz and 10 b/s/Hz.

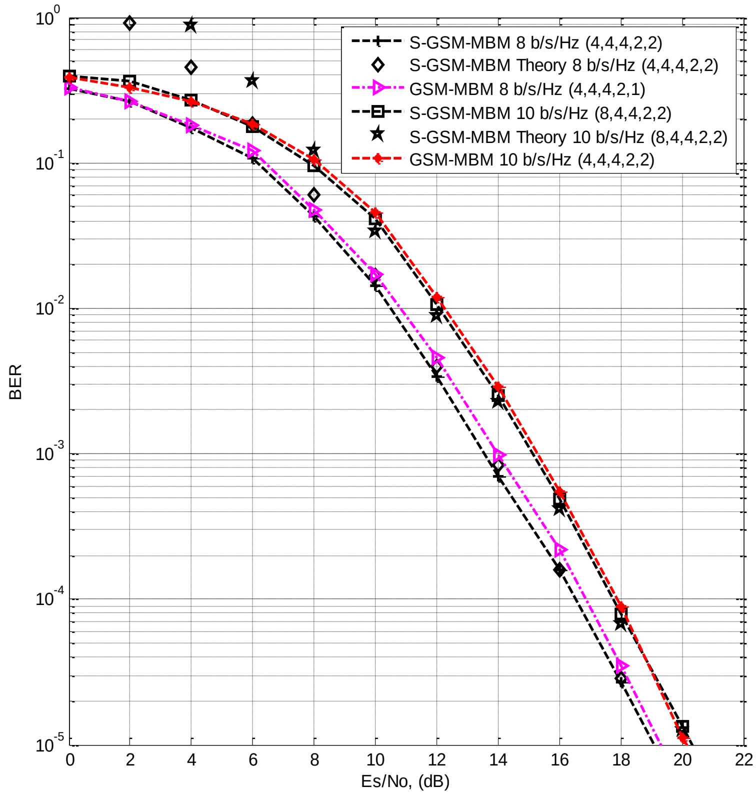

Figure 3.2 BER performance of S-GSM-MBM ($N_a = 2$) for 8 b/s/Hz and 10 b/s/Hz.

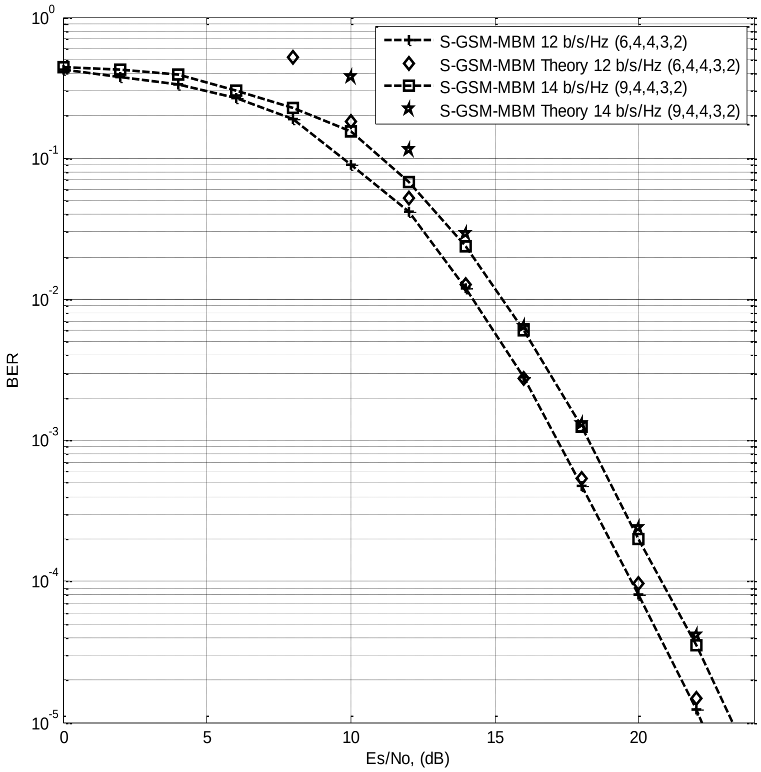

Figure 3.3 BER performance of S-GSM-MBM ($N_a = 3$) for 12 b/s/Hz and 14 b/s/Hz.

In Figure 3.3, the S-GSM-MBM scheme is equipped with three active transmit antennas ($N_a = 3$), considering a 12 b/s/Hz and14 b/s/Hz system. The Monte Carlo simulation results obtained revealed a tight fit with the average theoretical result obtained validating the scheme.

Figure 3.4(a) and Figure 3.4(b) present the performance comparison between the conventional GSM, SM, MB-SM and the proposed S-GSM-MBM system with the same spectral efficiency of 8 b/s/Hz and 10 b/s/Hz, respectively. From the Monte Carlo simulation results obtained, the S-GSM-MBM system outperforms every other scheme considered both in 8 b/s/Hz and 10 b/s/Hz, respectively.

The SNR gain achieved with respect to the proposed S-GSM-MBM system in Figure 4(a) and Figure 4(b), respectively with two active transmit antennas $N_a = 2$, i.e. taking S-GSM-MBM with two active transmit antennas as the reference point to calculate the SNR gain achieved is tabulated in Table 3.3.

Considering the improved error performance achieved in media-based modulation via the selective use of the RF mirrors, which create different channel fade realizations that form the modulation alphabet [9] as against the conventional index modulation schemes, where the transmit antennas create the channel fade realizations.

Therefore, a single transmit antenna with two RF mirrors i.e. $m_{rf} = 2$ around it, will create four different channel fade realization ($2^{m_{rf}} = 4$) as against one channel fade realization in conventional index modulation scheme. Hence, the availability of eight transmit units will exhibit an improved error performance when compared to four transmit units.

It is clearly evident from the Monte Carlo simulation results obtained that employing a media-based modulation technique based on RF mirrors achieved better system performance. At a BER of 10^{-5}, a significant improvement is achieved with an SNR gain of approximately 3.5 dB when compared to MB-SM. In addition, the result of the theoretical framework for each configuration setting also demonstrates a tight fit with the simulation results, which validates the proposed scheme.

The notation $(N_T,\ N_{R,}\ M)$ is employed for the GSM and SM system while notation $(N_T,\ N_{R,}\ M,\ m_{rf})$ and $(N_T,\ N_{R,}\ M, N_a, m_{rf})$ is employed for the MB-SM and S-GSM-MBM configuration settings, respectively.

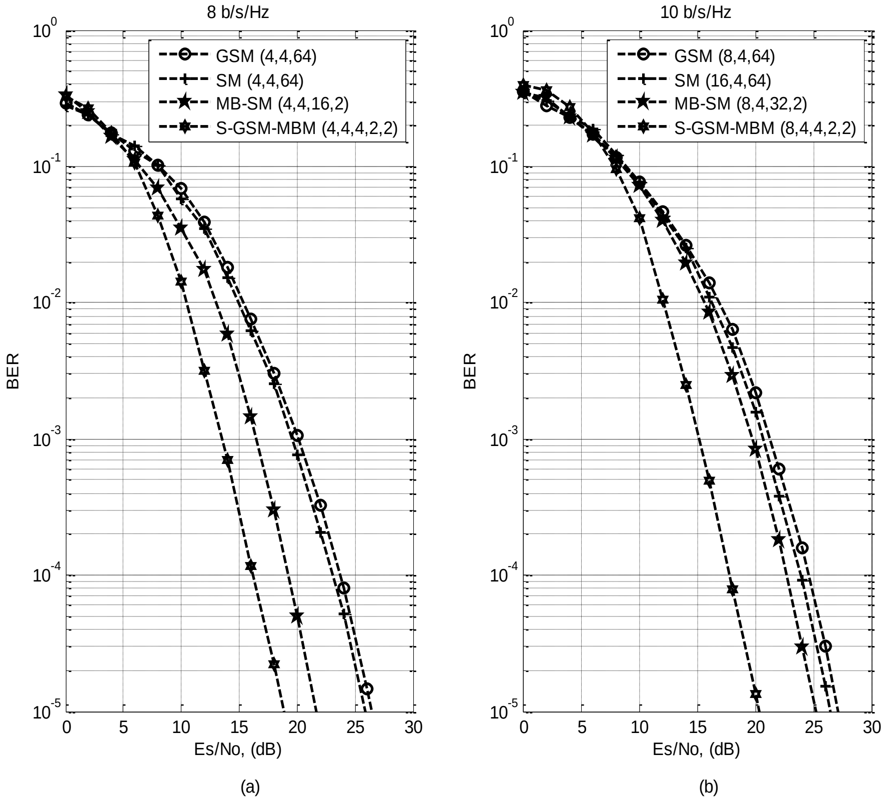

Figure 3.4 BER performance comparison of GSM, SM, MB-SM, and S-GSM-MBM for 8 b/s/Hz and 10 b/s/Hz, respectively.

Table 3.3: SNR gain (dB) achieved, with respect to the S-GSM-MBM system

Schemes	8 b/s/Hz	10 b/s/Hz
GSM	7.5 dB	6.5 dB
SM	6.5 dB	5.5 dB
MB-SM	3.5 dB	5 dB

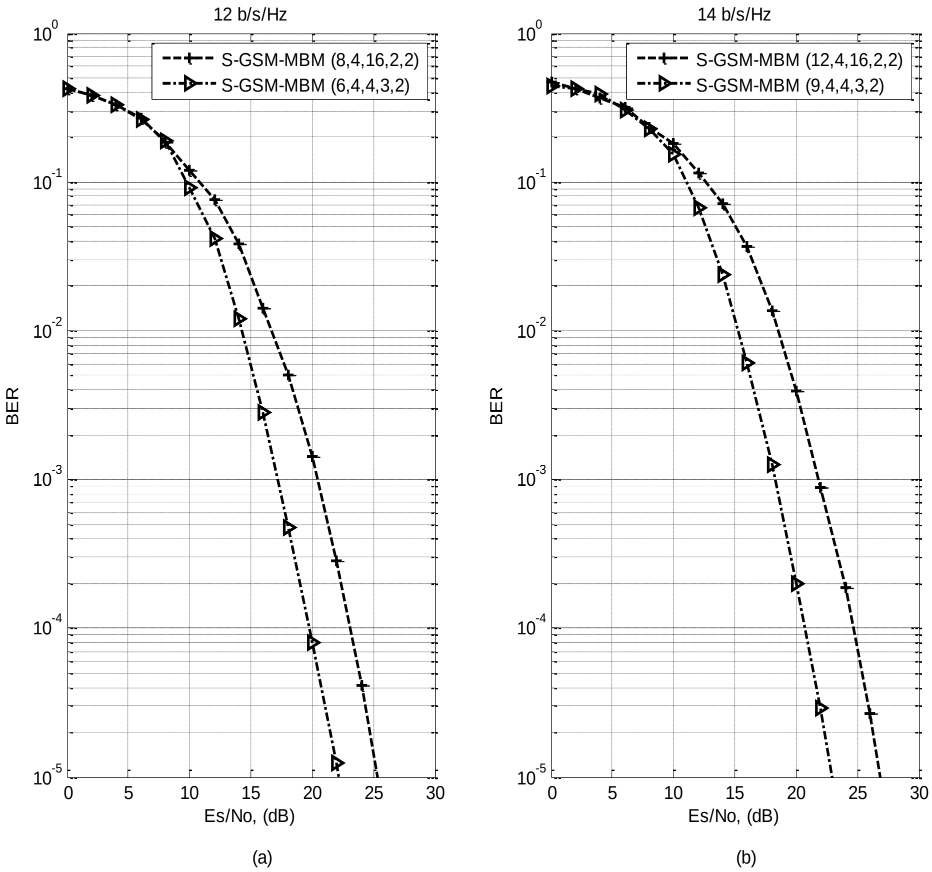

Figure 3.5 BER performance comparison of S-GSM-MBM ($N_a = 3$) and S-GSM-MBM ($N_a = 2$) employing for 12 b/s/Hz and 14 b/s/Hz.

Figure 3.5(a) and Figure 3.5(b) presents the performance comparison between S-GSM-MBM system with $N_a = 3$ and $N_a = 2$ for 12 b/s/Hz and 14 b/s/Hz, respectively. The Monte Carlo simulation results obtained revealed that S-GSM-MBM with $N_a = 3$ outperforms every other scheme considered. The SNR gain achieved with respect to S-GSM-MBM with $N_a = 3$ in Figure 3.5(a) and Figure 3.5(b) is tabulated in Table 3.4.

Table 3.4: SNR gain (dB) achieved, with respect to the S-GSM-MBM with $N_a = 3$.

Schemes	12 b/s/Hz	14 b/s/Hz
S-GSM-MBM ($N_a = 2$)	3.2 dB	3.5 dB

3.5.2 Average BER performance of S-GSM-MBM with MAP selection

Figure 3-6(a) and Figure 3-6(b) presents the Monte Carlo simulation results obtained for the S-GSM-MBM system employing MAP selection algorithm. In the MAP selection algorithm, we considered $N_a = 2$ and $N_R = 2$ with a spectral efficiency of 8 b/s/Hz and 10 b/s/Hz, respectively.

The notation $(N_T,\ N_{R,} M,\ \ m_{rf})$ is employed for the conventional S-GSM-MBM system, while the notation $(N_T,\ N_{R,} M, M_{rf,} m_{rf})$ is employed for the MAP based schemes.

The performance comparison between the conventional MB-SM, S-GSM-MBM and S-GSM-MBM with the MAP selection algorithm is revealed in Fig. 3-6(a) and Fig. 3-6(b), respectively. In the Monte Carlo simulation results obtained, S-GSM-MBM with MAP selection algorithm exhibits a superior performance than the conventional S-GSM-MBM system. However, S-GSM-MBM with the MAP selection algorithm based on EDAS outperforms every other scheme considered. Furthermore, S-GSM-MBM with norm-correlation MAP selection algorithm outperforms the S-GSM-MBM with norm-based MAP selection algorithm. Significant improvement is achieved in terms of error performance in S-GSM-MBM with MAP selection algorithm compared to the conventional S-GSM-MBM system. An SNR gain of approximately 9.5 dB is achieved at a BER of 10^{-5} with respect to EDAS technique when compared to the conventional MB-SM and 8 dB when compared to the S-GSM-MBM system. The SNR gain achieved with respect to S-GSM-MBM with optimal mirror activation pattern (MAP) algorithm (EDAS) with two active transmit antennas $N_a = 2$ in Figure 3.6(a) and Figure 3.6(b) is tabulated in Table 3.5.

Table 3.5: SNR gain (dB) achieved, with respect to the S-GSM-MBM with EDAS.

Schemes	SNR gain of S-GSM-MBM with EDAS	
	8 b/s/Hz	10 b/s/Hz
MB-SM	9.5 dB	8 dB
S-GSM-MBM	8 dB	6 dB
S-GSM-MBM (Norm-based)	6 dB	2 dB
S-GSM-MBM (Norm-Corr)	5.5 dB	1.5 dB

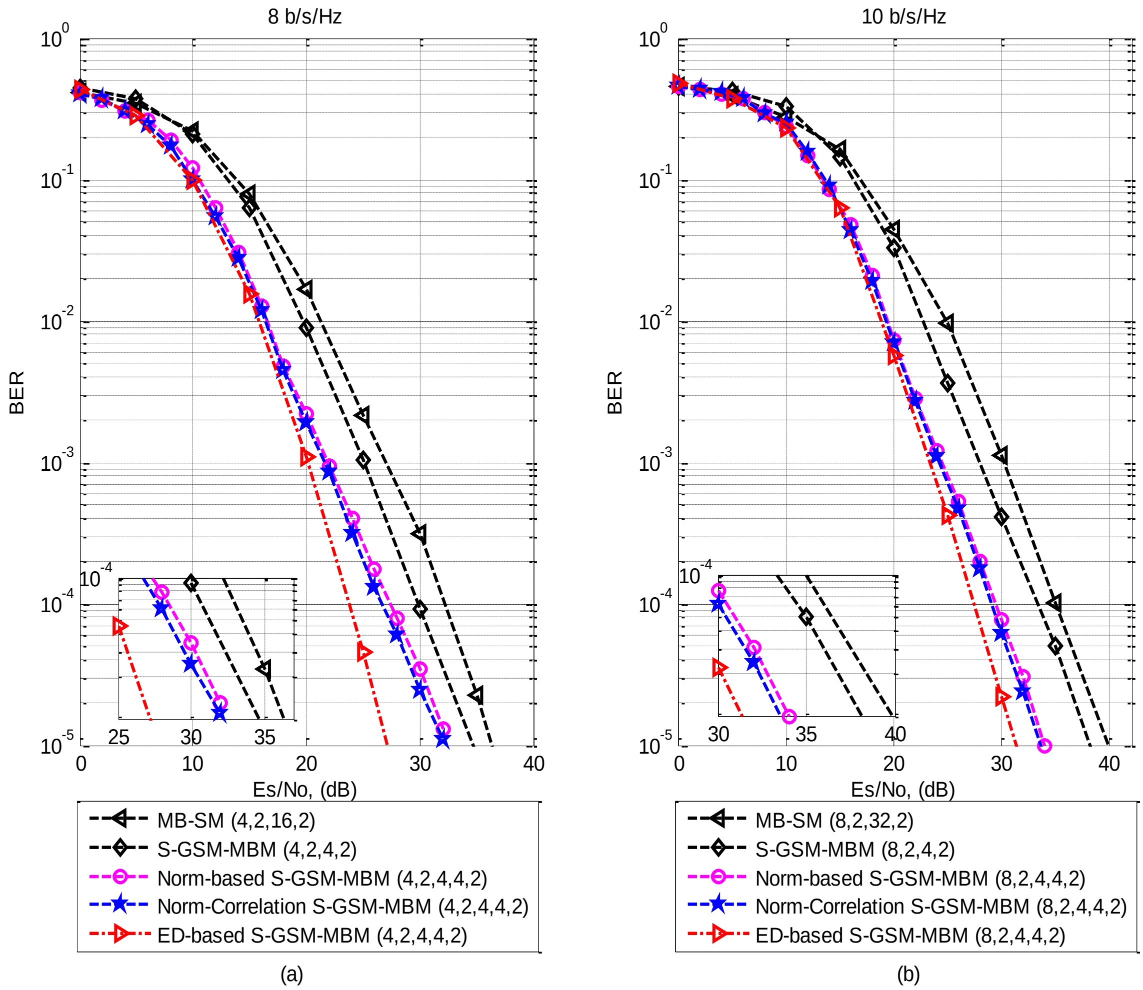

Figure 3.6 BER performance comparison of MB-SM, S-GSM-MBM and S-GSM-MBM with MAP algorithm for 8 b/s/Hz and 10 b/s/Hz.

3.6 Conclusion

In this Chapter, media-based modulation was investigated in the GSM system, based on antenna combination per transmission instant incorporated with RF mirror to enhance the spectral efficiency and improve the error performance of the system. The topology based on the S-GSM-MBM technique exhibits an improved error performance when compared to the conventional GSM, SM and MB-SM system of the same spectral efficiency. Likewise, the effect of MAP selection algorithm has been investigated in the S-GSM-MBM system. The Monte Carlo simulation results obtained revealed a trade-off between the optimal and sub-optimal MAP selection algorithm considered, in terms of the error performance and CC.

References

[1] R. Y. Mesleh, H. Haas, S. Sinanovic, A. Chang Wook, and Y. Sangboh., "Spatial Modulation," *IEEE Transactions on Vehicular Technology,* vol. 57, no 4, pp. 2228-2241, 2008.

[2] P. Wolniansky, G. J. Foschini, D. Golden, and R. Valenzuela, "V-BLAST: an architecture for realizing very high data rates over the rich-scattering wireless channel," in *Proceedings of the International Symposium on Signals, System and Electronics. (ISSSE)*, pp. 295-300, Sep. 1998.

[3] A. Younis, N. Serafimovski, R. Mesleh, and H. Haas, "Generalised spatial modulation," in *Proceedings of the 2010 Conference Record of the Forty-Fourth Asilomar Conference on Signals, Systems and Computers*, pp. 1498-1502, 2010.

[4] W. Jintao, J. Shuyun, and S. Jian, "Generalised Spatial Modulation System with Multiple Active Transmit Antennas and Low Complexity Detection Scheme," *IEEE Transactions on Wireless Communications,* vol. 11, no. 4, pp. 1605-1615, Apr. 2012.

[5] A. Khandani, "Media-based modulation: Converting static Rayleigh fading to AWGN," in *Proceedings of the IEEE International Symposium on Information Theory*, 2014.

[6] N. Pillay, H. Xu, "Quadrature Spatial Media-based Modulation with RF Mirrors," *IET Communications*, vol. 11, no. 16, pp. 2440-2448, Nov. 2017.

[7] N. Pillay, H. Xu, "Uncoded Space-Time Labeling Diversity-Application of Media-based Modulation with RF Mirrors," *IEEE Communications Letters*, vol. 22, no. 2, Feb. 2017.

[8] Y. Naresh and A. Chockalingam.: "On media-based modulation using RF mirrors," in *Proceedings of the Information Theory and Applications Workshop (ITA),* pp. 1-10, Feb. 2016.

[9] Y. Naresh, A. Chockalingam, "On Media-based Modulation using RF Mirrors," *IEEE Transactions on Vehicular Technology,* vol. 66, no. 6, pp. 4967 - 4983, Oct. 2016.

[10] J. R Castillo-Soria, R. Ramirez-Gutierrez, "Generalized Quadrature Spatial Modulation Scheme using Antenna Grouping," *Electronics and Telecommunications Research Institute Journal,* vol. 39, no. 5, pp. 707-717, Oct. 2017.

[11] N. R. Naidoo, H. Xu, and T. Quazi, "Spatial modulation: optimal detector asymptotic performance and multiple-stage detection," *IET Communications*, vol. 5, no. 10, pp. 1368 - 1376, Jul. 2010.

[12] H. Xu, "Symbol error probability for generalized selection combining reception of M-QAM," SAIEE Africa Research Journal, vol. 100, no. 3, pp 68 - 71, Sep. 2009.

[13] N. R. Naidoo, "Performance analysis and enhancement schemes for spatial modulation," MSc Thesis, School of Electrical, Electronics and Computer Engineering, University of KwaZulu-Natal, Dec. 2010.

[14] R. Rajashekar, K. V. S. Hari, and L. Hanzo, "Antenna Selection in Spatial Modulation Systems," *IEEE Wireless Communications Letters,* vol. 17, no. 3, pp. 521-524, Jan. 2013.

[15] N. Pillay, H. Xu, "Comments on "Antenna Selection in Spatial Modulation Systems", *IEEE Wireless Communications Letters,* vol. 17, no. 9, pp. 1681-1683, Aug. 2013.

[16] N. Pillay, H. Xu, "Low-complexity transmit antenna selection schemes for spatial modulation," *IET Communications,* vol. 9, no. 2, pp. 239-248, Jan. 2015.

[17] N. Pillay, H. Xu, "Low Complexity Detection and Transmit Antenna Selection for Spatial Modulation," *SAIEE Africa Research Journal*, vol. 105, no. 1, Mar. 2014.

[18] P. Yang, Y. L. Guan, Y. Xiao, M. Di Renzo, S. Li, and L. Hanzo, "Transmit Pre-coded Spatial Modulation: Maximizing the Minimum Euclidean Distance Versus Minimizing the Bit Error Ratio," *IEEE Transactions on Wireless Communications,* vol. 15, no. 3, pp. 2054-2068, Nov. 2015.

[19] W. Nan, L. Wenlong, M. Hongzhi, J. Minglu, and H. Xu, "Further Complexity Reduction Using Rotational Symmetry for EDAS in Spatial Modulation," *IEEE Communications Letters*, vol. 18, no. 10, pp. 1835-1838, Oct. 2014.

[20] Z. Zhou, N. Ge, and X. Lin, "Reduced-Complexity Antenna Selection Schemes in Spatial Modulation," *IEEE Communications Letters*, vol. 18, no. 1, pp. 14-17, Jan. 2014.

CHAPTER 4

Conference Article 1

This article has been published in the proceedings of SATNAC 2018. The detail is as follows:

S. Oladoyinbo, N. Pillay, H. Xu, "Single-Symbol Generalized Quadrature Spatial Modulation," in *Proceedings of the South African Telecommunication Networks and Applications Conference (SATNAC)* pp. 370-375, Sep. 2018.

Single-Symbol Generalized Quadrature Spatial Modulation

4 Introduction

An innovative form of multiple-input multiple-output (MIMO) system is spatial modulation (SM) [1], which requires a single radio frequency (RF) chain at every transmission interval and improves on the major setbacks experienced in the conventional MIMO system. The basic idea behind SM is the use of a transmit antenna index to convey additional information in conjunction with amplitude/phase modulation (APM). The attractiveness of the SM scheme brought about a great interest in the research community.

The requirement of a large number of transmit antennas to achieve a high data rate in the SM system impose high complexity [2, 3], which limits its practical implementation in terms of complexity/cost. This brought about generalized spatial modulation (GSM) [4], an SM-based scheme, which maps information bits to the index of a transmit antenna combination, allowing a relatively large number of points to be chosen in the spatial constellation. Thus, reducing the required number of transmit antennas for transmission. However, the performance of the GSM system is degraded when compared to the SM system due to the average power effect [4].

Similarly, another criticism of SM is the logarithmic relationship between the number of transmit antennas and the spectral efficiency. This is unlike vertical Bell Laboratories layered space-time architecture (V-BLAST) [5], which has a linear relationship. This brought about an enhanced spectral efficient form of SM called quadrature spatial modulation (QSM) [6].

QSM employs transmit antennas in an innovative manner to convey additional information by extending its spatial dimension to the in-phase and quadrature dimensions. The APM symbol is further decomposed into real and imaginary components. This allows significant enhancement in the overall throughput of the system. Significant improvement in terms of spectral efficiency/error performance is achieved in QSM when compared to SM and single-symbol GSM [4].

QSM maintains the benefit of SM, as outlined earlier, by modulating the decomposed symbol into cosine and sine carriers, respectively, eliminating inter-antenna synchronization and inter-channel interference experienced in the conventional MIMO system, making the system more energy-efficient [7].

Nevertheless, higher data rates are always desirable in wireless communication, but an increase in data rate in these systems requires additional transmit antennas, imposing high complexity.

This led to generalized quadrature spatial modulation (GQSM) [8], which employs a unique symbol transmitted across multi-active transmit antenna groups. The spectral efficiency associated to the GQSM system [8] is $n_b(\log_2(M)+2)$ b/s/Hz, where n_b is the number of transmit antenna groups and M is the APM modulation order. Hence, a $4 \times 4, 4$-QAM configuration setting in GQSM, yields a spectral efficiency of 8 b/s/Hz as against 6 b/s/Hz in the conventional QSM system.

GQSM [8], experiences several limitations, such as the requirement of multiple RF chains, due to simultaneous transmission of unique symbols, imposing high computational complexity (CC). Hence, limiting practical implementation. This motivates us to investigate a single-symbol GQSM (SS-GQSM) scheme, which requires only a single RF chain, thus, imposing a low hardware complexity.

The contributions of this paper are as follows: we investigate the use of an identical symbol set transmitted across a unique transmit antenna group for the proposed SS-GQSM system. This will allow the use of a single RF chain, thereby reducing the complexity of the system. Furthermore, the theoretical average bit error rate (BER) of the proposed scheme is formulated to validate the Monte Carlo simulation results obtained.

Finally, the effect of link adaptation is investigated in the proposed SS-GQSM and multi-symbol GQSM schemes, employing an optimal technique to select the transmit antennas that maximizes the minimum Euclidean distance. Likewise, a sub-optimal low-complexity transmit antenna selection algorithm based on the maximization of the channel amplitude and minimization of the antenna correlation is investigated. This technique exhibits a low CC when compared to the Euclidean distance antenna selection (EDAS) technique, coupled with superior performance when compared to other sub-optimal transmit antenna selection techniques in the literature.

The structure of the remainder of the paper is as follows: In Section II, the proposed SS-GQSM system model is presented and analysis of the average BER is presented in Section III. The formulated CC is presented in Section IV, while the proposed closed-loop SS-GQSM system is presented in Section V. Numerical analysis of the proposed schemes is presented in Section VI, while conclusions are drawn in Section VII.

Notation: Bold italic lowercase/uppercase symbols denote vectors/matrices, while regular letters represent scalar quantities. $\|\cdot\|_F$ represents Frobenius norm, $Q(\cdot)$ represents the Gaussian Q-function, $\underset{w}{\operatorname{argmin}}(\cdot)/\underset{w}{\operatorname{argmax}}(\cdot)$ represents the minimum/maximum value of an argument with respect to w, $\binom{\cdot}{\cdot}$ represents the binomial coefficient, i represents a complex number, $R\{\cdot\}$ represent the real component of the complex number, $|\cdot|$ represents the Euclidean norm, $[\cdot]^T$ represent transpose and $\lfloor\cdot\rfloor$ represents the nearest integer less than the input argument.

4.1 Generalized quadrature spatial modulation

In [8], simultaneous transmission of a unique symbol is introduced to the QSM system termed GQSM, in which n_b symbols are transmitted across n_b transmit antenna groups. The spectral efficiency is given as: $m = n_b(\log_2(M) + 2)$ b/s/Hz, where M is the APM modulation order, n_b is the number of transmit antenna groups, such that each group is equipped with two transmit antennas, i.e. $n_b = \frac{N_T}{2}$. This configuration setting exhibits an improved error performance at the cost of high complexity [8].

4.1.1 Proposed single-symbol generalized quadrature spatial modulation system model

The spectral efficiency m associated to the proposed SS-GQSM is $2n_b + \log_2(M)$ b/s/Hz, for example a 6×4, 16-QAM setting in SS-GQSM requires an 8×4, 16-QAM setting to yield the same spectral efficiency of 10 b/s/Hz in QSM. The $\log_2 M$ bits modulates the vector $\boldsymbol{x}_q^j$, which is further decomposed into real and imaginary components and $2n_b$ bits select the transmit antenna required for transmission. Thereafter, the modulated vector $\boldsymbol{x}_q^j$ is transmitted over a complex channel matrix $\boldsymbol{H}_j$ of dimension $N_R \times N_{T_\ell}$, where N_{T_ℓ} is the number of transmit antennas associated with each group, i.e. $N_{T_\ell} = 2$. The channel $\boldsymbol{H}_j$ is assumed to be independent and identically distributed (i.i.d) with distribution $CN(0,1)$ in the presence of additive white Gaussian noise (AWGN) $\boldsymbol{n}$, of dimension $N_R \times 1$. The $N_R \times 1$ received signal vector $\boldsymbol{y}$ can be defined as:

$$\boldsymbol{y} = \sqrt{\rho/n_b} \sum_{j}^{n_b} \boldsymbol{H}_j \, \boldsymbol{x}_q^j + \boldsymbol{n} \tag{4-1}$$

where $\boldsymbol{x}_q^j$ is further decomposed into real and imaginary components of the form $\boldsymbol{x}_q^j = [\, x_R^{q_j} \; i x_I^{q_j}]^T$ of dimension $N_{T_\ell} \times 1$, $j \in [1\!:\!n_b]$, $q \in [1\!:\!M]$, ρ represents the average signal-to-noise ratio (SNR) at each receive antenna.

Figure 4.1 presents the system model for the SS-GQSM system, where N_T transmit antennas and N_R receive antennas are assumed. Likewise, Table 4.1 presents an illustration of the mapping process for the SS-GQSM system.

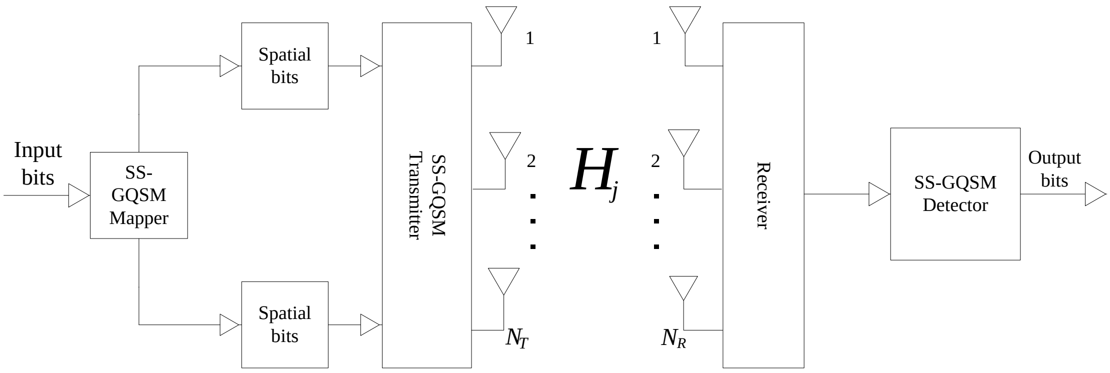

Figure 4.1 System model for the SS-GQSM system.

Table 4.1 Mapping process for the proposed SS-GQSM system

Configuration	Input bits	First	Second	Third	Fourth	Group 1	Group 2	Group 3
	$m = 2n_b +$ $\log_2(M)$ b/s/Hz	Antenna bits	Antenna bits	Antenna bits	$\log_2(M)$ bits	$-$	$-$	$-$
$M = 4$ $N_T = 4$ $n_b = 2$	101101	[10] $N_{T_1} = 2$ $N_{T_2} = 1$	[11] $N_{T_1} = 2$ $N_{T_2} = 2$	$-$	[01] $-1-1i$	$[-1i, -1]$	$[0, -1-1i]$	$-$
$M = 16$ $N_T = 6$ $n_b = 3$	1101011010	[11] $N_{T_1} = 1$ $N_{T_2} = 1$	[01] $N_{T_1} = 1$ $N_{T_2} = 2$	[01] $N_{T_1} = 1$ $N_{T_2} = 2$	[1010] $3-3i$	$[3-3i, 0]$	$[3, -3i]$	$[3, -3i]$

4.1.2 Detection

The received signal vector $\boldsymbol{y}$ of dimension $N_R \times 1$ is demodulated optimally employing maximum likelihood (ML) detection, such that:

$$\left[\hat{j}_1, \cdots, \hat{j}_{n_b}, \boldsymbol{x}_{\hat{q}}^{j}\right] = \underset{\substack{j\in[1:n_b] \\ q\in[1:M]}}{\operatorname{argmin}} \left(\left\| \boldsymbol{y} - \sqrt{\rho/_{n_b}} \sum_{j}^{n_b} \boldsymbol{H}_j \, \boldsymbol{x}_q^j \right\|_F^2 \right) \tag{4-2}$$

$$\left[\hat{j}_1, \cdots, \hat{j}_{n_b}, \boldsymbol{x}_{\hat{q}}^{j}\right] = \underset{\substack{\ell\in[1:n_b] \\ q\in[1:M]}}{\operatorname{argmin}} (\|\boldsymbol{g}\|_F^2 - 2R\{\boldsymbol{y}^H \boldsymbol{g}\}) \tag{4-3}$$

where $\boldsymbol{g} = \boldsymbol{H}_j \, \boldsymbol{x}_q^j$.

4.2 Average BER analysis for Single-Symbol Generalized Quadrature Spatial Modulation

A lower bound approach is employed to formulate the theoretical average BER for the proposed SS-GQSM, based on the analysis of the conventional SM system [3]. Considering identical symbol is transmitted across multi-active antennas/groups. The general expression is given as:

$$\begin{aligned} P_e &\geq 1-((1-P_a)(1-P_b)) \\ &= P_a + P_b - P_a P_b \end{aligned} \tag{4-4}$$

where P_a is the bit error probability of the antenna index given that symbol is perfectly detected and P_b is the bit error probability of the estimated symbol given that the antenna index is perfectly detected.

In the SS-GQSM system, we treat the system as if a single antenna was employed, similar to SM, but the antenna error P_a and symbol error P_b are modified, employing an average SNR $\frac{\rho}{N_T}$ and $\frac{\rho}{n_b}$, respectively, since multi-active transmit antennas convey the APM symbol over n_b antenna groups. These modifications result in a bound of the average BER for the SS-GQSM system.

Therefore, the average BER of the transmit antenna index estimation P_a is evaluated similar to [3] as:

$$P_a \leq \sum_{q=1}^{M}\sum_{j=1}^{N_T}\sum_{\hat{j}=1}^{N_T} \frac{N(j,\hat{j})P\left(\boldsymbol{x}_q^j \rightarrow \boldsymbol{x}_q^{\hat{j}}|\boldsymbol{H}_j\right)}{MN_T\log_2(N_T)} \tag{4-5}$$

where $P\left(\boldsymbol{x}_q^j \rightarrow \boldsymbol{x}_q^{\hat{j}}\right)$ is the conditional pairwise error probability (PEP) of choosing $\boldsymbol{x}_q^j$ given that $\boldsymbol{x}_q^{\hat{j}}$ was transmitted and $N(j,\hat{j})$ is the number of bit errors associated to the transmit antennas.

To obtain the average PEP, we compute the joint probability distribution of the channel gain employing the moment generating function and alternative form of Q-function over a frequency-flat Rayleigh fading channel. The derived PEP of the transmit antenna index P_a, considering the symbol is perfectly detected can be computed similar to [3], employing the triangle inequality rule with some modifications. The closed-form expression for the PEP becomes [3]:

$$P\left(\boldsymbol{x}_q^j \rightarrow \boldsymbol{x}_q^{\hat{j}}|\boldsymbol{H}_j\right) = \mu^{N_R}\sum_{k=1}^{N_R-1}\binom{N_R-1+w}{w}[1-\mu]^w \tag{4-6}$$

where $\mu = \frac{1}{2}\left(1-\sqrt{\frac{\alpha}{\alpha+1}}\right)$ and $\alpha = \frac{\rho}{N_T}|x_R^{q_j} + ix_I^{q_j}|^2$, considering N_T active transmit antennas.

The bit error probability of the symbol P_b can be estimated similar to [3] and [9], assuming the antenna index is perfectly detected.

The closed-form expression of P_b over a frequency-flat Rayleigh fading channel is presented in [3] and [9] as:

$$P_b(k) = \frac{1}{\log_2 M}\left(\frac{a}{c}\left[\frac{1}{2}\left(\frac{2}{b\rho+2}\right)^{N_R} - \frac{a}{2}\left(\frac{1}{b\rho+1}\right)^{N_R} + (1 - a)\sum_{i=1}^{c-1}\left(\frac{2\sin^2\theta}{b\rho+2\sin^2\theta}\right)^{N_R} + \sum_{i=c}^{2c-1}\left(\frac{2\sin^2\theta}{b\rho+2\sin^2\theta}\right)^{N_R}\right]\right) \quad (4\text{-}7)$$

where $a = 1 - \frac{1}{\sqrt{M}}$, $b = \frac{3}{M-1}$, $\theta = \frac{i\pi}{4c}$, c is the number of summations $c > 10$, for convergence of the trapezoidal approximation of the Q-function [10] and $\rho = \frac{\rho}{n_b}$.

4.3 Computational complexity analysis

The receiver complexity of the proposed SS-GQSM system is formulated based on complex multiplications and complex additions of the ML algorithm of (4-2). The ML detector searches over $q \in [1{:}M]$ across n_b antenna groups resulting in 2^m points. Considering the received signal vector $\boldsymbol{y}$ of dimension $N_R \times 1$ with channel matrix $\boldsymbol{H}_j$ of dimension $N_R \times N_{T_\ell}$, $j\epsilon[1{:}n_b]$ and the symbol $\boldsymbol{x}_q^j$ of dimension $N_{T_\ell} \times 1$ across n_b transmit antenna groups. $\boldsymbol{g}$ and $||\boldsymbol{g}||_F^2$ yields $N_R n_b$ complex multiplications and N_R complex multiplications, respectively across M. Resolving $\boldsymbol{y}^H\boldsymbol{g}$ yields N_R complex multiplications and $N_R - 1$ complex additions.

Hence, the receiver complexity of (4-2) for SS-GQSM across n_b groups with 2^m points is:

$$\delta_{SS-GQSM} = 2^m(N_R(Mn_b + 3) - 1) \quad (4\text{-}8a)$$

In addition, GQSM of [8] employs unique symbols across n_b groups. Therefore, the ML detector searches over M^{n_b}. Hence, resolving (2) in [8], $\boldsymbol{g}$ and $||\boldsymbol{g}||_F^2$ yields $N_R n_b M^{n_b}$ complex multiplications and N_R complex multiplications, respectively. Resolving $\boldsymbol{y}^H\boldsymbol{g}$ yields N_R complex multiplications and $N_R - 1$ complex additions. Hence, the receiver complexity of (4-2) for the GQSM of [8] across n_b groups with 2^m points is:

$$\delta_{GQSM[8]} = 2^m(N_R(M^{n_b}n_b + 3) - 1) \quad (4\text{-}8b)$$

Table 4.2 illustrates the complexity comparison of the SS-GQSM and GQSM of [8], employing $N_R = 4$ and $M = 4$ for ML detector of (4-2).

Table 4.2 Receiver complexity comparison for GQSM of [8] and SS-GQSM.

Scheme	8 b/s/Hz $n_b = 2$	12 b/s/Hz $n_b = 2$	12 b/s/Hz $n_b = 3$
SS-GQSM	11,008	176,128	241,664
GQSM [8]	35,584	569,344	831,488

4.4 Improved Single-Symbol Generalized Quadrature Spatial Modulation via Link Adaptation

In this section, N_{Total} transmit antennas are allocated to each group, such that $n_b N_{Total}$ transmit antennas are available and $N_{Total} > N_{T_\ell}$. N_{T_ℓ} transmit antennas is selected for each antenna group at each transmission interval. Considering the CC of $n_b > 2$ is extremely high for the GQSM system rendering the method impractical. We considered $n_b = 2$ for all transmit antenna selection algorithm considered in this paper.

4.4.1 Euclidean distance-based transmit antenna selection

In this sub-section, the effect of EDAS technique is investigated in the SS-GQSM system, improving the performance of the system optimally, based on the transmit antennas that maximize the minimum Euclidean distance. The performance of the system is greatly improved but at a cost of high CC and memory size. $n_b N_{Total}$ transmit antennas are considered, where $N_{Total} > N_{T_\ell}$. Let $N_s = \binom{N_{Total}}{N_{T_\ell}}$, which denotes the number of enumerations of selecting N_{T_ℓ} antennas out of N_{Total} antennas for the ℓ^{th} group. The Euclidean distance metric for selecting the required transmit antenna for the SS-GQSM system can be formulated as [11]:

$$\iota_{ED}^{j} = \min_{\substack{k \in \boldsymbol{\chi} \\ q \in [1:M]}} \left\| \boldsymbol{h}_{j_R} x_R^{q_j} + i\boldsymbol{h}_{j_I} x_I^{q_j} - \boldsymbol{h}_{\hat{j}_R} x_R^{q_j} - i\boldsymbol{h}_{\hat{j}_I} x_I^{q_j} \right\|_F^2 \tag{4-9}$$

where $\boldsymbol{\chi}$ is the set of all transmit antenna combinations, the k^{th} combination is of the form $\left(k_1 \cdots k_{N_{T_\ell}}\right)$. $(\boldsymbol{h}_{j_R}, \boldsymbol{h}_{j_I})$ and $(\boldsymbol{h}_{\hat{j}_R}, \boldsymbol{h}_{\hat{j}_I})$ are the $N_R \times 1$ channel gain vectors representing the selected and estimated transmit antennas of the k^{th} combination, respectively.

The final optimal enumeration of antennas is chosen based on:

$$\iota_{choosen} = \underset{\iota \in [1:N_S]}{\operatorname{argmax}} \left(\iota_{ED}^{j} \right) \tag{4-10}$$

4.4.2 Channel amplitude and antenna correlation-based transmit antenna selection

The sub-optimal transmit antenna selection based on channel amplitude and antenna correlation of [12] is investigated in the SS-GQSM system and GQSM of [8]. This technique demonstrates a low CC when compared to the EDAS technique.

In the proposed topology, the channel vectors are arranged in ascending order such that the channel with the highest energy corresponding to each transmit antenna set is employed for next transmission interval. Such that:

$$\left\| \boldsymbol{h}_{j_1} \right\|_F^2 \geq \left\| \boldsymbol{h}_{j_2} \right\|_F^2 \geq \cdots \geq \left\| \boldsymbol{h}_{j_{N_{Total}}} \right\|_F^2 \tag{4-11}$$

where $\boldsymbol{h}_{j_{N_{Total}}}$, $j \in [1: n_b]$ is the channel gain vector corresponding to the j^{th} antenna group.

Furthermore, antenna correlation, which concept was investigated in [12], discarding transmit antennas based on high correlation is further employed to eliminate the worse channel among the chosen set, employing the angle of correlation [2, 12] for all possible pairs combinations.

$$\theta = \arccos \left(\frac{\left| \overline{\boldsymbol{h}}_{j_1}{}^{H} \overline{\boldsymbol{h}}_{j_2} \right|}{\left\| \overline{\boldsymbol{h}}_{j_1} \right\|_F \left\| \overline{\boldsymbol{h}}_{j_2} \right\|_F} \right) \tag{4-12}$$

where the number of pairs combination is given by $\binom{N_{T_\ell}+1}{n_b}$.

The selected channel vector are relayed to the transmitter via the perfect feedback link and employed in the next transmission interval.

4.5 Numerical analysis

The notation $\left(N_T,\ N_{R,}\, M,\ \ n_b\right)$ is employed for the SS-GQSM and GQSM system of [8] in the Monte Carlo simulation results obtained.

In Figure 4.2, the performance comparison for the GQSM of [8], SS-GQSM and QSM system is presented. The GQSM of [8], SS-GQSM and QSM system are equipped with $4 \times 4, 4$ QAM, $4 \times 4,$ 16-QAM with $n_b = 2$, 6×4, 4-QAM with $n_b = 3$ and 4×4, 16-QAM, respectively, which yields a spectral efficiency of 8 b/s/Hz. The Monte Carlo simulation results obtained reveal that the GQSM of [8] exhibits significant improvement over the SS-GQSM and QSM scheme. However, the SS-GQSM imposes a low CC of approximately 70% reduction over the GQSM of [8].

The trade-off between that GQSM of [8] and the proposed SS-GQSM, in terms of performance and complexity is revealed in the Monte Carlo simulation results obtained and the computed CC in Section IV. As the GQSM of [8] outperform the SS-GQSM at a cost of high CC, at a BER of 10^{-5} at high SNR region, a significant improvement is achieved in 8 b/s/Hz configuration settings with $n_b = 2$ and $n_b = 3$ with an SNR gain of approximately 0.9 dB and 4.8 dB, respectively.

In addition, as the number of group increases, i.e. as the required number of transmit antennas increases the performance of the SS-GQSM is improved compared to the GQSM of [8].

The theoretical average BER result for each setting demonstrates a tight fit with the Monte Carlo simulation results, validating the proposed scheme.

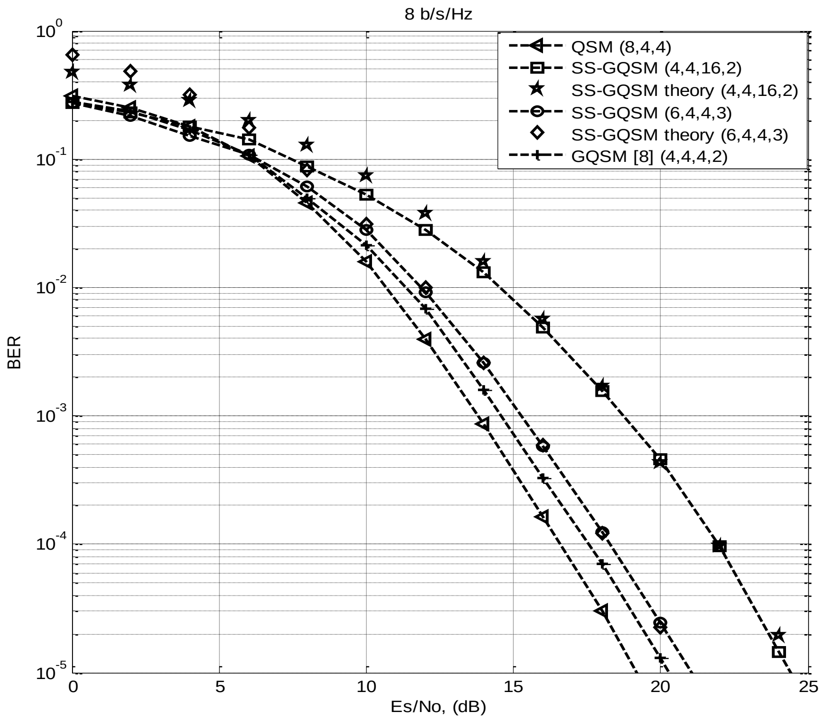

Figure 4.2 BER performance comparison of GQSM, SS-GQSM and QSM for 8 b/s/Hz.

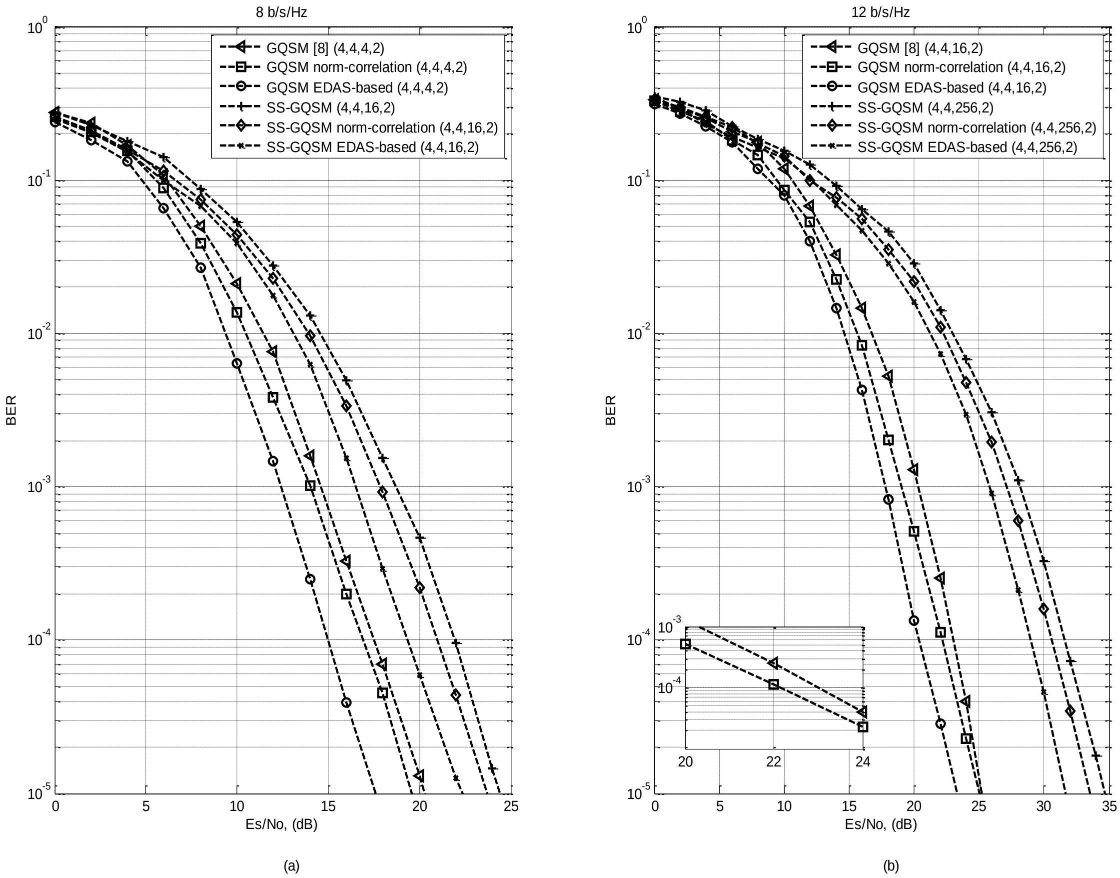

Figure 4.3 BER performance comparison of improved GQSM and improved SS-GQSM for 8 b/s/Hz and 12 b/s/Hz, respectively.

Likewise, the performance comparison for the GQSM of [8] and SS-GQSM is presented in Figure 4.3. The GQSM based on the EDAS technique outperforms the SS-GQSM based on the EDAS technique, norm-correlation based SS-GQSM and norm-correlation based GQSM. Furthermore, GQSM with a norm-correlation based antenna selection algorithm outperforms the SS-GQSM with EDAS based antenna selection algorithm. Significant improvement is achieved in terms of error performance in the GQSM and SS-GQSM scheme with antenna selection algorithm compared to the conventional GQSM and SS-GQSM. An SNR gain of approximately 3 dB is achieved at a BER of 10^{-5} with respect to GQSM based on the EDAS technique when compared to the conventional GQSM and an SNR gain of 2 dB when compared to the SS-GQSM scheme with respect to SS-GQSM based on EDAS technique.

Generating a BER at a high SNR region is difficult and takes time, considering the BER becomes very low in this region. For example, a BER at 10^{-5} means only one bit out of millions of bits will be in error. Therefore, ensuring the results obtained are statistically correct and significant, each SNR of interest we simulate in this paper most generates a prescribed number of errors. As we need about 1000 (or more) errors at each SNR point in the low SNR region and about 100 errors at the high SNR region, to have confidence that our BER is statistically valid.

4.6 Conclusion

The SS-GQSM scheme has been investigated in this Chapter, based on antenna grouping per transmission instant with the requirement of a single RF chain to reduce the complexity of the system. The topology, which is based on the SS-GQSM approach, exhibits a low CC when compared to the GQSM system of [8] with the same spectral efficiency. Likewise, the effect of link adaptation has been investigated in the SS-GQSM system. The Monte Carlo simulation results obtained reveal a trade-off in the optimal and sub-optimal transmit selection algorithm considered in terms of the error performance and CC.

References

[1] R. Y. Mesleh, H. Haas, S. Sinanovic, A. Chang Wook, and Y. Sangboh, "Spatial Modulation," *IEEE Transactions on Vehicular Technology,* vol. 57, no. 4, pp. 2228-2241, Jul. 2008.

[2] N. Pillay, H. Xu, "Low Complexity Detection and Transmit Antenna Selection for Spatial Modulation," *SAIEE Africa Research Journal,* vol. 105, no. 1, pp. 4-12, Mar. 2014.

[3] N. R. Naidoo, H. Xu, T. Quazi, "Spatial modulation: optimal detector asymptotic performance and multiple-stage detection," *IET Communications,* vol. 5, no. 10, pp. 1368 - 1376, Jul. 2010.

[4] A. Younis, N. Serafimovski, R. Mesleh, and H. Haas, "Generalised spatial modulation," in *Proceedings of the Conference Record of the Forty Fourth Asilomar Conference on Signals, Systems and Computers*, pp. 1498-1502, 2010.

[5] P. Wolniansky, G. J. Foschini, D. Golden, and R. Valenzuela, "V-BLAST: an architecture for realizing very high data rates over the rich-scattering wireless channel," in *Proceedings of the International Symposium on Signals, System and Electronics. (ISSSE 98),* pp. 295-300, Sep. 1998.

[6] R. Mesleh, S. S. Ikki, H. M. Aggoune, "Quadrature Spatial Modulation," *IEEE Transactions on Vehicular Technology,* vol. 64, no. 6, pp. 2738-2742, Jul. 2014.

[7] J. Jeganathan, A. Ghrayeb, L. Szczecinski, "Spatial modulation: optimal detection and performance analysis," *IEEE Wireless Communications Letters,* vol. 12, no. 8, pp. 545-547, Aug. 2008.

[8] F.R Castillo-Soria, R. Ramirez-Gutierrez, "Generalized Quadrature Spatial Modulation Scheme using Antenna Grouping," *Electronics and Telecommunications Research Institute*, vol. 39, no. 5, pp. 707-717, Oct. 2017.

[9] H. Xu, "Symbol error probability for generalized selection combining reception of M-QAM," *SAIEE Africa Research Journal*, vol. 100, no. 3, pp. 68 - 71, Sep. 2009.

[10] E. Basar, U. Aygolu, "Full-rate full-diversity STBCs for three and four transmit antennas," *Electronics Letters*, vol. 44, no. 18, pp. 1076-1077, Aug. 2008.

[11] S. Naidu, N. Pillay, H. Xu, "Transmit Antenna Selection Schemes for Quadrature Spatial Modulation," *Wireless Personal Communications*, vol. 99, no. 1 pp. 299–317, Nov. 2017.

[12] N. Pillay, H. Xu, "Low-complexity transmit antenna selection schemes for spatial modulation," *IET Communications*, vol. 9, no. 2, pp. 239-248, Jan. 2015.

CHAPTER 5

Conference Article 2

This is article is ready for submission to IEEE INFOCOM 2021: IEEE International Conference on Computer Communications 2021. The detail is as follows:

S. Oladoyinbo, N. Pillay, H. Xu, “Generalised Quadrature Spatial Modulation in Two-way Decode-and-Forward Relaying Cooperative Networks,” [*Ready for submission to IEEE International Conference on Computer Communications 2021*].

Generalised Quadrature Spatial Modulation in Two-way Decode-and-Forward Relaying Cooperative Networks

5 Introduction

Tremendous promise has been shown over the years with regards to the high-capacity transmission and improved link reliability in multiple-input multiple-output (MIMO) systems [1]. This has led to several innovative forms of MIMO schemes being proposed in the literature [2-5].

An example to consider is spatial modulation (SM) [2], an improved MIMO scheme, which requires only a single radio frequency (RF) chain per transmission interval and improves upon the major setbacks experienced in the conventional MIMO systems. The basic idea behind SM is the use of a transmit antenna index to convey additional information in conjunction with the amplitude/phase modulation (APM). However, the requirements of a large number of transmit antennas to achieve a high data rate in SM limits its practical implementation in terms of complexity/cost. This brought about generalized spatial modulation (GSM) [3].

GSM is an SM-based scheme, which maps information bits to the index of a transmit antenna combination, allowing a relatively large number of points to be chosen in the spatial constellation. This reduces the number of transmit antennas required for transmission. However, the system performance of GSM is degraded when compared to SM due to the average power effect [3].

Similarly, in the study of Jinlin *et al.* [4], a multi-symbol GSM system (M-GSM) was proposed, where multiple APM symbols are transmitted via the selected transmit antenna combination. It is evident from the Monte Carlo simulation results obtained [5] that M-GSM achieves a significant improvement in terms of error performance over the conventional GSM system. However, M-GSM requires multiple RF chains, which impose high system complexity; hence, limiting practical implementation. This led to an enhanced spectral efficient form of SM called quadrature spatial modulation (QSM) [5].

QSM employs transmit antennas in an innovative manner to convey additional information by extending its spatial dimension to the in-phase and quadrature dimensions. The APM symbol employed in QSM is decomposed into its real and imaginary components, which are modulated into cosine and sine carriers, respectively. QSM requires a single RF chain and is more energy-efficient compared to GSM. Furthermore, QSM exhibits an improved error performance compared to SM and GSM [3].

More recently, an improved spectral efficient QSM scheme termed generalized quadrature spatial modulation (GQSM) was proposed [6]. In GQSM, the available transmit antennas are divided into n_b groups, which transmits a unique symbol across the multi-active transmit antenna groups. The data rate associated with the GQSM system [7] is $n_b(\log_2 M + N_{T_\ell})$ b/s/Hz, where n_b is the number of transmit antenna groups, N_{T_ℓ} is the number of transmit antennas in each group and M is the APM modulation order. A GQSM scheme requires 4 transmit antennas coupled with 4-quadrature amplitude modulation (QAM) to achieve a data rate of 8 b/s/Hz. The same configuration settings in the conventional QSM system yields a data rate of 6 b/s/Hz. Hence, GQSM achieves a relatively high data rate with few transmit antennas when compared with SM, GSM, M-GSM and QSM [6].

Cooperative relay-based communication systems have shown tremendous promise in terms of enhancing link reliability. This is achieved by employing multiple relay nodes (active or passive nodes) available in the communication network as a virtual antenna to transmit user information [7].

The commonly known cooperative relay configurations are decode-and-forward (DF) and amplify-and-forward (AF) [7]. In DF, the received signal at the relay node is decoded and re-transmitted to the destination. Similarly, in AF, the received signal at the relay node is firstly amplified then forwarded to the destination. In both cases, the communication between the source and the target node is conducted over two-time slots/phases [8]. Thus, enhancing the reliability of the system.

Motivation: In the literature [8-11], two -way relaying has been proven as a spectral efficient relaying scheme. This technique employs two or more source nodes, which are allowed to simultaneously transmit a message block to the relay node. The relay node estimates the received signal and applies the network coding principle on the received messages, such that one data block is extracted and transmitted towards all source nodes. Each source node can then obtain the message block of the other node via reversing the operation performed at the relay [8].

In the study of Asil *et al.* [9], a two-way relaying technique was investigated in SM to improve the error performance of the conventional SM system. This was achieved by employing the multiple relay nodes available in the network as a virtual antenna to improve the error performance of the system coupled with improved spectral efficiency.

Similarly, in [8], the two-way DF relaying technique is investigated in QSM. This exhibits significant improvement over the conventional QSM and one-way DF-QSM relaying system in terms of error performance. Meanwhile, as stated earlier, GQSM exhibits several advantages over QSM, such as the requirement of fewer transmit antennas to achieve a high data rate. Likewise, GQSM outperforms QSM in terms of error performance. Hence, two-way DF-GQSM is expected to outperform two-way DF-QSM in terms of error performance. This motivates us to investigate two-way DF relaying with GQSM.

Contributions: The contributions of this paper are as follows: a) We investigate the two-way DF relaying technique with two source nodes, which simultaneously transmit a message block to the relay node employing the GQSM modulation technique. The received signal at the relay node is decoded, employing a maximum-likelihood (ML) detection algorithm and a network coding principle is employed to formulate a new message block, which is forwarded towards all source nodes. Each source node can then obtain the message block of the other node via network coding.

b) Secondly, we investigate one-way DF relaying for GQSM as a benchmark by transmitting information from a single node to the relay node. The received signal at the relay node is DF to the destination node over two-time slots/phases.

The structure of the remainder of the paper is as follows: In Section 5.1, the system model of the proposed scheme is presented. The one-way relaying DF for GQSM is presented in Section 5.2 and numerical analysis of the proposed scheme is presented in Section 5.3, while conclusions are drawn in Section 5.4.

Notation: Bold italic lowercase/uppercase symbols denote vectors/matrices, while regular letters represent scalar quantities. $\|\cdot\|$ represents Frobenius norm, $\mathrm{Q}(\cdot)$ represents the Gaussian Q-function, $\underset{w}{\operatorname{argmin}}(\cdot)\backslash\underset{w}{\operatorname{argmax}}(\cdot)$ represents the minimum/maximum value of an argument with respect to *w*, $\binom{\cdot}{\cdot}$ represents the binomial coefficient, $|\cdot|$ represents the Euclidean norm, $\oplus$ represents the XOR operator, $E\{\cdot\}$ is the expectation operator and $[\cdot]^T$ represents transpose.

5.1 System model

In two-way DF-GQSM, data transmission is performed over two-time slots/phases, namely, the transmission phase and the relaying phase. In the transmission phase, both source nodes (Node A and Node B) transmit its message blocks $\boldsymbol{x}_A$ and $\boldsymbol{x}_B$ to the relay node (Node R), simultaneously.

The transmitted message blocks from Node A and Node B are detected optimally at the relay node. After that, network coding is employed to pre-code the estimated bits to generate a new message block $\boldsymbol{x}_R$. This is transmitted to both source nodes (Node A and Node B), simultaneously, in the relaying phase, such that Node R is the source node, while Node A and Node B represent the destination nodes.

Figure 4.1 presents the system model of a half-duplex two-way DF relaying scheme for GQSM, which consists of two source nodes (Nodes A and Node B), exchanging information via Node R.

Node A, Node B and Node R are equipped with N_{T_A}, N_{T_B} and N_{T_R} transmit antennas, respectively, coupled with the same number of RF chains. Likewise, the number of receive antennas is denoted as N_{R_A}, N_{R_B}, N_{R_R} for Node A, Node B and Node R, respectively, coupled with the same number of RF chains. The antennas used for transmission in one phase are also used for reception in the other phase. In both phases, the GQSM transmission model is employed to transmit the message block.

For ease of presentation, we consider a typical system model of the conventional GQSM system [6], which consists of a transmitter (source) as Node X and a receiver (destination) as Node Y. The source node is equipped with N_{T_X} transmit antennas and the destination node is equipped with N_{R_Y} receive antennas. The total number of transmit antennas available in the system N_{T_X} are divided into n_b, i.e. $n_b = \frac{N_{T_X}}{2}$ transmit antenna groups, such that each group is equipped with 2 transmit antennas. The spectral efficiency associated with the GQSM scheme is given as: $m = n_b(\log_2 M + 2)$ b/s/Hz, where M is the M-QAM modulation order.

In each group, $\log_2 M$ bits modulate the M-QAM symbol and the remaining 2 bits is mapped to the transmit antenna indices corresponding to the group, such that $n_b \log_2 M$ bits modulate n_b M-QAM symbols and $2n_b$ bits are mapped to the transmit antenna indices across all groups. If the indices of the transmit antennas of a group are different, the M-QAM symbol of that group is decomposed into its real and imaginary components. Therefore, each transmit antenna corresponding to that group transmits either the real (x_{Re}) or the imaginary (x_{Im}) component of the decomposed symbol, such that $E\{|x_{Re} + ix_{Im}|^2\} = 1$.

However, if the transmit antenna selected to transmit the real (x_{Re}) and the imaginary (x_{Im}) component of the M-QAM symbol of a group is the same; then, the symbol is transmitted as an undecomposed symbol. Hence, $x_{Re} + x_{Im}$ is transmitted via the selected transmit antenna and the other transmit antenna is silent. The complete transmission message block: $\boldsymbol{x}_X = \left[\boldsymbol{x}_X^1 \cdots \boldsymbol{x}_X^{n_b}\right]^T$ of dimension $N_{T_X} \times 1$, which is composed of a concatenated output of all groups, where $\boldsymbol{x}_X^{\ell}$, $\ell \epsilon [1{:}\, n_b]$ of dimension 2×1, is the message vector corresponding to the ℓ^{th} group.

Taking an example of a GQSM system with the following configuration settings: $M = 4, N_{T_X} = 4, \text{i.e.}\, n_b = 2$, a spectral efficiency of 8 b/s/Hz is yielded. Assuming the input bits $m =$ [0 0 1 1 0 1 0 1], the first 4 bits, i.e. [0 0 1 1] are employed in Group 1 and the last 4 bits, i.e. [0 1 0 1] are employed in Group 2, such that the first two bits [0 0] in Group 1 and the first two bits [0 1] in Group 2 selects the 4-QAM symbol $-1 + i1$ for Group 1 and $-1 - i1$ for Group 2, respectively. Likewise, the last two bits [1 1] in Group 1 and the last two bits [0 1] in Group 2 selects the required transmit antennas for Group 1 and Group 2, respectively. Based on the input bits, the message vector in Group 1 given by $\boldsymbol{x}_X^1$ is $[0, -1 + i1]^T$, considering the transmit antenna indices are the same. Likewise, the message vector in Group 2 given by $\boldsymbol{x}_X^2$ is $[-1, -i1]^T$, considering the transmit antenna indices are different. Thus, $\boldsymbol{x}_X = [0, -1 + i1, -1, -i1]^T$.

The message block $\boldsymbol{x}_X$ is transmitted over a Rayleigh frequency-flat fading channel represented by the complex channel gain matrix $\boldsymbol{H}_{Y_X}$ of dimension $N_{R_Y} \times N_{T_X}$ with independent and identically distributed (i.i.d) entries and CN(0,1) distribution. The modulated message block is received in the presence of additive white Gaussian noise (AWGN) $\boldsymbol{n}_Y$ of dimension $N_{R_Y} \times 1$ with CN(0,1) i.i.d entries. Hence, the received signal vector $\boldsymbol{y}_Y$ at Node Y can be written similar to [8] as:

$$\boldsymbol{y}_Y = \sqrt{\frac{\rho}{n_b}} \boldsymbol{H}_{Y_X} \boldsymbol{x}_X + \boldsymbol{n}_Y \tag{5-1}$$

where $\frac{\rho}{n_b}$ represents the average signal-to-noise ratio (SNR).

The message block is detected optimally employing the ML detector at Node Y, which searches the entire signal space of constellation points and all possible transmit antenna indices. The ML detector is defined as:

$$[\hat{\boldsymbol{x}}_X] = \underset{\boldsymbol{x}_X \epsilon \boldsymbol{X}_X}{\operatorname{argmin}} \left\| \boldsymbol{y}_Y - \sqrt{\frac{\rho}{n_b}} \boldsymbol{H}_{Y_X} \boldsymbol{x}_X \right\|_F^2 \tag{5-2}$$

where $\boldsymbol{X}_X$ is the set of all possible message blocks from Node X.

Now we extend the above GQSM transmission model to the two-way DF-GQSM relaying scheme.

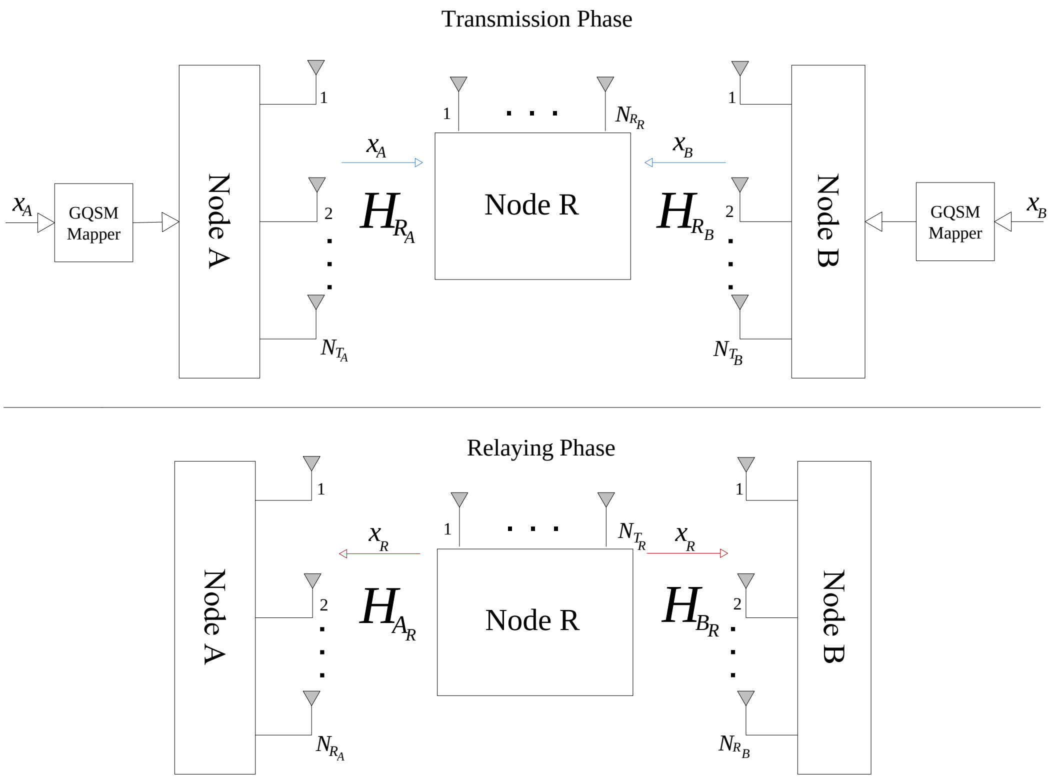

Figure 5.1 System model of the proposed two-way DF-GQSM relaying system

5.1.1 Phase 1: Transmission phase

In the transmission phase, Node A and Node B simultaneously transmit m bits to Node R employing the GQSM modulation technique. The input bits $\boldsymbol{a} = [a_1, \cdots, a_m]$ at the source Node A with the length given by n_b $(\log_2 M_A + 2)$ bits, where M_A is the M_A-QAM modulation order employed at Node A is mapped to the message block $\boldsymbol{x}_A$. Likewise, the input bits $\boldsymbol{b} = [b_1, \cdots, b_m]$ at the source Node B with the length given by n_b $(\log_2 M_B + 2)$ bits, where M_B is the M_B-QAM modulation order employed at Node B is mapped to the message block $\boldsymbol{x}_B$. The received message blocks at the relay node from both source nodes are decoded, resulting in an estimate of $2m$ bits.

In a situation where the number of transmit antennas $N_{T_A} \neq N_{T_B}$, the modulation orders M_A and M_B are adapted accordingly, such that the target spectral efficiency is achieved.

The modulated message block is transmitted over a Rayleigh frequency-flat fading channel represented as $\boldsymbol{H}_{R_A}$ and $\boldsymbol{H}_{R_B}$ of dimension $N_{R_R} \times N_{T_A}$ and $N_{R_R} \times N_{T_B}$ for Node A and Node B, respectively, with i.i.d entries and CN(0,1) distribution. The message blocks $\boldsymbol{x}_A$ and $\boldsymbol{x}_B$ are received in the presence of AWGN $\boldsymbol{n}_R$ of dimension $N_{R_R} \times 1$ with i.i.d entries and CN(0,1) distribution. Hence, the received signal vector $\boldsymbol{y}_R$ at Node R can be written as:

$$\boldsymbol{y}_R = \sqrt{\frac{\rho_A}{n_b}}\,\boldsymbol{H}_{R_A}\,\boldsymbol{x}_A + \sqrt{\frac{\rho_B}{n_b}}\,\boldsymbol{H}_{R_B}\,\boldsymbol{x}_B + \boldsymbol{n}_R \tag{5-3}$$

where $\frac{\rho_A}{n_b}$ and $\frac{\rho_B}{n_b}$ represents the average SNR corresponding to the transmission from Node A and Node B, respectively, $\boldsymbol{H}_{R_A}$ and $\boldsymbol{H}_{R_B}$ represents the complex channel matrices corresponding to Node A and Node B, respectively. An ML detector is employed to estimate the transmitted message block from the received signal vector $\boldsymbol{y}_R$ at the relay node and is defined as:

$$[\widehat{\boldsymbol{x}}_A, \widehat{\boldsymbol{x}}_B] = \underset{\substack{\boldsymbol{x}_A \epsilon\, \boldsymbol{X}_A \\ \boldsymbol{x}_B\, \epsilon\, \boldsymbol{X}_B}}{\operatorname{argmin}} \left\| \boldsymbol{y}_R - \left(\sqrt{\frac{\rho_A}{n_b}}\boldsymbol{H}_{R_A}\boldsymbol{x}_A + \sqrt{\frac{\rho_B}{n_b}}\boldsymbol{H}_{R_B}\boldsymbol{x}_B \right) \right\|_F^2 \tag{5-4}$$

where $\boldsymbol{X}_A$ and $\boldsymbol{X}_B$ are the set of all possible transmission vectors corresponding to Node A and Node B, respectively.

5.1.2 Phase 2: Relaying Phase

In the relaying phase, the relay pre-codes the estimated bits employing an XOR operation to generate the bits $\boldsymbol{r} = [r_1, \cdots, r_m]$ using [8]:

$$\boldsymbol{r} = \widehat{\boldsymbol{a}} \oplus \widehat{\boldsymbol{b}} \tag{5-5}$$

where $\widehat{\boldsymbol{a}}$ and $\widehat{\boldsymbol{b}}$ are the estimated bits for Node A and Node B, respectively at Node R. The vector $\boldsymbol{r}$ bits modulates the block $\boldsymbol{x}_R$, which is forwarded to both nodes (Node A and Node B) at the second time-slot/phase, employing the GQSM modulation technique. This is transmitted from Node R over a Rayleigh frequency-flat fading channel represented as a complex channel matrices $\boldsymbol{H}_{A_R}$ and $\boldsymbol{H}_{B_R}$ for Node A and Node B of dimension $N_{R_A} \times N_{T_R}$ and $N_{R_B} \times N_{T_R}$, respectively, with i.i.d entries as CN(0,1). The message block is received in the presence of AWGN $\boldsymbol{n}_A$ and $\boldsymbol{n}_B$ for Node A and Node B, respectively, with i.i.d entries as CN(0,1) of dimension $N_{R_A} \times 1$ and $N_{R_B} \times 1$, respectively. The $N_{R_A} \times 1$ and $N_{R_B} \times 1$ received signal vectors $\boldsymbol{y}_A$ and $\boldsymbol{y}_B$ at Node A and Node B, respectively, can be written as:

$$\boldsymbol{y}_A = \sqrt{\frac{\rho_{R_A}}{n_b}}\,\boldsymbol{H}_{A_R}\boldsymbol{x}_R + \boldsymbol{n}_A \tag{5-6}$$

$$\boldsymbol{y}_B = \sqrt{\frac{\rho_{R_B}}{n_b}}\,\boldsymbol{H}_{B_R}\boldsymbol{x}_R + \boldsymbol{n}_B \tag{5-7}$$

where $\frac{\rho_{R_A}}{n_b}$ and $\frac{\rho_{R_B}}{n_b}$ denotes the received SNR from the relay corresponding to Node A and Node B, respectively. $\boldsymbol{H}_{A_R}$ and $\boldsymbol{H}_{B_R}$ are the Rayleigh frequency-flat fading channels between the relay and the source for Nodes A and Node B, respectively. An ML detection algorithm is employed to detect the transmitted message block at both nodes. This is defined accordingly as:

$$[\hat{\boldsymbol{x}}_{R_A}] = \underset{x_R \in \boldsymbol{X}_R}{\operatorname{argmin}} \left\| \boldsymbol{y}_A - \sqrt{\frac{\rho_{R_A}}{n_b}} \boldsymbol{H}_{A_R} \boldsymbol{x}_R \right\|_F^2 \tag{5-8}$$

$$[\hat{\boldsymbol{x}}_{R_B}] = \underset{x_R \in \boldsymbol{X}_R}{\operatorname{argmin}} \left\| \boldsymbol{y}_B - \sqrt{\frac{\rho_{R_B}}{n_b}} \boldsymbol{H}_{B_R} \boldsymbol{x}_R \right\|_F^2 \tag{5-9}$$

where $\boldsymbol{X}_R$ is the set of all possible message blocks from Node R. The detected vector is mapped to the corresponding bit block for each node. Let $\hat{\boldsymbol{r}}_A$ represent the obtained bits block at Node A and $\hat{\boldsymbol{r}}_B$ be the obtained bits block at Node B. An estimated version of the transmitted bits can be extracted from the other node by performing an XOR operation with its own transmitted bits, such that [8]:

$$C_A = \hat{\boldsymbol{r}}_A \oplus \boldsymbol{a} \tag{5-10}$$

$$C_B = \hat{\boldsymbol{r}}_B \oplus \boldsymbol{b} \tag{5-11}$$

where C_A is the estimated version of $\boldsymbol{b}$ obtained at Node A and C_B is the estimated version of $\boldsymbol{a}$ obtained at Node B, thus, estimating the $2m$ bits.

In the next sub-section, we investigate one-way DF relaying for the GQSM scheme, which will serve as a benchmark for comparison with the two-way DF-GQSM relaying technique.

5.2 Benchmark: One-way DF relaying for DF-GQSM

In one-way DF relaying, Node A transmits its message block to Node R. The message block is decoded at Node R and then transmitted to the destination (Node B). The spectral efficiency associated to one-way DF-GQSM relaying is $m = \frac{n_b\,(\log_2 M_A + 2)}{2}$ b/s/Hz, where M_A is the M_A-QAM modulation order employed at Node A.

Note, in two-way DF-GQSM relaying, the spectral efficiency was given by $n_b(\log_2 M_A + 2)$ b/s/Hz. Hence, for identical spectral efficiency, a higher modulation order or a larger number of transmit antennas are required in the one-way relaying technique.

Considering an example of a two-way DF-GQSM system with the following configuration settings: $M_A = 4, N_{T_A} = 4, n_b = \frac{N_{T_A}}{2} = 2$, this yields a spectral efficiency of 8 b/s/Hz. In one-way DF-GQSM relaying, the following configuration settings are required to match the spectral efficiency of the two-way DF-GQSM relaying: $M_A = 64, N_{T_A} = 4, n_b = \frac{N_{T_A}}{2} = 2$.

In the first time-slot/transmission phase, the complete transmission message block $\boldsymbol{x}_A$ of dimension $N_{T_A} \times 1$ modeled earlier in Section 5.1 is transmitted from Node A to Node R over a Rayleigh frequency-flat fading channel $\boldsymbol{H}_{R_A}$ of dimension $N_{R_R} \times N_{T_A}$ with entries modeled as i.i.d complex Gaussian random variables with distribution CN(0,1). The message block is received in the presence of AWGN $\boldsymbol{n}_R$ of dimension $N_{R_R} \times 1$ with i.i.d entries distributed as CN(0,1). Therefore, the $N_{R_R} \times 1$ received message block $\boldsymbol{y}_R$ at the relay can be written as:

$$\boldsymbol{y}_R = \sqrt{\frac{\rho_A}{n_b}} \boldsymbol{H}_{R_A} \boldsymbol{x}_A + \boldsymbol{n}_R \tag{5-12}$$

The message block is detected optimally at the relay node employing the ML detection algorithm to estimate the transmitted message block. The ML detector is defined as:

$$[\hat{\boldsymbol{x}}_A] = \underset{\boldsymbol{x}_A \in \boldsymbol{X}_A}{\operatorname{argmin}} \left\| \boldsymbol{y}_R - \sqrt{\frac{\rho_A}{n_b}} \boldsymbol{H}_{R_A} \boldsymbol{x}_A \right\|_F^2 \tag{5-13}$$

where $\boldsymbol{X}_A$ is the set of all possible message blocks from Node A.

In the second time-slot/transmission phase, the decoded message block at the relay node is transmitted from Node R to Node B, employing the GQSM modulation technique over a Rayleigh frequency-flat fading channel $\boldsymbol{H}_{B_R}$ of dimension $N_{R_B} \times N_{T_R}$ with entries modeled as i.i.d complex Gaussian random variables with distribution CN(0,1). The transmitted message block is received in the presence of AWGN $\boldsymbol{n}_B$ of dimension $N_{R_B} \times 1$ with i.i.d entries distributed as CN(0,1). The $N_{R_B} \times 1$ received message block $\boldsymbol{y}_B$ at Node B can be written as:

$$\boldsymbol{y}_B = \sqrt{\frac{\rho_B}{n_b}} \boldsymbol{H}_{B_R} \boldsymbol{x}_B + \boldsymbol{n}_B \tag{5-14}$$

where $\boldsymbol{x}_B$ is of dimension $N_{T_R} \times 1$. ML detection is employed at the destination node to estimate the transmitted message block, which is defined as:

$$[\hat{\boldsymbol{x}}_B] = \underset{\boldsymbol{x}_B \in \boldsymbol{X}_B}{\operatorname{argmin}} \left\| \boldsymbol{y}_B - \sqrt{\frac{\rho_B}{n_b}} \boldsymbol{H}_{B_R} \boldsymbol{x}_B \right\|_F^2 \tag{5-15}$$

where $\boldsymbol{X}_B$ is the set of all possible message blocks from the relay node.

5.3 Numerical analysis and discussion

In this section, the Monte Carlo simulation results obtained for the two-way DF-GQSM relaying system is presented. We consider the average BER versus the SNR in dB. Full knowledge of the channel is assumed at the receiver.

The notation $2W$ and $1W$ represents two-way relaying and one-way relaying, respectively and the notation (N_T, N_R, M, n_b) is employed for the DF-GQSM relaying system. In all cases, ML detection is employed.

It is clearly evident from the Monte Carlo simulation results obtained (Figure 5.2, Figure 5.3) that two-way DF-GQSM relaying with two groups, i.e. $n_b = 2$ achieves an improved system performance compared to when $n_b = 3$. At a BER of 10^{-5}, two-way DF-GQSM with $n_b = 2$ achieves an SNR gain of approximately 4 dB over two-way DF-GQSM relaying with $n_b = 3$.

Figure 5.2(a) presents the performance comparison between the two-way DF-GQSM relaying and one-way DF-GQSM relaying, employing $n_b = 2$ and 3, respectively. The Monte Carlo simulation results obtained revealed that the two-way DF-GQSM relaying exhibits superior performance over its counterparts considered, with an SNR gain of approximately 8 dB and 12 dB compared to the one-way DF-GQSM relaying with $n_b = 2$ and 3, respectively. Likewise, one-way DF-GQSM relaying with $n_b = 2$ outperform the one-way DF-GQSM relaying with $n_b = 3$ with an SNR gain of 9 dB. The notation $1W$ represents one-way relaying and the notation (N_T, N_R, M, n_b) is employed for the one-way DF-GQSM relaying.

The performance comparison between the two-way DF-GQSM relaying and two-way DF-QSM relaying is presented in Figure 5.2(b). This comparison is limited to only two-way DF QSM relaying as one-way DF-QSM will require 16 transmit antennas coupled with 256-QAM modulation order to match the spectral efficiency of one-way DF-GQSM. Similarly, only two groups, i.e. $n_b = 2$ is considered as two-way DF-QSM relaying requires higher modulation order coupled with a large number of transmit antennas to match the spectral efficiency of two-way DF-GQSM. This imposes high system complexity.

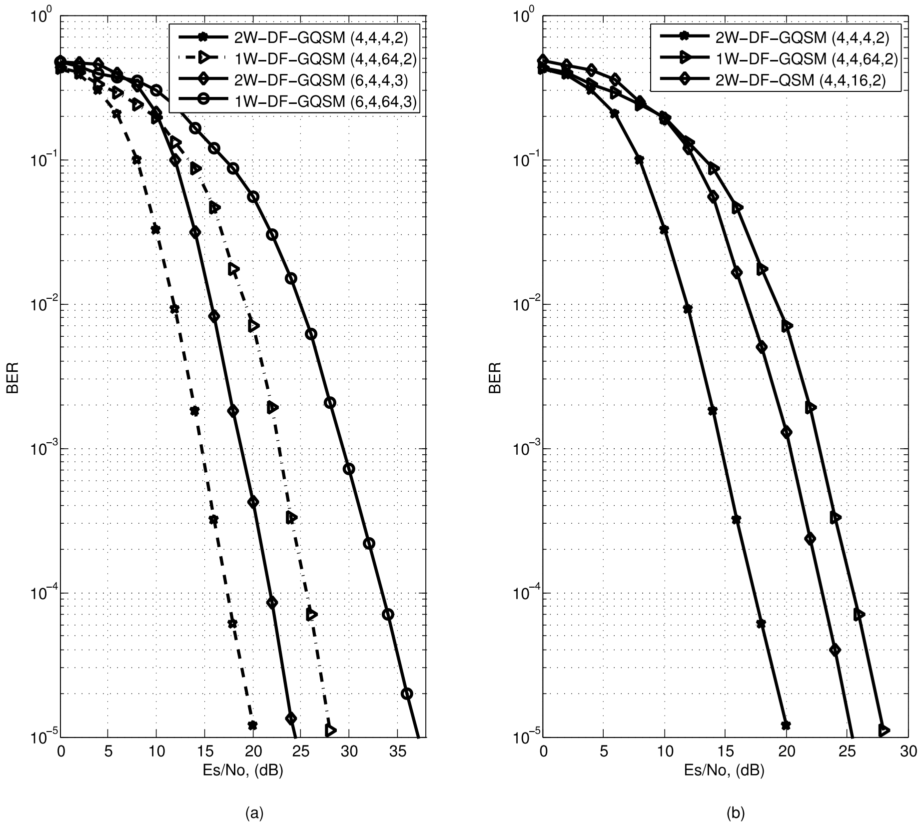

Figure 5.2 BER performance comparison of two-way DF-GQSM, one-way DF-GQSM and two-way DF-QSM.

The Monte Carlo simulation results obtained revealed that the two-way DF-GQSM relaying exhibits superior performance over the two-way DF-QSM relaying with an SNR gain of 5 dB. Furthermore, two-way DF-QSM relaying exhibits an improved system performance when compared to one-way DF-GQSM relaying as expected with an SNR gain of 2.5 dB.

In Figure 5.3, a comparison is drawn between the conventional QSM system, GQSM system, two-way DF-GQSM relaying, two-way DF-QSM relaying and one-way DF-GQSM relaying. In this comparison, 12 b/s/Hz is considered for the QSM scheme as 128 transmit antennas coupled with 256-QAM modulation order is required to match the spectral efficiency of two-way DF-GQSM. Similarly, SM is not considered as 256 transmit antennas with a high modulation order is required to match the spectral efficiency, which is not practical realizable as this will impose high system complexity.

The Monte Carlo simulation results obtained revealed that the two-way DF-GQSM relaying exhibits superior performance over its counterparts with an SNR gain of approximately 13 dB compared to the conventional QSM system. In addition, two-way DF-QSM relaying exhibits an improved system performance when compared to one-way DF-GQSM relaying, GQSM and QSM while GQSM outperforms one-way DF-GQSM with an SNR gain of approximately 0.5 dB.

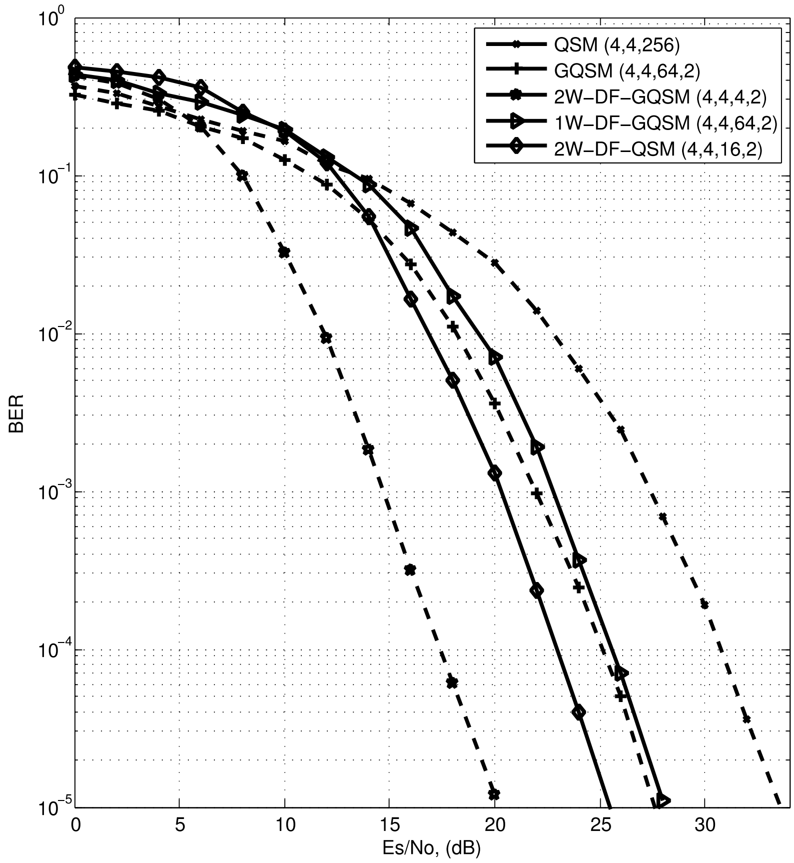

Figure 5.3 BER performance comparison of QSM, GQSM, two-way DF-GQSM, two-way DF-QSM and one-way DF-GQSM

The comparison drawn in Figure 5.2 and Figure 5.3 reveals that significant improvement is achieved in terms of error performance in a two-way DF-GQSM relaying technique compared to its counterparts.

The Monte Carlo simulation results obtained with respect to the two-way DF-GQSM relaying in Figure 3 revealed an SNR gain of approximately 4 dB, 5 dB, 8 dB, 17 dB compared to two-way DF-GQSM relaying with $n_b = 3$, two-way DF-QSM relaying, one-way DF-GQSM relaying with $n_b = 2$, one-way DF-GQSM relaying with $n_b = 3$, respectively.

Similarly, in Figure 5.3, the two-way DF-GQSM relaying reveal an SNR gain of approximately 7.5 dB, 8 dB and 13 dB compared to the conventional QSM system, the conventional GQSM system and one-way DF-GQSM relaying, respectively.

5.4 Conclusion

In this Chapter, two-way DF relaying is investigated with GQSM to improve the error performance of the system. The topology based on the two-way DF-GQSM relaying technique employed n_b groups coupled with two source nodes to transmit user information via the relay node. The received information at the relay node is decoded via an ML detection algorithm and a network coding principle is employed to create a new message block, which will be forwarded to the destination at the second time slot. Each source node can then obtain the message of the other node via reversing the operation performed at the relay.

Likewise, a one-way DF-GQSM is introduced as a benchmark, which is compared to the proposed two-way DF-GQSM in terms of error performance. In the Monte Carlo simulation results obtained, the two-way DF-GQSM relaying with two groups exhibits an improved error performance compared to the two-way DF-GQSM relaying with three groups, two-way DF-QSM relaying and one-way DF-GQSM relaying.

References

[1]. A. Goldsmith, Wireless Communications, 1st ed., New York: Cambridge University Press, 2005.

[2]. R. Mesleh, H. Haas, S. Sinanovic, A. Chang Wook, and Y. Sangboh, "Spatial Modulation," *IEEE Transactions on Vehicular Technology,* vol. 57, no. 4, pp. 2228-2241, Jul. 2008.

[3]. A. Younis, N. Serafimovski, R. Mesleh, and H. Haas, "Generalised spatial modulation," in *Proceedings of the 2010 Conference Record of the Forty-Fourth Asilomar Conference on Signals, Systems and Computers*, pp. 1498-1502, 2010.

[4]. F. Jinlin, H. Chunping, X. Wei, Y. Lei, and H. Yonghong, "Generalised spatial modulation with multiple active transmit antennas," in *Proceedings of the IEEE GLOBECOM Workshops (GC Wkshps),* pp. 839-844, Dec. 2010.

[5]. R. Mesleh, S. S. Ikki, and H. M. Aggoune, "Quadrature Spatial Modulation," *IEEE Transactions on Vehicular Technology,* vol. 64, no. 6, pp. 2738-2742, Jul. 2014.

[6]. J. R Castillo-Soria, R. Ramirez-Gutierrez, "Generalized Quadrature Spatial Modulation Scheme using Antenna Grouping," *Electronics and Telecommunications Research Institute Journal,* vol. 39, no. 5, pp. 707-717, Oct. 2017.

[7]. Y. Li, M. Daneshmand, and Duan W, “A cooperative relay method and performance for wireless networks,” in *Proceedings of the 2nd International Symposium on Intelligence Information Processing and Trusted Computing, Hubei,* pp. 31-34, Dec. 2011.

[8]. S. Althunibat, R. Mesleh, “Performance analysis of quadrature spatial modulation in two-way relaying cooperative networks,” *IET Communications*, vol. 12, no. 4, pp. 466-472, Mar. 2018.

[9]. A. Koc, I. Altunbas, and E. Basar, “Two-way full-duplex spatial modulation systems with wireless powered AF relaying,” *IEEE Wireless Communications Letters*, vol. 7, no. 3, pp. 444-447, Jun. 2018.

[10]. B. Rankov, A. Wittneben, “Achievable rate regions for the two-way relay channel,” in *Proceedings of the IEEE International Symposium on Information Theory, Seattle, WA*, pp. 1668-1672, Dec. 2006.

[11]. H. Ju, E. Oh, and D. Hong, "Catching resource-devouring worms in next-generation wireless relay systems: Two-way relay and full-duplex relay," *IEEE Communications Magazine*, vol. 47, no. 9, pp. 58-65, Sep. 2009.

[12]. N. R. Naidoo, H. Xu, and T. Quazi, "Spatial modulation: optimal detector asymptotic performance and multiple-stage detection," *IET Communications*, vol. 5, no. 10, pp. 1368 - 1376, Jul. 2010.

[13]. H. Xu, "Symbol error probability for generalized selection combining reception of *M*-QAM," *SAIEE Africa Research Journal*, vol. 100, no. 3, pp 68 - 71, Sep. 2009.

CHAPTER 6

Conclusion and Future Work

The conclusion and suggested future work of this thesis is presented in this chapter

6 Conclusion

The background study coupled with the transmission model for the conventional MIMO schemes was presented in Chapter 1, stating the benefits and the setbacks experienced in the scheme. This led to several innovative forms of MIMO schemes found in the literature, which improves/mitigates these setbacks. Thereafter, the contribution of this thesis is presented in the preceding chapters

In Chapter 2, an adaptive scheme for media-based SIMO schemes was investigated. A decision metric employed was based on minimizing the IBEP at every transmission instant. Hence, the IBEP for each candidate mode considered was derived and the candidate mode with the minimum IBEP was selected as the transmission mode. The Monte Carlo simulation results obtained demonstrated an enhanced performance over its counterparts, viz. the conventional SIMO, MB-SSK and SIMO-MBM.

In Figure 2.2, a spectral efficiency of 4 b/s/Hz and 6 b/s/Hz was considered for the Monte Carlo simulation with M-QAM, it was clearly evident in the results obtained that the proposed ASIMOMBM scheme achieves a better performance compared to its counterparts.

Similarly, in Figure 2.3, M-PSK was considered for the Monte Carlo simulation results and ASIMOMBM scheme exhibits an improved error performance when compared to its counterparts. The SNR gains achieved with respect to the proposed ASIMOMBM scheme is tabulated in Tables 6.1 and 6.2 for M-QAM and M-PSK, respectively.

Table 6.1: SNR gain (dB) of the ASIMOMBM system, based on M-QAM employing $N_R = 2$

Schemes	4 b/s/Hz	6 b/s/Hz
SIMO	4.4 dB	5.1 dB
MB-SSK	2.1 dB	1.3 dB
SIMO-MBM	1.1 dB	1.0 dB

Table 6.2: SNR gain (dB) of the ASIMOMBM based on M-PSK with $N_R = 2$

Schemes	4 b/s/Hz	6 b/s/Hz
SIMO-PSK	7.5 dB	14.5 dB
MB-SSK-PSK	0.7 dB	1.3 dB
SIMO-MBM-PSK	0.6 dB	1.0 dB

In Chapter 3, the application of RF mirrors was investigated with GSM to enhance the spectral efficiency and improve the error performance of the system at a reduced hardware complexity. The theoretical average bit error probability for the proposed scheme was formulated. In addition, the effect of MAP selection algorithm was investigated in the S-GSM-MBM system. The S-GSM-MBM technique demonstrates an improved system performance compared to the conventional GSM, SM and MB-SM system of the same spectral efficiency.

The Monte Carlo simulation results obtained revealed that a media-based modulation technique based on RF mirrors improves the system performance of the conventional GSM scheme. Similarly, the proposed S-GSM-MBM achieves better performance when compared to MB-SM in the literature. The theoretical analysis conforms well with the Monte Carlo simulation results, which validates the proposed S-GSM-MBM scheme. The SNR gains achieved with respect to the S-GSM-MBM scheme is tabulated in Table 6.3.

Table 6.3: SNR gain (dB) achieved, with respect to the S-GSM-MBM system

Schemes	8 b/s/Hz	10 b/s/Hz
GSM	7.5 dB	6.5 dB
SM	6.5 dB	5.5 dB
MB-SM	3.5 dB	5 dB

In addition, a MAP selection algorithm was introduced to the proposed S-GSM-MBM, which further improved the error performance of the scheme. The S-GSM-MBM scheme with EDAS based MAP selection outperforms its counterparts, followed by the S-GSM-MBM with norm-correlation based MAP selection algorithm. The SNR gain achieved with respect to S-GSM-MBM with EDAS based MAP selection algorithm with $N_a = 2$ is tabulated in Table 6.4.

Table 6.4: Achieved SNR gain (dB) with EDAS based S-GSM-MBM.

Schemes	8 b/s/Hz	10 b/s/Hz
MB-SM	9.5 dB	8 dB
S-GSM-MBM	8 dB	6 dB
S-GSM-MBM (Norm-based)	6 dB	2 dB
S-GSM-MBM (Norm-Corr)	5.5 dB	1.5 dB

Likewise, a comparison is drawn between the conventional index modulation schemes and the proposed topology based on the optimal and sub-optimal MAP selection algorithm considered, which revealed the trade-off in terms of the error performance and CC.

Similarly, in Chapter 4, we investigated a SS-GQSM scheme based on antenna grouping with the requirement of a single RF chain to reduce complexity/cost. The proposed scheme exhibits a low CC compared to the GQSM system of [8] with the same spectral efficiency. Furthermore, the effect of link adaptation was investigated in the proposed SS-GQSM system and the theoretical framework for the proposed scheme is derived. The Monte Carlo simulation results obtained reveal a trade-off in the optimal and sub-optimal transmit selection algorithm considered in terms of the error performance and CC.

The conventional GQSM scheme outperforms the SS-GQSM at the cost of high CC. The trade-off in terms of error performance and complexity is evident in the Monte Carlo simulation results obtained and the computed CC. The comparison is tabulated in Table 6.5 and Table 6.6.

Table 6.5 SNR gain (dB) achieved, with respect to the GQSM system

Schemes	$n_b = 2$	$n_b = 3$
S-GSM-MBM	0.9 dB	4.8 dB

Table 5.6 illustrates the complexity comparison of SS-GQSM and the conventional GQSM scheme with $N_R = 4$ and $M = 4$.

Table 6.6 Receiver complexity comparison for GQSM and SS-GQSM.

Scheme	8 b/s/Hz, $n_b = 2$	12 b/s/Hz, $n_b = 2$	12 b/s/Hz, $n_b = 3$
SS-GQSM	11,008	176,128	241,664
GQSM	35,584	569,344	831,488

The last contribution of this thesis was presented in Chapter 5, where we investigated two-way DF relaying with GQSM to enhance the link reliability and improve the error performance of the system. This was based on two-way DF-GQSM relaying technique employing N_{T_ℓ} groups coupled with two source nodes to transmit user information via the relay node. The received information at the relay node was decoded via ML detection algorithm and a network coding principle was employed to extract the new bits, which was forwarded to the destination at the second time slot.

In addition, we introduced a one-way DF-GQSM as a benchmark to draw comparisons in terms of system performance. The results obtained revealed that the two-way DF-GQSM relaying with two groups outperform all other configurations and schemes considered, as shown in Figure 5.4.

6.1 Future work

This study can be further aimed at providing future research advances in the following direction:

1. Improving receiver complexity: investigating a low complexity detector, such as sub-optimal detector in S-GSM-MBM and SS-GQSM to further reduce the complexity of the scheme to make the proposed scheme more realizable.
2. A decision metric of the minimum BER can be investigated in ASIMOMBM coupled with a low-complexity detector.
3. Transmit antenna combination with minimized antenna correlation can be introduced to the S-GSM-MBM system, such that each group employs a less correlated antenna combination.